The Bartlett Centre for Advanced Spatial Analysis

UCL

Thesis submitted for the degree of

Doctor of Philosophy

Multifractality applied to the study of spatial inequality in urban systems

Author
Hadrien Salat

Supervisors
Dr. Elsa Arcaute
Prof. Michael Batty
Dr. Roberto Murcio

February 7, 2019

I, Hadrien, Pierre, Pablo Salat confirm that the work presented in this thesis is my own. Where information has been derived from other sources, I confirm that this has been indicated in the thesis.

Abstract

This thesis investigates multifractality as a tool to analyse the spatial patterns emerging from urban inequality. In our context, inequality is defined as a difference between individuals in economic welfare (in the tradition of Dalton and Sen). As such, it considers the typical household income distribution, but also variables such as real estate and energy consumption. These variables can be transformed into mathematical measures which present diverse extent of self-similarities explained by the self-organisation processes resulting from an intense competition for space. The multifractal methodology can exploit these self-similarities to produce precise local statistical information even when the usual tools fail due to an excessive complexity.

The analysis is performed on large geographical datasets for London, Paris, New-York and Kyoto. The main results are a decrease in multifractality with modernisation that can be understood as an arguably positive homogenisation, but also a negative loss of diversity; striking similarities in the independent evolution of the spatial repartition of land and housing prices across the globe during the 20th century; and discrepancies between income and the other measures, in accordance with the idea that income alone is not enough to fully characterize inequality. The most important result, however, is the validation after comparison with the traditional inequality and segregation measures that multifractality is a high-performing spatial inequality indicator. It is in particular able to extend the exposure and clustering dimensions of segregation to ordinal continuous variables.

Impact statement

The impact of this thesis is twofold. From an academic perspective, it brings a new methodology to the study of inequality and segregation in the urban environment that solves some of the issues usually encountered. It also invites urban planners and policy makers to measure more accurately the impact on inequality induced by their future projects. In September 2015, the United Nations General Assembly identified combating inequality as the 10^{th} goal of sustainable development for their 2030 agenda, the present thesis is a step forward towards achieving this goal.

The traditional academic framework for the analysis of inequality is based on a-spatial inequality measures producing a global estimate of the inhomogeneities inside the distribution of a wealth variable, usually income. However, these estimates contain by nature no spatial information. In parallel, segregation measures evaluate the spatial separation between two or more groups living in different parts of a city. When the definition of the groups is based on an ordinal variable, such as income, these measures describe the spatial patterns emerging from inequality. However, ordinal segregation measures may suffer from computational efficiency issues, are sensitive to the modifiable areal unit problem and usually only provide one global parameter that is difficult to interpret. We propose a methodology, multifractal analysis, which does not suffer from these issues and which provides a spectrum of results allowing to characterise the spatial distribution of inequality with unprecedented subtlety.

Our methodology is more than a simple application of an already existing mathematical theory. We have carefully adapted it to the urban context and we have explored a novel way of interpreting it tailored to the analysis of economic spatial inequality. This should make its implementation in practice easy for urban planners and policy makers. To that effect, we propose in the appendix our own modelling framework linking the potential redevelopment of residential areas or modification of the transport network with the resulting spatial patterning of income inequality. Although not realistic at this stage, this model demonstrates how the methodology we develop throughout the thesis can be applied to real life situations.

Two articles have been published based on the content of the thesis (Salat et al., 2017, 2018). They respectively aim to introduce the methodology and to disseminate its application to studying inequality.

Contents

List of Tables

List of Figures

Introduction

At the most basic level, *inequality* can be understood as the socioeconomic gap separating the wealthy from the poor. Traditionally, it is characterised either by the shape or the spread of a particular household income distribution. Some policy advice is then derived with the aim of smoothing the distribution and reducing its spread at a regional, national or international level. This approach was most successfully carried by Piketty (2014) and Atkinson (2015). However, ever since the notion of inequality was scientifically formalised, it has been emphasised that income alone may not be sufficient to capture the true differences in "economic welfare" between individuals (Dalton, 1920; Atkinson, 1970; Sen, 1997). Recently, Martin et al. (2015) attempted to theorize the problem of tackling inequality from an architectural perspective. They define inequality as "a seemingly endless chain of inequities around which both individuals and social groups hold conflicting interests" and include in these inequities social issues typically infused by urban development, such as racial and gender discrimination.

We propose our own definition of inequality as any economic or social trait that results in some individuals being worse off than others, without the moral connotation implied by the term "inequity"[1]. It does not only include direct economic welfare characteristics, such as the traditional income difference or housing inequality, but also the social prejudice potentially induced by economic segregation. Our focus is nevertheless narrower than studying all manifestations of inequality: we are mainly interested in analysing the spatial patterns that emerge from inequalities. Space plays a fundamental role in the perception of inequality as it determines the number and quality of jobs accessible, but also the composition of neighbouring leisure and commercial amenities that create social interactions and outside of work quality of life. It is therefore unsurprising that wealth inequality triggers a

[1]See for example Nielsen (2017): "People are not good at assessing the overall level of inequality in a large impersonal society. They tend to visualize the structure of society as a whole in terms of the social positions of people they are familiar with (their reference group, the counterpart of the hunting-and-gathering band of the ancestral environment). Complete equality of outcomes is not the preferred situation; inequality based on hard work or superior talents is accepted as long as opportunities to achieve these outcomes are equal. Inequality generates moral outrage [inequity] when disparities are interpreted as a form of "cheating" or denial of a fair share in a (perhaps putative) exchange relationship."

competition for space resulting in turn in housing, income and accessibility inequality. In particular, this competition induces segregation which in turn acts as a lever that maintains or degrades the existing socioeconomic unequal situation (Jacobs, 1961; Massey and Denton, 1993).

The importance of including space in the analysis of inequality has already been underlined by Reardon and O'Sullivan (2004); Reardon et al. (2006) who call for defining better economic segregation measures that allow to take into account both the variable and spatial distribution of economic ordinal variables. As a matter of fact, measuring inequality is already a daunting task, even before considering the spatial aspect of it. It requires, for example, to decide which is the most important factor between on the one side the spread of the welfare gap between different social groups, and on the other side the relative proportion of the population that falls inside each group. A method inspired by *multifractal theory* could offer a solution to integrate the role of space in the analysis of inequality while solving many of the technical issues usually encountered by the traditional inequality and segregation indices. Multifractal theory was originally developed to study mathematical measures defined on geometrical complex sets and to study fully developed turbulence in physics. It relies on exploiting the underlying scaling properties sometimes found in chaotic complex systems to gather compelling statistical information that allow to describe the spatial heterogeneity of the system.

Multifractality is only relevant when strong self-similarities exist and when more than one scaling exponent is needed to describe them. For cities, the frequent occurrence of such scaling properties is well established (Batty and Longley, 1994; Frankhauser, 1994; Bettencourt et al., 2007; Batty, 2008*b*; Bettencourt and Lobo, 2016). Meanwhile, the insufficiency of using only one scaling exponent for an entire city has been recently emphasised (Thomas et al., 2012; Arcaute et al., 2015; Cottineau et al., 2017). The theories to explain the existence of self-similarities in urban systems are varied, but are mostly centred around the creation of nonlinearities as a result of the competitive self-organisation bottom-up processes shaping cities. We have already underlined that this competition for space results in housing, income and accessibility inequality. It is therefore natural to ask if multifractality could be used as a tool to gain better statistical insights on inequality in urban development compared to the current inequality and segregation measures. In particular, can multifractality characterise the spatial patterns that emerge from inequality in cities?

In order to answer this question, we first need to identify which urban characteristics are multifractal. By characteristics we mean distributions

such as income, land and house prices or energy consumption. Given our context, we are only interested in those when they carry a sense of economic welfare. We also need to assess the relative importance given by our methodology to the spatial patterning in comparison to the distributional characteristics of the inequality characteristics that we have identified. We finally need to prove that the multifractal methodology offers new insights on spatial inequality and more generally is an improvement over current inequality measures.

The first step of our methodology consists in discriminating a set of measures representing economic welfare and testing the multifractality of these measures using highly detailed dataset in four different cities: London, New York, Paris and Kyoto. We then test our results against the different inequality and segregation indicators that have been traditionally in use since the beginning of the 20^{th} century. Our focus is resolutely oriented towards developing a sound and powerful scientific measurement method rather than towards giving policy advice. However, such policy implications should be a natural extension of the work presented here, and we already hint at it with the urban development model proposed as an appendix.

The thesis is structured as follows. The first chapter reviews the literature both on the study of inequality applied to an urban context and on the place of monofractality and multifractality in urban science. The second chapter presents a formal definition of multifractality and critically compares the different methods that have been developed to put it in practice. We explain in particular our choice of a particular method and our own adaptations of it. Chapter III approaches multifractality from an interpretative perspective both in general and tailored for the urban inequality context. It explains and justifies in detail the epistemology of our approach. Multifractality is presented again with a heuristic approach trimmed of the complex technicalities of the previous chapter so that the reader less interested in the mathematics of multifractality will find sufficient information to fully understand the following chapters. Chapter IV gathers case studies based on real estate, income, energy consumption and accessibility datasets in London, New York, Paris and Kyoto. It proves that multifractality is a valid approach and presents some original results. Finally, the last chapter compares some of our results to the results obtained from the classical inequality indicators. We prove definitively that our methodology is efficient, provides more coherent results than the traditional framework and is able to capture facets of segregation that cannot usually be attained by classical segregation measures.

CHAPTER I

Review of inequality measures and urban multifractality

We define inequality as any economic or social trait that results in some individuals being worse off than others. This chapter will show that this definition encompasses both the traditional household income analysis (Persons, 1909; Dalton, 1920; Atkinson, 1970), any other potential indicator of disparities in economic welfare (Dalton, 1920; Sen, 1997), and the social and economic segregation perspective (Burgess, 1928; Massey and Denton, 1988; Reardon and O'Sullivan, 2004). We review the technical development and particularities of these different historical approaches in the chapter's first section. We also present the studies that emphasize the role played by the singularities of urban systems in giving rise to inequality and segregation, and enlighten some of the difficulties usually encountered by the classical methods.

A new tool potentially able to resolve these difficulties, multifractality, is presented in the second section. It is particularly focused on the study of spatial patterns emerging from inequalities. We first justify why the geometric properties necessary for multifractality to exist, self-similarities, are frequently found in urban environments. We then present some interesting case studies from the literature that prove multifractality has already been found for some urban measures such as land prices and street intersection densities. These measures are a good basis to support the use of the multifractal methodology for urban systems. We gather further support with ideas from the broader multifractal field that could be relevant for urban environments. Finally, we review the development of the theoretical foundations of multifractal theory and the development of the four main methodologies usually adopted for practical studies.

1. Measuring inequality in urban systems

The usual approach to measuring inequality, particularly brought into prominence by Atkinson (1970), consists in gathering indices that give a global estimate of the statistical dispersion inside a given distribution, or an

estimate of the deviation of said distribution compared to an equal distribution. The distribution is usually assumed to be household income (Atkinson, 1983, 2015), although Sen (1997) argues that income alone is not necessarily an adequate representation of the welfare of an individual (an idea that was already pointed out by Dalton as soon as 1920 Dalton, 1920). For example, the total disposable money may differ once we subtract the basic needs (including potential disabilities) that may be different from an individual to another; or the money may be unequally distributed inside the household. These indices are not meant to account for the role of space, and focus exclusively on the disparities inside the distribution of wealth. As such, we will call them *a-spatial inequality measures*. They are detailed in the first subsection below.

In the urban context, another separate approach can be considered: *segregation*. It consists in gathering indices that measure "the degree to which two or more groups live separately from one another in different parts of the urban environment" (Massey and Denton, 1988). These indices usually do not provide any information on the relative gap between each group, but give a measurement of the clustering and lack of spatial uniformity. These inhomogeneities may translate into a different experience of life quality for groups belonging to different segregation clusters, hence characterizing spatially inequality. In addition, Jargowsky (1996); Watson (2006) and Reardon et al. (2006) have extended the notion to social groups defined through an ordinal variable. In particular, the ordinal variable can be household income, as was used for the a-spatial inequality measures. The segregation measures are detailed in the second subsection.

These two approaches appear to have attracted most of the focus of the social scientist efforts. Some additional measures have been developed based on spatial autocorrelation techniques used in Geography (Chakravorty, 1996; Dawkins, 2007). They meet the objectives of the segregation measures with a strengthened account of the spatial characteristics of the distribution. We now detail both the a-spatial and the segregation and autocorrelation approach, then see how they have been applied to the specific urban context, and finally discuss their shortcomings and emphasise the need, as underlined by Reardon et al. (2006), for new measures that integrate both the distributional and spatial traits of the inequality variables in a more convincing way.

1.1. A-spatial inequality measures. Early research on the topic of inequality advocated for measuring disparities in income distributions as in any distribution of a biological or physical characteristic (Persons, 1909). The necessity of relating income to economic welfare was then introduced

(Dalton, 1920). Dalton intended to do it using a functional, later renamed *utility function*, obeying some mathematical rules to express the perceived welfare stemming from income. The comparison between the functional and a fully equal distribution was coined the *Dalton index*. Consider a distribution $\{x_i\}_{i=1}^n$ of average μ, then the Dalton index D is defined as

$$\mathrm{D} = \frac{\sum_i U(x_i)}{nU(\mu)}, \tag{1}$$

where U is the utility function. However, further developments of this idea were severely constrained by the lack of computational power in these days. In 1970, Atkinson reworked the concept to make the index invariant through linear transformations of the utility function (Atkinson, 1970). It resulted in the *Atkinson index*, classically defined as

$$\mathrm{A} = 1 - \frac{1}{\mu}\left(\frac{1}{n}\sum_i x_i^{1-\varepsilon}\right)^{\frac{1}{1-\varepsilon}}, \tag{2}$$

for the same distribution as before. In this formulation, the utility function operates implicitly through the "inequality aversion" coefficient $0 \leq \varepsilon < 1$. The closer ε is to 1, the more impact the lower end of the distribution has, and the closer ε is to 0, the more impact the higher end of the distribution has. In his seminal review, Sen (1973) argues that both these approaches are valid, and defines a "normative" category to group all such indices that relate income to welfare.

In parallel, a simpler approach was developed in Italy in the early twentieth century (Gini, 1912; Ricci, 1916, partial translations by Ceriani and Verme (2012)). It focuses on the description of the statistical characteristics of the wealth distribution, without any particular link to economic welfare (Yntema, 1933, for a classic early 1930s review of this approach). This sort of indices form therefore the "descriptive" category according to Sen (1973). It encompasses basic indices, such as the range, relative mean deviation, variance, coefficient of variation and standard deviation of logarithms measures. It also contains the Gini index which has undoubtedly been the most fructuous one. The Gini index compares the Lorenz curve (Lorenz, 1905), i.e. the curve representing the proportion of overall income enjoyed by the bottom x% of the population, to a straight line representing absolute equality. More explicitly, it is defined for $\{x_i\}_{i=1}^n$ as

$$\mathrm{G} = \frac{\sum_i \sum_j |x_i - x_j|}{2n^2\mu}. \tag{3}$$

It is the only index, together with the coefficient of variation, that ensure that "any transfer from a poorer person to a richer person, other things remaining

the same, always increase the variance", which is the minimal condition that any inequality measure should have according to Dalton (1920) (who was influenced on this by (Pigou, 1912)).

Alternatively, Theil (1967) uses Shannon's entropy formula to derive an inequality measure. We want to avoid opening a Pandora's box here by trying to define precisely entropy, and abide by John Neumann's famous quote addressed to Shannon about his formula: "You should call it entropy, because nobody knows what entropy really is, so in a debate you will always have the advantage." (as reported by Tribus and McIrvine, 1971). For now, we can understand entropy as a measure of uncertainty. Counterintuitively, when applied to the share of income going to individuals, the formula reaches its maximum when absolute equality is obtained. The *Theil index* is then defined as the difference of the distribution's entropy to the maximum case, which reduces for our distribution $\{x_i\}_{i=1}^n$ to

$$\mathrm{T} = \sum_i \frac{x_i}{n\mu} \log\left(\frac{x_i}{\mu}\right). \tag{4}$$

According to Sen (1973), it is somewhat arbitrary, and the lack of clear interpretation place it in the descriptive category. It does however satisfies the Dalton minimal condition. The Theil index is defined similarly to *redundancy* in information theory. It computes the difference between the maximum possible entropy in the system (in the sense of Shannon's entropy, so $\log(n)$) and the actually observed entropy. The upper bound of the Theil index, $\log(n)$, depends on the system's characteristics. As a result, it is only useful when comparing the evolution of a singular system, or several systems with similar number of observations n.

It is noteworthy that both the Gini and Theil indices obey the requirement made by Atkinson (1970) of invariance through linear transformations of the income distribution (as can be easily verified from the equations). In the context of segregation, Reardon et al. (2006) further require that measures are invariant to any order preserving change of the distribution. As a matter of fact, this is part of a larger unresolved debate. Assume that the entire population is divided into several income classes. Is the number of people inside each income class more important than the gaps between those classes? Reardon's stance means that it is from their point of view. Likewise, for continuous distributions, is the shape of the Lorenz curve more important than the total income spread? This debate, together with the debate about the necessity of introducing a utility function to interpret income in terms of economic welfare, are not settled. The a-spatial inequality

field has otherwise known little technical evolution since the 1970s. More recently, the emphasis has been increasingly put on measuring segregation.

1.2. Segregation indicators. The idea of relating social distance to spatial distance is not new (Park, 1924, 1926). It was first convincingly formulated by Burgess (1928). Since then, there have been trends and many debates as to which segregation indices should be used, with for example a long-lived emphasis on the *interaction index* invented by Bell (1954), which has been through a series of enhancements in the eighties (Lieberson (1981); Jakubs (1981); Morgan (1983), among many others). It is usually defined as

$$\sum_i \left(\frac{x_i}{X}\right)\left(\frac{y_i}{N_i}\right), \tag{5}$$

where x_i is the population of minority class X in an areal unit i, X its population in the entire system, y_i the population of majority class Y in unit i, and N_i the total population of unit i. In 1955, it appeared Duncan and Duncan (1955) had settled the argument with the epiphany of the *dissimilarity index*,

$$\mathrm{D} = \frac{1}{2}\sum_i \left|\frac{x_i}{X} - \frac{y_i}{Y}\right|, \tag{6}$$

where x_i and y_i are the population of class X and Y (respectively) in an aeral unit i, and X and Y are the total population of class X and Y in the entire system. This position was further strengthened by the work of Taeuber and Taeuber (1965). However, the truce came to an end in 1976 when the objections by Cortese et al. (1976) relaunched the debate. In 1988, Massey and Denton (1988) listed up to twenty different indices for the purpose of measuring residential segregation. In this section, we only present the general segregation framework, rather than the details and mathematical definitions of each of the many indices. Those details are postponed until chapter V.

In 1986, Stearns and Logan (1986) distinguished three "dimensions" to segregation, they are *(un)evenness*, *concentration* and *probability of interaction*. Massey and Denton (1988) increased the number to five by replacing probability of interaction with *exposure*, *centralisation* and *clustering*. They define these notions as follows.

- **Evenness** is defined as the "differential distribution of two social groups among areal units in a city";
- **Exposure** is the "degree of potential contact, or possibility of interaction, between minority and majority group members within geographic areas of the city";

- **Concentration** is the "relative amount of physical space occupied by a minority group in the urban environment";
- **Centralisation** is the the "degree to which a group is spatially located near the centre";
- **Clustering** is the "extent to which areal units/minority adjoin one another".

For example, the dissimilarity index and the Gini coefficient are measures of evenness, while the interaction index is a measure of exposure. The five dimensions are illustrated in figure I.1. Depending on how the classes and areal unit are defined, the different dimensions may overlap. Indeed, in the bottom right image representing clustering, there is an obvious separation of the distribution and space in four different classes and neighbourhoods that will lead to mutually exclusive areal units, hence to maximum unevenness.

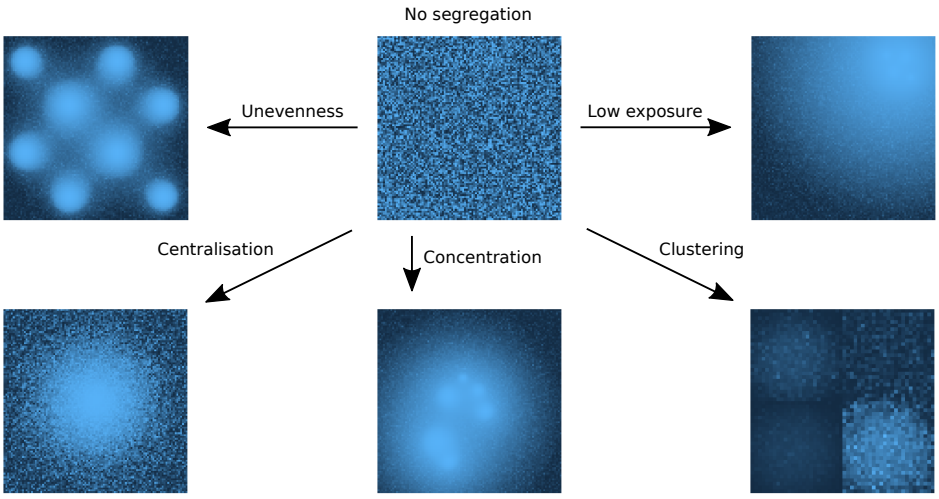

FIGURE I.1. **The five dimensions of segregation.** Assume that the brighter a pixel is, the higher the average income is in its corresponding area. The image in the middle represents no segregation. On the left, the distribution is uneven: rich and poor neighbourhoods are mutually exclusive. On the right, the rich and the poor are not exposed to one another since they are separated by the middle class. On the bottom left, the richest occupy the centre. On the bottom middle, they are concentrated around the bottom right corner and occupy a low amount of space. On the bottom right, the population is clustered in four different classes.

In 2004, Reardon and O'Sullivan (2004) argued that only exposure and evenness indices met satisfactorily the criteria they had identified to evaluate the quality of segregation measures. Indeed, they ask of a measure to have

"scale interpretability", which in their case means reaching 0 when group proportions are uniform and reaching the maximum value only when there is no proximity between any two members of each group. They further require independence from arbitrary boundaries, invariance to local population density and to total population composition (meaning that only the position in space should matter). In addition, the measure should obey three "algebraic property" which they call "location equivalence" (similar to class equivalence in mathematics), "additive spatial decomposability" and "additive grouping decomposability" (similar to σ-additivity in mathematics). They finally define some rules tackling transfers and exchanges of individuals between areal units. We will see in the conclusions and in appendix B how our multifractal measures fare against these rules.

The measures referenced above are only statistically meaningful if the sample size is large enough in each areal unit. This means that the size of the units may become excessive to relate to the perception of proximity at human scale. It also means that the shape of the unit and the shape of its artificial boundary may have a large impact on the results. Wong (1993) emphasizes this issue and proposes to incorporate the length of the boundary and shape of the areal units as a weight into the definition of the dissimilarity index. Ideally, we would want a "continuous" map of segregation where each location is at the centre of its own unit. As a matter of fact, (Reardon et al., 2006) call for new economic segregation measures that take into account the role of space in a more ambitious way, while being insensitive to the choice of category thresholds, boundary definitions[1], and shape-preserving changes in the variable distribution.

They summarise existing measures by categorising them into three different groups of measures. These measures are relatively difficult to define and put in practice, we therefore only mention them here and postpone a more detailed description of them until chapter V. The first group is made of categorical segregation measures. An extensive compilation of such measures has been established by Apparicio et al. (2014). These may be appropriate for racial segregation, but they are not suitable for economic segregation, since they only allow either two or a small number of categories that do not represent well economic measures such as income. A second group is made of ordinal variation-ratio segregation measures, forefronted by the Neighbourhood Sorting Index (NSI) (Jargowsky, 1996; Jargowsky and Kim, 2005) and the Centile Gap Index (CGI) (Watson, 2006). They compare the ratio of the between-neighbourhood variation to the total population variation for some

[1]This particular issue is usually referred to as the Modifiable Areal Unit Problem or MAUP.

definitions of social variation (Berry and Mielke, 1992; Kvalseth, 1995*a*,*b*). Their main limit is that they do not obey well the three criteria of category, boundary and shape-preserving change invariance. Finally, the third group is made of spatial measures, including those based on the autocorrelation geographic principle (Chakravorty, 1996; Dawkins, 2007) and some custom ones proposed by the authors.

Before we explore in more details the shortcomings of these segregation measures, as well as the shortcomings of the inequality measures from the previous section, we summarize some of the well establish results we expect to recover, or at least not contradict, with our own methodology, and take note of some recent methodological ideas that can prove useful while defining our own measures.

1.3. Inequality in urban systems. Some archetypal results include the observation that there is an opposition between American and European cities with a pauperisation of the centre for the former that is not observed for the latter (Brueckner et al., 1999; Glaeser et al., 2008). This pauperisation of the centre may further generate sprawl that is considered largely detrimental for the environment and health (due in particular to the increase use of driving) and is a source of segregation as new homogeneous exclusively residential zones are created (Squires, 2002, and in particular, Jargowsky (2002)). There is additionally a common gentrification process in most developed cities, potentially creating heterogeneity and uncontrolled displacement of some social classes (Atkinson and Bridge, 2005). High segregation is associated with health problems for the lower classes (Lobmayer and G., 2002), and ghettoisation self-perpetuating processes that can have social and economic negative repercussions (Massey and Denton, 1993), in particular urban decay (Jacobs, 1961; Andersen, 2002).

In contrast, the Japanese city is presented as a model of low residential segregation by Fujita and Hill (1997). They have identified in particular a decreasing trend in segregation during modern times that diverges distinctly from the other highly developed societies. Those results were later mitigated by Fielding (2004), who criticises the methodology and in particular the influence that the spatial scales and artificial boundary definitions used may have had on the low segregation scores. Nonetheless, Fielding points

out seven socio-economic reasons[2] that would explain why segregation is expected to be much lower for Japanese cities compared to American cities. We will test this hypothesis in chapter IV with our methodology.

Due to the lack of ordinal segregation measures until the mid nineties (Jargowsky, 1996), and due to the rapidly decreasing efficiency of categorical segregation measures when the number of categories is greater than two (Reardon et al., 2006), most of the segregation analysis has historically revolved around racial segregation, and particularly black and white segregation in American cities (Taeuber and Taeuber, 1965; Lieberson, 1981; Reardon et al., 2009). Our methodology is however based around ordinal variables. Even though they are rarer, some noteworthy contributions do exist in this direction such as the studies by Watson (2006, 2009) that evidence a correlation between a rise in income a-spatial inequality and a rise in residential segregation.

In terms of a-spatial inequality indices, the greatest successes have been achieved by Piketty (2014) and Atkinson (2015). Their work is entirely policy oriented. More precisely, it is primarily aimed at governmental policy-making in contrast to local planning. This is well in line with the aim of a-spatial indices that provide only one global number for a given distribution. In contrast, an interesting comparison of the UK Census results in 2001 and 2011 is proposed by Lloyd (2016). In this study, most of the results are focused on comparing between urban and rural areas and between the different cardinal directions at a nation wide scale, and little is said of intra-urban inequalities. Despite that, the variogram methodology used is particularly relevant for our study. In fact, Lloyds attempts at linking inequality and space in a way that varies from the segregation approach. He plots the Census variables (such as ethnicity, employment or housing tenure) into variograms that relate the differences in variable proportion between pairs of locations with the distance between said locations. The main difference with other indices consists in plotting the full curve of variations versus distance, and interpreting the differences between different dates or location types across an entire curve in opposition to only one global number.

Finally, in a noteworthy contribution, Louf and Barthelemy (2016) introduce some important methodological elements. They applied a custom exposure measurement method to the 2014 American Community Survey and found that the population could be sorted in 3 main income classes, with higher-income households being proportionally more present in larger cities

[2]The fact that transportation costs are covered by the employer; the higher renewal rate of the built housing stock; the lesser social status value attributed to housing; the reliance on small scale planning in contrast to large scale planning; the lack of gentrification; the low level of ethnic diversity; and the narrower global income range in Japan.

and higher density zones. They use these results to refute the assumption of increased social polarisation and explain some of the differences between American and European cities. A key element was to measure the deviation from the fully random "null" model, rather than taking the index directly. Another significant methodological aspect was to use density instead of distance to define neighbourhoods. It allows in particular to take into account the polycentricity of modern cities beyond the historical boundaries (Louf and Barthelemy, 2013).

Indeed, similarly to Fielding (2004) mentioned earlier, they point out the negative impact that artificially defined boundaries can have on the quality of the results, and try to tackle this problem with this improved methodology. Many more issues arise in the way that segregation and inequality is measured currently. We now describe these issues and advocate for the need of fresh measuring tools that approach the problem from a new angle.

1.4. Shortcomings of the classical indicators. As identified above, one of the first criticism of current inequality measures is their reliance on household income only, instead of actual individual economic welfare (Dalton, 1920; Sen, 1997). The solution supported by these authors is to introduce utility functions to relate income and welfare. We believe however that other criteria can account for economic welfare in addition to income. Indeed, home ownership is both a proxy of wealth and a clear sign of inequality when it is inaccessible for a part of the population. Similarly, energy consumption could be used to translate the intensity of activity of the professional sector or could be linked to the standard of living at the household level. We could also think of accessibility, air quality or diversity of nearby amenities as indicators of life quality at least partially uncorrelated to income. After taking technical feasibility into account, we chose a focus on real estate, income, energy consumption and accessibility to diverse amenities to build inequality measures.

The link between real estate and income inequality is rarely exploited aside from a few noteworthy works in architecture (Martin et al., 2015) and economy (Abeysinghe and Hao, 2014; Farzanegan et al., 2017). However, these references do not take into account the specificities of self-organised complex systems. The seminal review by McDonald and McMillen (2011) summarizes the traditional science of urban economics and real estate. Classic location models in Economy often adopt a utilitarian perspective where social interactions are neglected in favour of reducing transportation costs[3]. These theories also classically assume that there is a convergence towards an

[3]More comprehensive models are however presented by Tannier et al. (2016).

equilibrium, however Pumain (2017) and Batty (2017) argue that cities are in reality in a far from equilibrium state. In the appendix, we propose an urban model that can compare the evolution of the income distribution and the housing market under different urban development scenarios. We use an agent-based modelling approach to reintroduce both the social aspects of choosing an accommodation and the complex self-organising nature of cities.

Another issue pointed out above was the loss of spatial information with classical measures, especially since they provide only one global value. Chodrow (2017) criticizes the fact that a single scale is generally used for an entire region. He derives from information theory a creative multiscale approach to define new segregation measures. His approach being aimed at analysing racial segregation, it is quite efficient at computing categorical variables, but not ordinal variables. In addition, Louf and Barthelemy (2016) argue that using arbitrarily defined administrative boundaries incurs a loss of the relevant spatial information. Multifractal theory answers the spatial issues in two ways. First, it characterizes the studied variable through multiple scales, similarly to Chodrow (2017), including the finest, and therefore keeps track of the spatial environment better than large-scale administrative boundaries. Second, it provides a full curve of values that contains spatial information rather than one global value. We show in particular in chapter V that despite improving the situation, the new measures proposed by (Reardon et al., 2006) are still very sensitive to the choice of boundary definitions. We also demonstrate in that chapter that the multifractal approach does offer a better solution, while still performing adequately on the criteria of invariance to order-preserving changes in the distribution also supported by Reardon et al. (2006).

Finally, Louf and Barthelemy (2016) alert on the possible mistakes incurred by reliance on administrative boundary. This is particularly visible in the top left image of figure I.1. Indeed, if we were to divide the space in four squared neighbourhoods, then there would be minimal segregation, since all four neighbourhoods would be identical. In contrast, if we were to divide the space in sixteen squared neighbourhoods, then all neighbourhoods would either only contain rich individuals or only contain poor individuals. This would be a case of maximum segregation.

Let us now review and justify the use of this promising methodology in the urban context.

2. A new tool: Multifractals

Fractality is a notion originally invented to study irregular sets in geometry for which classical Euclidean tools failed (Mandelbrot, 1982). Its

concept is to extend the usual notion of dimension to sets whose topology at an infinitesimally small scale is better described by a higher (fractional) dimension than their standard Euclidean dimension. When they exist, the self-similarity properties of the set are heavily used to find this new dimension. By extension, the notion became somewhat of a synonym for self-similarity and more generally for scaling in physical complex systems. As Gomez-Lievano et al. (2016) put it, "scaling laws are important in science because they constrain the development of new theories: any theory that attempts to explain a phenomenon should be compatible with the empirical scaling".

Fractality is also called *monofractality* when it is necessary to differentiate it from *multifractality*. The idea behind multifractality is to extend the general notion of fractality to mathematical measures (Frisch and Parisi, 1983), which can be broadly understood as "layers" with some arithmetic properties on top of the physical space. A measure is considered multifractal when it possesses several local scaling exponents instead of a unique global one. The set formed by all points where the exponent is the same is in turn a fractal set (in the geometrical sense), whose dimension can be studied. Provided that these various scaling conditions are verified, multifractality can be a remarkable tool to study and compare spatial inhomogeneities for different systems. Luckily, as we will see below, multifractality is quite common in complex systems resulting from self-organization with random processes.

Cities are a perfect example of a complex system resulting from self-organization with random processes (Portugali, 2011; Portugali et al., 2012). Since we intend to use multifractality as a tool for analysing urban inequality, it is necessary to explain why it is especially well suited to study urban characteristics, and in particular those that can be related to inequality. This section will first show why, in view of the literature, scaling is frequently found in urban science, and why the study of its characteristics has sprawled in the last 20 years. It will then present case studies that encourage adding the more flexible multifractal formalism to the classical monoscaling analyses, with a focus on those that relate to the inequality factors identified in the previous section. The case studies will be separated in two groups: those directly applied to urban systems, and those from the broader multifractal field that could find useful applications to cities. Lastly, we will briefly review the current theoretical and technical knowledge about multifractals.

2.1. Monofractality in urban environments: scaling's ubiquity?

The existence of fractality in cities, in the sense of self-similarity and presence of scaling power laws, has been identified since the 1980s (Batty and

Longley, 1986, 1994; Frankhauser, 1994). These findings have since operated a paradigm shift in the study of cities and launched an exponential craze for finding power laws in urban parameters. The milestones of this new approach include the *Science* paper by Batty (2008*b*), followed by two pioneering books defining a new science of cities (Batty, 2005, 2013), and some proposed, although contested, empirical proofs of the concept's universality in urban development (Bettencourt et al., 2007; Bettencourt and Lobo, 2016; Youn et al., 2016).

Pumain (2004), influenced by the work of West (1997) on scaling in biological systems in general and by the work of Banavar et al. (1999) on efficiency in transportation networks, identifies the potential role of transportation means, and more precisely their speed variations through the ages, in creating spatial nonlinearities in urban human activity. This idea has since been refined by Batty (2008*b*) who formulates the origin of fractality as a result of cities growing from bottom up processes resulting from an intense competition for space. In this approach, the scaling emerges from the constraints imposed on the underlying network inducing a varying growth of the number of links compared to the number of nodes. It was notably supported by the later work of Arbesman et al. (2009); Pan et al. (2013); Bettencourt (2013) and Yakubo et al. (2014). Another hypothesis proposed by Salingaros and West (1999) and Frankhauser (2004) is the combination of bottom-up processes (both from individual actions and collective actions) with top-down planning. In contrast, Schweitzer and Steinbrink (2002) assume that fractal patterns emerge from contradictory decisions at individual level only, such as a conflict between minimizing the distance both to the centre of the city and to the countryside.

More recently, Gomez-Lievano et al. (2016) propose an explanation for the existence of power laws in rank-size distribution of cities, based on a combination of two factors. The first one is that the more complex a phenomenon is, the more complementary factors must be simultaneously present for it to happen. The second one is that Darwinian selection processes transform the distribution into a logarithmic distribution exacerbating extreme values. Applied to cities, this would mean that the selection process caused by cities' attractivity induces a logarithmic distribution of the number of factors depending on population size, which is the very definition of a power law.

A lot of the interest in urban scaling laws comes from their potential applications to economic efficiency. West (1997, 2006, 2017) has associated sublinearity (i.e. a scaling exponent smaller than one) in quantities accounting for infrastructure as an identifier of scale economies, and superlinearity

(i.e. a scaling exponent greater than one) as a condition for the creation of wealth and innovation (and as a potential risk of crises). In particular, Bettencourt et al. (2007) used these ideas to show the necessity of exponential innovation and growth to avoid the collapse of an urban economy. However, the applicability of this approach to cities was criticized by Pumain (2012), who argues that the necessary ergodicity assumption is not met by the evolutionary processes generating cities. Nonetheless, the study of urban scaling laws has proved fruitful over time, with applications for example in transport network efficiency (Derrible and Kennedy, 2010*a*,*b*; Louf et al., 2014; Louf and Barthelemy, 2015) and in accessibility optimisation for urban planning (Tannier et al., 2012). Fractal methods have also been used to characterise urban morphology (e.g. Batty and Longley, 1986; Fotheringham et al., 1989; Frankhauser, 1994) and in particular to define the boundaries of cities (Longley and Batty, 1989; Tannier et al., 2011; Tannier and Thomas, 2013), which, as we will now see, turns out to be an important stake for asserting the validity of scaling laws in cities.

Indeed, despite its great potential, limits to urban fractality have been increasingly pointed out in recent years. Thomas et al. (2012) have shown that the scaling may be different for the whole city than for its neighbourhoods. Similarly, Arcaute et al. (2015) and Cottineau et al. (2017) have evidenced that varying the often arbitrary definition of city boundaries can induce large variations of the value of fractal exponents calculated inside the city. In particular, Arcaute et al. (2015), propose a systematic method, further developed by Masucci et al. (2015), to define the "natural" boundaries of cities in an attempt to solve this particular issue. Arcaute et al. (2016) also propose a percolation clustering approach for the same purpose. These authors point out that the formalism used to measure scaling laws is not rigorous enough (see also Leitão et al., 2016). Harsher criticism is thrown by Louf and Barthelemy (2014), who denounce wrong fractal estimates based on inadequate estimations and a general lack of understanding of the underlying fractal mechanisms. They alert on possible "unforeseen, disastrous consequences" that could stem from using inadequately obtained fractal results for policy making.

Even though the universality of the conclusions that can be drawn from empirical fractal analysis is discussed, and as much criticism as some particular technical implementations receive, there is a clear consensus on the factual existence of strong underlying scaling laws in urban systems. Part of the errors pointed out by (Louf and Barthelemy, 2014) could be explained by the lack of subtlety of the monofractal model in the sense that it forces to fit a single scaling exponent over an entire dataset. Because of the considerable

randomness in social processes, it appears more suitable to use the more sophisticated multifractal model that allows fitting multiple exponents. In addition, contrary to the monofractal dimension that only provides one global a-spatial parameter, the multifractal approach retains the spatial nature of the variable (in addition to still providing a range of global parameters). In fact, we have pointed out in the previous section that this characteristic was identified by Reardon et al. (2006) as being especially desirable and usually insufficiently conveyed by classical segregation measures.

2.2. Multifractality in urban environments: a new paradigm. Roughly speaking, when a space possesses a characteristic that is not a power law, but instead a collection of local power laws with different scaling exponents, then this characteristic is called a multifractal. To be more precise, it is required that said characteristic can be transformed into a proper mathematical measure, i.e. a function that associates each sub-space with a non-negative number so that the measure of a countable union of sub-spaces is the sum of the measure for each sub-space[4]. It has already been proved that many urban measures are indeed multifractal. The work by Hu et al. (2012, 2013) is particularly relevant, since it deals with land prices, a proxy of wealth. Two different multifractal methods are tested over the land price distribution of the Chinese city of Wuhan. The first article introduces the idea of predictive value with a temporal analysis, although the narrow range of dates considered (only three close years: 2001, 2004 and 2007) limits the strength of its findings. The second one is aimed at urban planning with insights on measuring how much of the price distribution can be explained by the geographical background. Those two papers are positive arguments to hypothesize the multifractality of land prices in cities.

Two articles, one by Ariza-Villaverde et al. (2013) and one by Murcio et al. (2015), report multifractality for street network intersection densities in Cordoba and London respectively. The first one concludes by stating the insufficiency of monofractals to describe street networks, that should be described instead using multifractals. The second one is complemented by a modelisation of the loss of multifractality induced by constrained boundaries on the development of street networks represented by a DLA model. They invite to build measures on street networks, and more widely on other transportation networks, to study the possible multifractality of accessibility.

An interesting discovery in these two articles is an apparent loss of multifractality, or more precisely a convergence towards monofractality, through

[4]In practice, this transformation is often left implicit. For example, "counting the number of intersections in a network" is an implicit way of defining the measure μ so that $\mu(\{x\}) = 1$ if x is an intersection.

time. Indeed, in the article by Murcio et al. (2015), it is a clear consequence of the shrinkage of the multifractal spectra representing street intersections densities in London at 9 time intervals between 1786 and 2010. In the case of Ariza-Villaverde et al. (2013), it is not reported as a result, but implied by the relative width of the spectra corresponding to the historic Roman-Arab-Christian developed parts of Cordoba compared to the parts redeveloped in the 1950s. This temporal loss of multifractality can be related to the work by Nie et al. (2015), which reports similar results for a measure corresponding to the fraction of urban impervious surface in each pixel of landsat images of Shanghai between 1997 and 2010. In fact, full multifractality was found only in 1997, while mulitfractality was only found along the W-E axis in 2002, and no multifractality was found in 2010. This trend of urban measures converging to a monofractal through time structure will be largely confirmed by the results of this thesis.

As stated previously, self-organization under competition for space results in strong scaling characteristics. It is therefore not surprising to also find multifractality in city form and population growth processes (Chen, 2008; Chen and Wang, 2013), the dynamics of city-size and settlement distributions (Haag, 1994; Chen and Zhou, 2004; Chen, 2014), and other more loosely related topics such as agricultural land use (Wang et al., 2010). All these papers, although not directly related to potential inequality parameters, prove the frequent multifractal nature of measures arising from urban development.

Aside from a noteworthy attempt at making multifractal analysis practical by Chen (2016), whose purpose was to find a method to distinguish between urban and rural areas, the common shortcomings of all those articles, however, are the emphasis on description over practical interpretation. In contrast, the very recent work by Yamu and Frankhauser (2015); Yamu and van Nes (2017), and Frankhauser et al. (2018) attempts at reducing urban sprawl through multifractal urban simulation with a home-made software called *Fractalopolis*. The software is meant to construct new optimized urban development by iterating a multifractal pattern taking into account a number of accessibility, environmental and social rules. The goal is to find the most efficient way to limit sprawl while maintaining the life quality of the citizens. The second article in particular is framed within the objectives of the UN 2015 Paris agreements.

This thesis aims at operating a similar shift from description towards optimizing urban development, while adding a necessary interpretative intermediary step. Although mainly focused on relating multifractality and inequality, the interpretation framework can contribute to a better general

understanding of the multifractal spectrum. It should be, at least partly, transferable to other topics arising in the field of urban multifractals. An opening towards a more planning oriented approach is proposed in appendix A where an agent-based model to test the impact of urban development scenarios on inequality is proposed. This work should encourage the inclusion of inequality rules to the accessibility, environmental and social rules taken into account for example by Yamu and Frankhauser (2015) in their approach.

2.3. Interesting ideas from the broader multifractal field. Outside of the urban context, some applications of multifractality have already flourished. In particular, some studies on the analysis of retinal vessels (Mainster, 1990; Stosic and Stosic, 2006; Talu, 2013), are an interesting source of inspiration, since the network structure of blood vessels is reminiscent of the network structure of some street patterns. It shares in particular the planar property and tree-like aspect. However, we find the method used in these papers, which consists in analysing the network as a black and white "photography", limited in comparison to the rich literature that has been developed on applying multifractal analysis directly to the network topological structure (e.g. Wang et al., 2012; Liu et al., 2015; Song et al., 2015; Rendon de la Torre et al., 2017).

Another fruitful application domain is offered by financial markets. Fractal structures have been studied in finance and real estate since the 1990s (e.g. Mandelbrot, 1997; Kaizoji, 2003; Ohnishi et al., 2012), while multifractal structures have been more and more evidenced since the early 2000s (notably by Mandelbrot, 1999; Muzy et al., 2000; Bacry et al., 2001; Di Matteo et al., 2003; Di Matteo, 2007; Barunik et al., 2012; Morales et al., 2012, 2013; Buonocore et al., 2016, 2017; Jiang et al., 2018). The techniques used are specifically designed for time-series, which are difficult to obtain with a sufficiently wide range when associated with their geographical data for urban land and house prices. However, since the spatial distribution of real estate is, in a sense, a projection of its immaterial market, these results are a strong encouragement to investigate if we can find multifractal properties in real estate spatial patterns.

Finally, an article by Ihlen and Vereijken (2013) identifies multifractal structures in human behaviour. The focus is on performance to motor control tests, with hypothesised applications to a more general understanding of underlying cognitive processes in human behaviour. The direction followed by these findings is still in a preliminary state, but already show the potentially intrinsic nature of multifractality in complex systems relying on the behaviour of humans. Multifractal analysis is a relatively new field with promising and fast developing applications. We intend to add the study of

spatial inequality as one of these new and meaningful applications. To this aim, we now review the theoretical and methodological multifractal knowledge currently available.

2.4. Multifractal theoretical foundations and its methodologies. From an historical perspective, the idea of extending fractals to measures was first hinted by Mandelbrot (1982). The actual theorization and naming of the multifractal notion started from the mid eighties for the specific purpose of studying turbulence signals (Frisch and Parisi, 1983; Benzi et al., 1984; Chhabra et al., 1989; Meneveau and Sreenivasan, 1989). In the nineties, Mandelbrot et al. (1990); Evertsz and Mandelbrot (1992); Brown et al. (1992); Olsen (1995); Riedi (1995) and Pesin (1997) developed strong mathematical multifractal theories, restoring in a sense the original geometrical intent of the notion. At this day, Falconer (2003) can be considered the seminal book detailing the mathematical notion of fractality, with one chapter in particular devoted to multifractals.

The *Nature* article by Stanley and Meakin (1988) popularized multifractality and helped giving incentive to develop applications outside of the turbulence field. From that point on, the multifractal methodology has crystallised around five main groups of methods that optimise the computations depending on the type of data studied (griddable data such as images, time-series and networks).

The moment method and its variants were the first ones to be introduced, and are studied in almost all of the historical papers cited above. The moment method can still be considered the reference method in the field because of the simplicity of its implementation, adaptability to many different types of data, as well as the existence of many variants to enhance its accuracy and computational efficiency (Atmanspacher et al., 1989; Chhabra et al., 1989; Chhabra and Sreenivasan, 1991; Cheng, 1999*a*,*b*; Salat et al., 2017). Its main use is for griddable data, historically images. As such, it can be easily adapted to Geographical Information Systems (GIS) by concentrating the measure on the centroids of any relevant geographical sub-division, and gridding the resulting cloud of points. The general mathematical formalisation of the method is canonically detailed by Falconer (2003).

The histogram method (Arneodo et al., 1987; Meneveau and Sreenivasan, 1989; Evertsz and Mandelbrot, 1992) is another method geared towards gridded data. Compared to the moment method, it improves significatively the run time, particularly for spaces of a dimension greater than 2, and is less reliant on error generating techniques. However, it only works for data offering a wide variety of scaling ranges, and is constructionally inaccurate.

Because of these drawbacks, it is only rarely used in this thesis, and only as an alternative method to confirm the results from other methods.

Multifractal detrended fluctuation analysis (MDFA) (Kantelhardt et al., 2002; Gu and Zhou, 2006; Kantelhardt, 2012) is a generalization of detrended fluctuation analysis (DFA), which was originally created to detect long-range monofractal correlations in DNA nucleotide sequences (Peng et al., 1994; Ossadnik et al., 1994). It is used to remove artifacts created by nonstationarities in one-dimensional time series and otherwise uses the core idea of the moment method as its mechanics. This "detrending" effect is particularly useful to remove undesirable traits such as inflation in land prices, and could be advantageous for studying inequality should long and detailed spatial time-series become available. The simplicity of its implementation allows to extend the method to higher dimensions to recover the spatial interpretation we are seeking, at the cost of a sharp decrease in performance.

In order to study intrinsically continuous phenomena (originally time-series), some wavelets based methods have been created. A first method called Wavelet transform modulus maxima (WTMM) was developed successively by Holschneider (1988); Muzy et al. (1991); Bacry et al. (1993) and Arneodo et al. (2002). A second method called Wavelet leaders was developed later by Lashermes et al. (2005); Jaffard et al. (2007) and Wendt et al. (2009). Although there is some dispute between these two groups of scientists about the respective merits of each method, they both accomplish the same result which is replacing the square boxes of gridded data by wavelets that "glide" smoothly along the data. These methods are better suited for a generalization to higher dimensions than MDFA, are highly customizable, and are able to extend, in a sense, the multifractal formalism to nonconservative and continuous phenomena. Their main drawback is the bursting complexity of their implementation due to the continuous framework that contrasts with the discretized framework of the previous methods.

Since data relating to real estate, income, energy and land use is planar, we naturally focus on the moment-based group of methods for our analyses. The histogram and MDFA methods are used as controls to ensure that the results are not artefacts created by our particular methodology. In contrast, the wavelets-based methods are not well adapted for our datasets and will not be used. We now critically justify these choices in the next two chapters.

CHAPTER II

Formal Multifractal Theory and its Methods

We first introduce monofractality and present a formal definition of multifractality. We then give all the necessary details to put in practice the main historical methodologies. We justify from their respective advantages and disadvantages which methods we choose to apply and to what extent. This chapter should allow anyone to implement the different methods, however familiarity with topology and measure theory may be necessary to fully understand the complexity of the notions. Chapter III will reintroduce multifractality using a more intuitive approach and should be sufficient to understand the application of the methodology to studying inequality. This chapter is largely adapted from Salat et al. (2017).

1. Monofractals: Characterizing space

The notion of *monofratality*, that we will simply call *fractality*, is closely related to the notions of *dimension* and *topological continuity*. The dimension of a vector space can be defined as the minimal number of vectors necessary to identify all the points in the space from an origin. We can then easily extend this notion to homeomorphic deformations of vector spaces a.k.a. manifolds. It is tempting to extend further the notion to sets that can intuitively be decomposed or rearranged into manifolds. Consider the following example. A finite segment is of dimension 1 (figure II.1(a)). A countable number of disjoint segments is also of dimension 1 since they can be concatenated into one bigger segment or one line (figure II.1(b)). Now, consider two lines. It is possible to divide each line into segments of size one, then place these segments next to each other alternatively to create one new line (figure II.1(c)). For an infinite countable number of lines, the same idea can be applied, although it requires more work. Indeed, we can use the known existence of an infinite number of prime numbers to associate each line with a prime number, then divide it into segments of size 1, and finally attach each segment on a new line at a place corresponding to a power of that prime number (figure II.1(d)). Then, all segments of all lines are identified on the new line, and form one continuous line after "cutting" the holes between two consecutive powers of prime numbers.

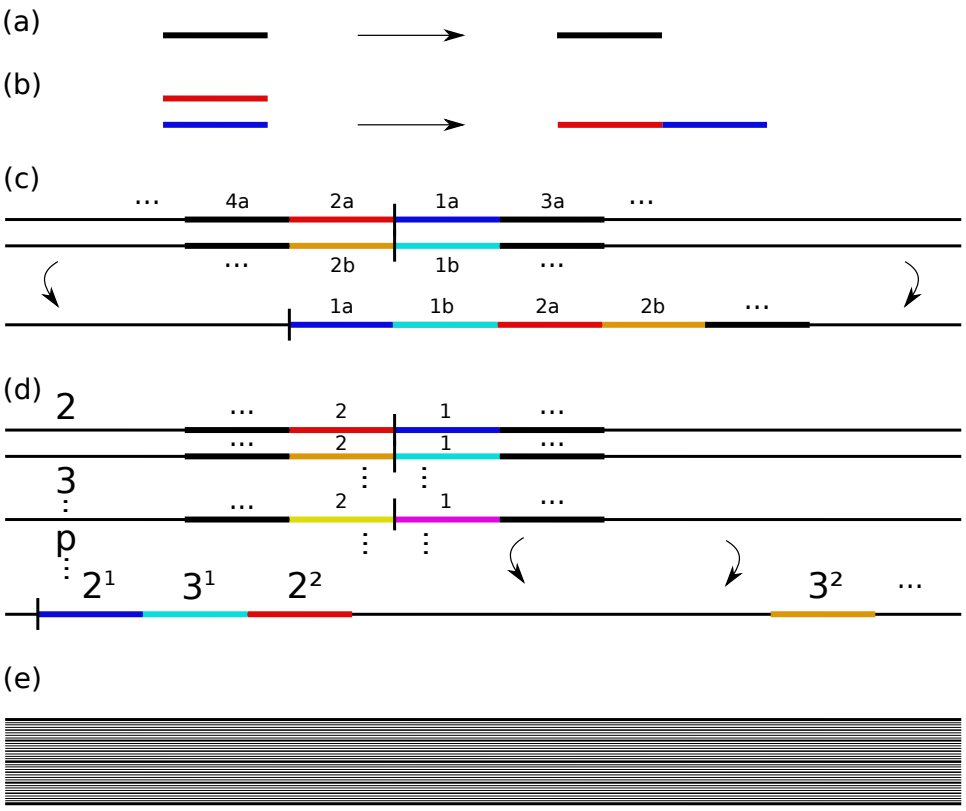

FIGURE II.1. **One-dimensional spaces.** (a) A segment is of dimension 1. (b) Two segments can be transformed into one. (c) Two infinite lines can be transformed into one. (d) A countable number of lines can still be transformed into one. (e) A non-countable infinite number of lines corresponding to the dichotomic division of [0,1] (including the boundaries).

Consider now a non-countable number of lines. For example a line associated to each real number contained in $[0, 1]$. It is no longer possible to transform this set into one line, but since $[0, 1]$ is "continuous", we can use two vectors instead to identify all the points in the set. The dimension has therefore jumped to two. However, there are sets that lie somewhere in-between the two previous examples. Consider for example the subset of the previous set made only of the lines associated to a point corresponding to the dichotomic dividing of $[0, 1]$ (figure II.1(e)). This set is quite complex: it is transversally totally disconnected, which prevents us from defining a proper second vector, but shares a density property with the full set: every transversal segment of type $[\frac{n}{2^k}, \frac{n+1}{2^k}]$ contains at least one point of both sets, no matter how large k is. To characterise the dimension of these sets, Mandelbrot (1982) introduced the concept of *fractality*, coined from the latin

word "fractus", which means "broken", as in "too irregular to fit into classical geometry".

The usual dimension associated to fractals is the *Hausdorff dimension*. It uses a one-dimensional "benchmark" elevated to a power s to evaluate the "volume" of a set D. More precisely, consider a covering of the set D at an infinitesimal scale, and a function that sums the diameters raised to a power s of all its elements. As long as s is lower than the dimension of the space D, this function will return $+\infty$, and as soon as s becomes greater than the dimension of the space D, the function will return 0. The Hausdorff dimension is then defined as the s value for which the function transitions from $+\infty$ to 0. To understand intuitively this mechanic, consider a square. Lines (power $s = 1$) are of negligible size compared to it, so an infinite number of them is needed to cover the square. In contrast, the square is negligible compared to a cube (power $s = 3$), so, only an infinitesimally small portion of the cube is needed to cover it, or approximately 0 cube. Finally, if we use balls (power $s = 2$) to cover the square, then a finite and positive number of balls is enough to cover the square. We deduce that the dimension of the square is 2. Formally, if A is a metric space, $s \in \mathbb{R}^+$, and $D \subset A$, we define

$$\mathcal{H}_r^s(D) := \inf \left\{ \sum_{i \in I} \left(\frac{\operatorname{diam}(A_i)}{2} \right)^s,\ \{A_i\}_{i \in I} \subset A, \right. \\ \left. \text{with } D \subset \cup_{i \in I} A_i, \text{ and } \sup_{i \in I} \operatorname{diam}(A_i) \leq r \right\}, \tag{7}$$

and

$$\mathcal{H}^s(D) = \sup_{r>0} \left(\mathcal{H}_r^s(D) \right). \tag{8}$$

Then, the Hausdorff dimension is defined as

$$\begin{aligned} \dim_{\mathcal{H}} D &:= \inf \{ s \geq 0,\ \mathcal{H}^s(D) = 0 \} \\ &= \sup \{ s \geq 0,\ \mathcal{H}^s(D) = +\infty \}. \end{aligned} \tag{9}$$

The Hausdorff dimension is particularly convenient from a mathematical point of view, as it is defined for any set D. In practice, however, it is difficult to compute, and is usually replaced by the box-counting dimension. Formally, let $N_\delta(D)$ be the smallest number of balls of diameter at most δ necessary to cover D. Then, the box-counting dimension is defined as

$$\dim_B D := \lim_{\delta \to 0} -\frac{log(N_\delta(D))}{log(\delta)}. \tag{10}$$

Note that the limit may not exist, in which case we may consider the lower or upper limit instead.

For most rigorously self-similar subsets encountered, the Hausdorff and box-counting dimensions are in fact the same thing. Finding how much of the set A is "filled" by the fractal subset D is the same as finding by how much one needs to grow a sub-element of the figure to find the whole figure again. This is done through the relation

$$\dim_{\mathcal{H}} = -\frac{\log(\text{number of copies})}{\log(\text{scaling factor})}. \tag{11}$$

Because of this, self-similarity is often treated as a synonym of fractality in the literature. By extension, the word "fractal" is also used for phenomena described by *homogeneous* functions, i.e. functions $f : D \subset \mathbb{R}^n \to \mathbb{R}$ for which there exists an α such that

$$\forall \lambda \in \mathbb{R}, x \in D,\ f(\lambda x) = \lambda^{\alpha} f(x). \tag{12}$$

An emblematic example of an homogeneous function is the famous power-law (Ihlen and Vereijken, 2013), which is, in a sense, a representation of scale-invariance within the space D.

On the other hand, any dense subset made of a countable number of points is of dimension 0 for the Hausdorff dimension and of dimension equal to its closure for the box-counting dimension. For example $\mathbb{Q} \cap [0, 1]$ in $\mathbb{R}$ is of dimension 0 for the Hausdorff dimension and of dimension 1 for the box-counting dimension. Those definitions are therefore far from equivalent in all generality. A more detailed discussion on what elements are desirable to define a suitable fractal dimension can be found in chapter 3 from Falconer (2003).

An example of a fractal set is given in figure II.2. The middle third Cantor set is created from an initial segment of length 1, from which two sub-segments of length one third are extracted. This process is then repeated for each new segment, and so on. Since the resulting set is self-similar with two new copies of itself each scaled at a ratio of 1/3, one would get from equation (11) a Hausdorff dimension of $\log(2)/\log(3)$. Calculating directly the Hausdorff dimension without using equation (11) is more involving than one would expect even for such a simple set, hence the motivation to restrict the notion of fractals to self-similar sets. The value $\log(2)/\log(3)$ represents how much of the initial segment is still present in the Cantor set after an infinite number of iterations of the generating process.

To illustrate the universality of fractality, we can name other, more rarely seen, definitions of fractal dimension: the correlation dimension for sets of random points (Grassberger and Procaccia, 2004) and the packing dimension, a dual to the Hausdorff dimension (Tricot, 1982). Also, Barnsley (1988) proposes a more abstract approach. Denote (X, d) a complete metric space.

FIGURE II.2. **Fractal middle third Cantor set.** From an initial segment of length 1, two sub-segments of length one third are created, and so on for each new segment, generating a self-similar fractal of dimension $\log(2)/\log(3)$.

He defines $\mathcal{H}(X)$ as the set of all non-empty compact subsets of X, and considers the Hausdorff between elements of $\mathcal{H}(X)$. Recall that the Hausdorff distance is defined as

$$d_H(A,B) = \max\left\{\sup_{a\in A}\inf_{b\in B} d(x,y), \sup_{b\in B}\inf_{a\in A} d(x,y)\right\}. \tag{13}$$

From the observation that $(\mathcal{H}(X), d_H)$ is a complete metric space, Barnsley defines fractals as any subset of $(\mathcal{H}(X), d_H)$. This is indeed quite a general definition!

2. Multifractals: A theory of measures

While monofractals are mostly concerned with spaces, multifractals deal with measures. Recall that a measure μ defined on a space A is a function from the parts of A to $\mathbb{R}^+$, such that $\mu(\emptyset) = 0$, and such that if $\{B_i\}$ is a countable collection of pairwise disjoint sets in A, then $\mu(\cup B_i) = \sum \mu(E_i)$. A measure "assigns" a size to every subset of A. In practice, the data can be directly a mathematical measure (e.g. a probability measure), or any value distribution that can be transformed into a measure (e.g. a weighted set, a fractal landscape, a time-series, for example, or even a function using the WTMM method, see below). Even if the idea behind multifractals is also to study the complexity and to reveal the scaling properties of a mathematical object, it is somewhat distinct from monofractality. In particular, a measure can be a multifractal even when its support is not a monofractal (Stanley and Meakin, 1988). Let us consider a subset $D \subset \mathbb{R}^n$ on which are defined:

- a "fractal" measurement method $\mathcal{M}$;
- a finite measure μ which we want to study.

Here, $\mathcal{M}$ can be any method providing a way to compute a monofractal dimension, such as those quoted in the previous section, as deemed appropriate for the nature of the space D.

A *multifractal measure* μ on D is characterized by a distribution such that around any $x \in D$, the measure in a ball of radius r around x scales with r, i.e. is proportional to r^α for some α, provided r is small enough, and such that the sets formed by all points around which the scaling exponent is the same are monofractals for $\mathcal{M}$. The fractal dimension of the set corresponding to the local exponent α is denoted $f(\alpha)$.

Usually, the method $\mathcal{M}$ is based on defining a self-similar local measurement $\mathcal{M}_r$, such as the number of boxes of radius r necessary to cover the set for the box-counting dimension or the quantity $\mathcal{H}^s_r$ from equation (7) in the definition of the Hausdorff measure above. In that case, the multifractality of μ is equivalently characterized by a distribution such that the two following fundamental scaling relations hold for r small enough:

1. $\mu_r(x) \sim r^{\alpha_x}$ for an α_x around any $x \in D$, where $\mu_r(x)$ is the measure in a ball of radius r around x;
2. $\mathcal{M}_r(\alpha) \sim r^{-f(\alpha)}$ for an $f(\alpha)$, where $\mathcal{M}_r(\alpha)$ is the $\mathcal{M}_r$-measure of the set $\{x, \alpha_x = \alpha\}$.

The *multifractal spectrum* is the curve $f(\alpha)$ against α. It gives, roughly speaking, the "fractal dimension" $f(\alpha)$ of sets where the measure scales locally with the same exponent α. *Multifractal analysis* should be understood as a method to characterize and compare measures defined on D when they present enough scaling properties to alleviate the intrinsic complexity of (D, μ).

An example is given in figure II.3. The middle third Cantor set is made multifractal by weighting every right sub-interval twice as much as every left sub-interval, the total weight being normalized to 1 at each step. The first three steps of this process are illustrated in the top figure. Denote by r_k the size of the new sub-intervals at step k, and fix $r_0 = 1$. Then, at step $k = 3$, height sub-intervals are obtained, each of size $r_3 = (1/3)^3$ and carrying a weight that can be expressed as r_3^α for some α. At this macroscopic state, a broad $\mathcal{M}$ can be defined such that $\mathcal{M}_{r_k}(\alpha)$ denotes the number of sub-intervals scaling with r_k for an exponent α. This number can be in turn expressed as $r_k^{-f(\alpha)}$. For the particular α chosen in figure II.3, that is $\alpha = 1 - \frac{\log(2)}{3\log(3)}$, there are $3 = (1/3^3)^{-1/3}$ sub-intervals carrying this measure, hence $f(\alpha) = 1/3$. By repeating this calculation for each of the four different weights carried by the sub-intervals at step $k = 3$, the spectrum corresponding to the bottom line of the bottom figure is obtained.

Of course, at such a low level of iteration, $\mathcal{M}$ does not make much sense. But as k grows to infinity, the spectrum resulting from this $\mathcal{M}$ converges to the actual spectrum one would obtain for the Hausdorff measure and the proper totally disconnected weighted middle third Cantor set. The first

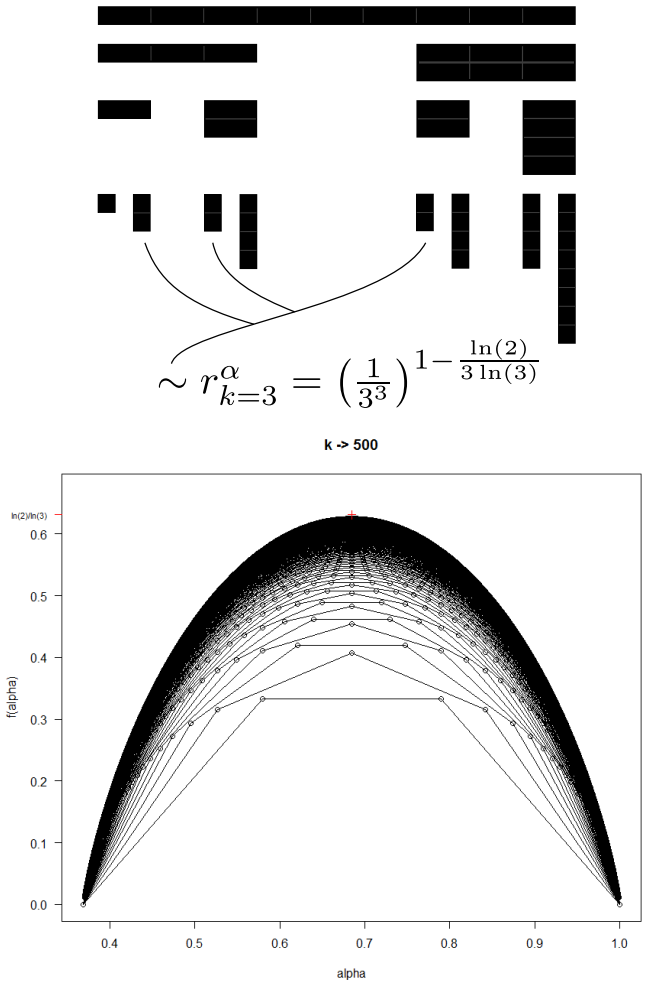

FIGURE II.3. **Multifractal middle third Cantor set.** On the top, the first three iterations of the generation of the weighted multifractal Cantor set are represented, while on the bottom the first 500 spectra corresponding to each successive iteration for $\mathcal{M}$ are plotted.

500 iterations are illustrated in figure II.3. It can be noted that the multifractality comes from the measure created by the weights, not from the physical support itself which is only the monofractal Cantor set presented in the previous section. In particular, the dimension of the support, here $\log(2)/\log(3)$, can be found at the peak of the spectrum.

Falconer (2003) derives two formal definitions of multifractal spectrum: the *singularity spectrum*, which can be considered the most canonical and universal definition, and the *coarse spectrum*, which is more adequate in practice.

Consider a topological space D and a finite measure μ on D. The local scaling exponent α_x of μ at $x \in D$ is given by the Hölder dimension $\dim_{loc}$,

defined by

$$\dim_{loc}\mu(x) := \lim_{r\to 0}\frac{\log\mu\left(B(x,r)\right)}{\log r}, \tag{14}$$

where $B(x,r)$ is the ball of center x and radius r for the topology of D. The *singularity spectrum* is then defined by the function

$$f_{\mathcal{H}}(\alpha) := \dim_{\mathcal{H}}\left\{x\in D,\ \dim_{loc}\mu(x)=\alpha\right\}. \tag{15}$$

Note that the Hausdorff dimension is chosen for $\mathcal{M}$ instead of the box-counting dimension since $\{x\in D,\ \dim_{loc}\mu(x)=\alpha\}$ is often dense in the support of μ, in which case the box-counting would result in a constant spectrum equal to the dimension of the support of μ.

Let us now consider an r-mesh grid covering D and count the number of cells for which μ is roughly r^{α}. Define,

$$N_r(\alpha) := \#\left\{r\text{-mesh cubes } C,\ \mu(C)\geq r^{\alpha}\right\}, \tag{16}$$

where # stands for "number of". Provided the limits do exist, the *coarse spectrum* is defined by the function

$$f_C(\alpha) := \lim_{\varepsilon\to 0}\lim_{r\to 0}\frac{\log^{+}\left(N_r(\alpha+\varepsilon)-N_r(\alpha-\varepsilon)\right)}{-\log r}, \tag{17}$$

where $\log^{+}(\cdot)$ stands for $\max(\log(\cdot),0)$.

When f_C does exist, then for all α,

$$f_{\mathcal{H}}(\alpha)\leq f_C(\alpha), \tag{18}$$

and the equality holds true for self-similar measures (Proposition 17.9 from Falconer (2003)). When f_C does not exist, one can define the *lower* and *upper* spectra by

$$\underline{f}_C(\alpha) := \lim_{\varepsilon\to 0}\liminf_{r\to 0}\frac{\log^{+}\left(N_r(\alpha+\varepsilon)-N_r(\alpha-\varepsilon)\right)}{-\log r}, \tag{19}$$

and

$$\bar{f}_C(\alpha) := \lim_{\varepsilon\to 0}\limsup_{r\to 0}\frac{\log^{+}\left(N_r(\alpha+\varepsilon)-N_r(\alpha-\varepsilon)\right)}{-\log r}. \tag{20}$$

In that case, according to lemma 17.3 of Falconer (2003),

$$f_{\mathcal{H}}(\alpha)\leq\underline{f}_C(\alpha)\leq\bar{f}_C(\alpha). \tag{21}$$

An example is given in figure II.4 for a binomial cascade of parameter $p=0.6$. The binomial cascade is a simpler version of the multifractal middle-third Cantor set introduced above. Here, an original interval of size 1 is divided into two sub-intervals of length 1/2 carrying a probability 0.6 for the left one and 0.4 for the right one. This process is then iterated on each

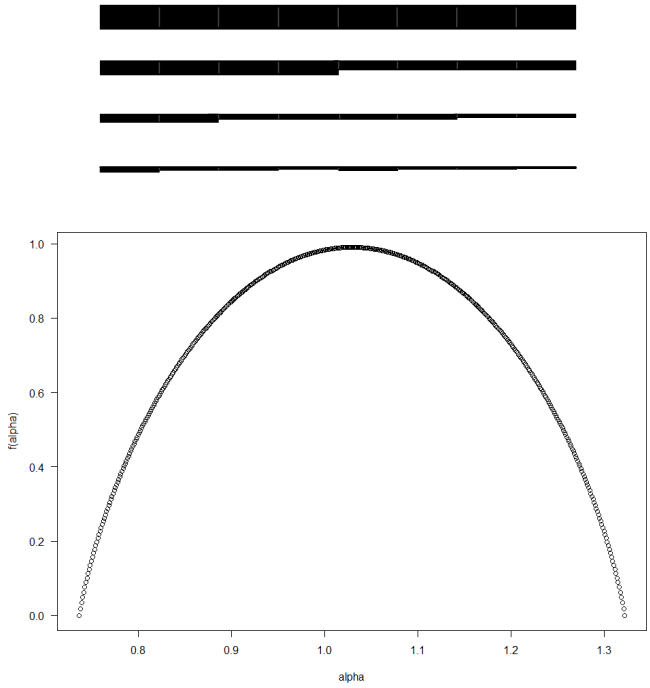

FIGURE II.4. **Multifractal binomial cascade.** On the top, an original interval of size 1 is divided into two sub-intervals of length 1/2 carrying a probability 0.6 for the left one and 0.4 for the right one. On the bottom, the corresponding multifractal spectrum.

resulting sub-intervals, and so on. The resulting singularity spectrum $f_{\mathcal{H}}$ in the bottom figure is computed using the same trick as for the Cantor set and is identical to the coarse spectrum $f_C = \underline{f}_C(\alpha) = \bar{f}_C(\alpha)$, since the measure is self-similar. Here, the fractal dimension of the support is 1 since the iterative process does not create "holes" in the initial segment.

3. Practical methods to compute the spectrum

3.1. Moment-based methods. Moment-based methods are particularly effective for spatial data and image analysis. They rely on counting the measure at different levels of aggregation and include a multitude of variants depending on the aggregation method chosen. They are meant to give correct results for "static" singular measures, and may not be adapted to continuous data and to nonconservative phenomena such as turbulent velocity profiles (see Kestener and Arneodo, 2003)). For those, wavelet based techniques are better suited.

The most basic aggregation technique, box-counting, consists in applying square grids of increasing resolutions to the data. If it suits the data better, grids can be based on another unit shape, such as a diamond or a triangle.

It may also be advantageous to consider ball neighbourhoods for calculation simplicity when using GIS software. We describe here the technique assuming that the grid is a mesh of unit r. Let us call D the domain it covers. We want to describe a phenomenon that occurs N times in D. Denote

$$p_i := N_i/N = \int_{i^{th}box} d\mu(x) \tag{22}$$

the probability that an instance of the phenomenon occurs in the i^{th} box, where μ is the corresponding probability measure. To interpret the two scaling rules from the previous section, one simply needs

1. $p_i \sim r^{\alpha_i}$;
2. $N(\alpha_i) \sim \rho(\alpha_i) d\alpha_i r^{-f(\alpha_i)}$,

where $N(\alpha_i)$ is the number of times α falls in each interval $[\alpha_i, \alpha_i + d\alpha_i]$, and ρ is a density function used to take into account the dimension of D.

To effectively compute f, we generally use a trick called *moment method* (Frisch and Parisi, 1983; Halsey et al., 1987; Atmanspacher et al., 1989). By raising p_i to its moment p_i^q for different q, one can force only one value of alpha for each q to make a significant contribution to the total value of the measure. Consider

$$\begin{aligned} Z(q) := \sum_i p_i^q &\sim \sum_i r^{\alpha_i q} \\ &\sim \int_\alpha N(\alpha) r^{\alpha q} \\ &\sim \int \rho(\alpha) r^{\alpha q - f(\alpha)} d\alpha, \end{aligned} \tag{23}$$

then, for r small enough, the value of $Z(q)$ is almost entirely given by the α such that

$$\tau(q) := \alpha q - f(\alpha) \tag{24}$$

is minimal. Let us call $\alpha(q)$ this value of α. It is easy to show by a Legendre transform that the minimality condition yields

$$\alpha(q) = \frac{d\tau(q)}{dq}; \tag{25}$$

and

$$f(\alpha(q)) = \alpha(q)q - \tau(q), \tag{26}$$

so that computing $\tau(q)$ from $Z(q)$ for each q between $-\infty$ and $+\infty$ is enough to obtain the full spectrum.

It is not possible in practice to use an infinite range of values for q, nor is it desirable since the method becomes less and less accurate for extreme values of q. To respect the constraints imposed by tangibility, it is necessary

to select only the values of q such that $f(\alpha) > 0$ and such that the *generalized dimension* D_q, defined by $D_q := \tau(q)/(q-1)$, remains lower than the euclidean dimension of the physical space that supports the phenomenon.

In practice, $\tau(q)$ is found directly as the slope in a log-log plot of $\sum_i \mu_i^q(r)$ versus r obtained for different grid sizes r, where $\mu_i(r)$ is the total measure of cell i of size r. Since this slope is independent of the normalization of the measure μ, μ does not need to be weighted as a probability measure. Explicitly, $\tau(q)$ can be found directly as the limit

$$\tau(q) = \lim_{r \to 0} \frac{\log(\sum_i \mu_i^q(r))}{\log(r)}. \tag{27}$$

Compared to the mathematical definitions of the multifractal spectrum (equations (15) and (20)), we have

$$f_{\mathcal{H}}(\alpha) \leq \underline{f}_C(\alpha) \leq \bar{f}_C(\alpha) \leq f_M(\alpha), \tag{28}$$

where f_M is the spectrum resulting from the moment method (corollary from Proposition 17.2 from Falconer (2003)).

Both finding $\tau(q)$ through linear fitting and applying numerical Legendre transforms have a cost on the accuracy of the results. The possibility of averaging over several samples can be extremely beneficial. There are two ways of doing this: averaging over a range of $\{f_j(\alpha_i)\}_j$ computed independently for different samples j, or averaging first over a range of $\{N_j(\alpha_i)\}_j$ and then deducing the corresponding $f(\alpha_i)$ from the relation $N(\alpha) \sim r^{-f(\alpha)}\rho(\alpha)d\alpha$ on the averaged values. The first solution guarantees to obtain a "classic" positive spectrum, but it can be unreliable if the fluctuations between the $f_j(\alpha_i)$ are too important. The second solution is more reliable, but may create an artificial negative part in the spectrum if $N(\alpha_i)$ falls below 1 for some α_i as a result of the averaging process.

Chhabra and Sreenivasan (1991) argue that this artificial negative part can still be of relevance when a strong underlying probabilistic process is suspected either as a cause of the phenomenon or as a result of the experimental methodology since it could describe the rarely occurring events. Unfortunately, since $\alpha \mapsto N(\alpha)$ decreases exponentially compared to $\alpha \mapsto f(\alpha)$ in the negative part, one would need an exponentially increasing number of samples as the resolution gets smaller to maintain accuracy while supersampling. Paradoxically, for a constant number of samples, a better resolution would mean a less accurate result.

To tackle this problem, Chhabra and Sreenivasan propose a multiplier method. The self-similarity of the measure implies the existence of an underlying scale-invariant multiplier distribution such that the α_i at resolution r_k are only the result of k composition of said multipliers. If there is no

correlation in the underlying probabilistic process from resolution r_{k-1} to resolution r_k for some k, then one can deduce the multipliers and hence α. In particular, if all levels of resolution are uncorrelated, one can choose $k = 1$, otherwise, one should choose the smallest k for which a level of resolution is uncorrelated to the previous one.

Denote r_0 the minimal resolution and r_k the resolution chosen as described above. Then, define

$$r := r_k/r_0, \tag{29}$$

and for each sample j and box i,

$$M_{ij} := \mu_{ij}(r_0)/\mu_{ij}(r_k). \tag{30}$$

Then, $\tau(q)$ and $\alpha(q)$ are given by

$$\frac{1}{N(r)}\tau(q) + d \approx -\frac{\log\left(1/N(r)\sum_{i,j} M_{ij}^q\right)}{\log(r)}; \tag{31}$$

$$\frac{1}{N(r)}\alpha(q) \approx -\frac{\sum_{i,j} M_{ij}^q \log(M_{ij})}{\sum_{i,j} M_{ij}^q \log(r)}. \tag{32}$$

where $N(r)$ is the number of non zero values of M_{ij} and d is the dimension of the physical support D. Because only two box sizes are considered by this method, the multiscale nature of multifractal analysis is not taken into account and must be ascertained *a priori*. In practice, we have tested several r_k and only kept the measures for which the resulting spectra were identical, proving scale invariance.

As will be shown in section 4 below, when applied to real data, the moment method has a tendency to fail for α values greater than the dimension of the space occupied by the measure (that is for negative q). This may be caused by the presence of flat noises (see Salat et al., 2018). In addition, Huang et al. (2010, 2011) have shown that underlying large-scale structures in the data may cause the method to fail. The multiplier method "bypasses" these noises and large scale biases by inducing a true power-law from the local behaviour of the measure around the point. In a way, this process can be thought of as fitting the best multifractal model to the data.

Another way to expand the set of sample points consists in using one grid and aggregate with a gliding box for different radii of said gliding box instead of using different grid sizes (Cheng, 1999*a*; Cheng and Agterberg, 1996). In that case, $\tau(q)$ is given by taking the limit for $r \to 0$ in

$$\frac{1}{N(r)}\tau(q) + d \approx \frac{\log\left(1/N(r)\sum_{i=1}^{N(r)} \mu_i^q(r)\right)}{\log(r)}, \tag{33}$$

where $N(r)$ is the number of gliding boxes of size r with non zero measure, $\mu_i^q(r)$ is the measure inside the i^{th} gliding box, and d is the dimension of the physical support D.

Since it is not required that gliding boxes are mutually exclusive, contrary to squares from a mesh grid, the number of values contributing to the analysis remains that of the smallest resolution at all scales. The trade-off is that only boxes which are completely bounded in D should be included, so that only the "inner portion" of the data can be analyzed, or the object of study needs to be surrounded by a large neighborhood of known values (see figure II.5). Using gliding boxes allows a higher raw number of sample points at the cost of restricting the range of study. It is of course possible to join gliding boxes and the multiplier method by adapting the definition of μ_{ij} and $N(r)$ in equations (30) and (31).

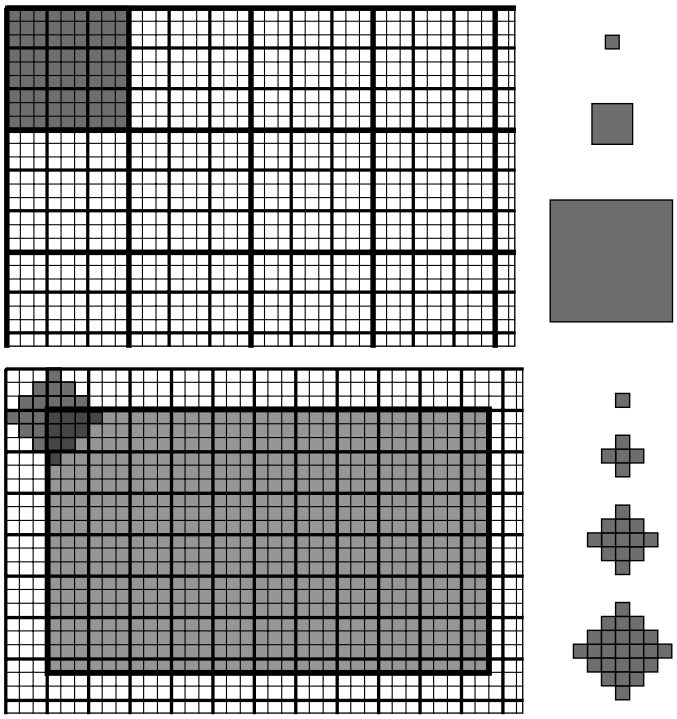

FIGURE II.5. **Comparison between grid and gliding box upscalings.** In the top image, the third level of aggregation, which is only 3^2 times the smallest resolution, only allows to fully place 8 boxes on the figure. In contrast, gliding boxes applied on the lowest image maintain 608 sample points at the cost of forcing to remove a wide border from the analysis.

A final variant is proposed by Chhabra et al. (1989) to avoid the Legendre transform of $\tau(q)$ when the measure arises from multiplicative processes.

Once the p_i have been established, compute

$$\mu_i^q(r) = \frac{p_i^q}{\sum_j p_j^q}. \tag{34}$$

Then, the Legendre transform can be directly integrated in the calculation of f and α through the formulas

$$f(q) = \lim_{r\to 0} \frac{\sum \mu_i^q(r) \log \mu_i^q(r)}{\log(r)}; \tag{35}$$

$$\alpha(q) = \lim_{r\to 0} \frac{\sum \mu_i^q(r) \log p_i(r)}{\log(r)}. \tag{36}$$

Note that here $\alpha(q)$ is the average value of α at resolution q. Unfortunately, this recipe does not remove the need for linear fitting when calculating the limits, which is usually the main cause of error.

3.2. Histogram method. A computationally fast and direct approach is offered by the *histogram method* (Arneodo et al., 1987; Meneveau and Sreenivasan, 1989). The idea consists in finding the cells with extremal values of total measure for different grid resolutions, and dividing the distance between those values into regular intervals to exploit the fact that exactly one value of α and one value of $f(\alpha)$ will correspond to an extremity of one of the new sub-intervals.

Let us call μ_i^k the total measure of cell i of a grid of unit r_k, and $N(X)$ the number of boxes presenting feature X. Step by step, the method breaks down as follows.

1. Find $X_i^k := \log(\mu_i^k)$ for each cell i of different grids of unit r_k;
2. Divide $[X_{min}^k, X_{max}^k]$ regularly in n smaller intervals for each k, where $X_{min}^k := \min\{X_i^k\}$ and $X_{max}^k := \max\{X_i^k\}$;
3. Deduce one value of α and $f(\alpha)$ from the slopes of X^k and $N(X^k)$ versus $\log(r_k)$ for each sub-interval;
4. Repeat for different grid positions for a better estimate.

In step 3, for $1 \le j \le n$, the value α_j is given by the slope of $X_{j,k}$ versus $\log(r_k)$ where $X_{j,k}$ is one of the extremities of the j^{th} sub-interval for grid resolution r^k. According to Meneveau and Sreenivasan (1989), the correct normalization of the total measure leads to an expression of $f(\alpha)$ as the slope of $\log(N(X_{j,k})\Delta X^{1/2})$ versus $log(r_k)$, where $N(X_{j,k})$ is the number of boxes of size r_k containing an X falling in the interval of size ΔX around $X_{j,k}$.

It is indeed a problem to find the correct normalizations of α and $f(\alpha)$ since the relations $p_i \sim r^{\alpha_i}$ and $N(\alpha_i) \sim \rho(\alpha_i) d\alpha_i r^{-f(\alpha_i)}$ depend on prefactors that are unknown *a priori*. Such a problem is absent in previous methods since those factors are cancelled while taking the limit for $r \to 0$, which is not done here.

3.3. Multifractal Detrended Fluctuation analysis. Some methods have been developed for the specific purpose of studying time series. They are therefore particularly well suited for one-dimensional data, but can be extended to any dimension at the expense of computational complexity. In this section, time series will be defined as one dimensional arrays of discrete values representing observations taken at regular intervals.

Multifractal Detrended Fluctuation Analysis (*MDFA*) is thoroughly described by Kantelhardt et al. (2002); Kantelhardt (2012). In the basic approach, time series are first sub-divided into smaller segments on which is subtracted a least-squares best-fit polynomial of a chosen order to remove the artifacts created by nonstationarities in the time series. A method similar to the moment method is then applied to the resulting detrended series. In details, MDFA consists of the following steps.

1. Replace a time series $f(\cdot)$ with its cumulative sum $F(\cdot)$;
2. Divide F into N_s segments containing s elements each for an array of s;
3. Detrend by removing a least-squares fitted polynomial of order n to F on each segment;
4. Denoting $\bar{F}$ the result of step 3, compute
$$F_q(s) := \left(\frac{1}{N_s} \sum_{\nu=1}^{N_s} \bar{F}(\nu, s)^q \right)^{1/q};$$
5. Find the scaling relation $F_q(s) \sim s^{h(q)}$.

Here, $h(q)$ is the *hurst exponent*, which relates to the classical $\tau(q)$ through the relation $\tau(q) = qh(q) - D_f$, where D_f is the fractal dimension of the physical support of f.

Step one ensures that the transformed series F is σ-additive, which is a necessary property to define a measure that the original series f may not possess. It also allows the use of simple polynomials of the form $a_n i^n + \cdots + a_0$ with $i \in \mathbb{N}$ to detrend in step three. It should be noted that the expression of F_q given above is not well defined for $q = 0$. It is indeed necessary to set

$$F_0(s) = \exp\left(\frac{1}{N_s} \sum_{\nu=1}^{N_s} \log\left(\bar{F}(\nu, s)\right) \right). \tag{37}$$

According to Kantelhardt et al. (2002), MDFA works only for positive h and becomes inaccurate for h close to 0. A solution consists in integrating by considering the sum $\sum F(\cdot, s)$ instead of F. Following the same steps, one would obtain $h(q) + 1$ instead of $h(q)$.

The use of $\tau(q)$ as an intermediary step is given to link the method to previous techniques (see equations (25) and (26)), but one can compute

directly α and $f(\alpha)$ using the expressions

$$\alpha(q) = h(q) + q\frac{dh(q)}{dq}; \tag{38}$$

$$f(\alpha(q)) = q(\alpha - h(q)) + D_f. \tag{39}$$

MDFA can be extended to 2 or more dimensions using multivariate polynomials, as proposed by Gu and Zhou (2006). The 3 dimensions extension is particularly useful to study the evolution of a two-dimensional spatial pattern simultaneously in space and time. Unfortunately, the necessity to choose a common array of s for all directions at the same time, and therefore constraining the precision and accuracy of the method to the direction along which the data is the most scarce or irregular, as well as the rapidly growing computational complexity are significant limiting factors.

3.4. Wavelet-based methods. Kestener and Arneodo (2003) argue that the moment method when applied to multifractal measures implicitly supposes that the underlying cascading process is conservative across all scales (which translates into $\tau(q) = (q-1)D_q$, and, in particular, $\tau(1) = 0$). They indicate that one can still detect and quantify the multifractal properties of measures that have a cancellation exponent $\tau(1) < 0$ by using the *Wavelet Transform Modulus Maxima* method (WTMM), introduced by Muzy et al. (1991). Although such non conservative measures are not properly defined mathematical measures[1], this direction allows to extend effectively the concept to continuous phenomena.

WTMM replaces the square grids of the moment-based methods by highly customizable wavelets. In particular, if those wavelets are chosen orthogonal to low order polynomials, a natural detrending happens. In addition, the "modulus maxima" technique refers to the computationally economic possibility of analysing the data along maxima lines only. With a judicious choice of wavelets, one can therefore integrate the advantages of MDFA and maintain adequate computational complexity for dimensions above 1 or 2.

In more detail, consider a function $f : \mathbb{R} \to \mathbb{R}$ representing either a continuous signal or the interpolation of a discrete time series and a wavelet ψ orthogonal to low-order polynomials. Note that the function f is not directly a mathematical measure here, but represents instead the density of a measure. It is implicitly transformed into a measure when integrated in the first step below. The wavelet ψ is a real valued function, preferably of

[1]The analysis of one such measure could be seen instead as the analysis of a sequence of measures approximating one "underlying" measure defined at scale $r \to 0$

zero mean to ensure that the method is invertible. WTMM is divided in the following steps.

1. Operate the wavelet transform by defining for any x_0:
$$T_\psi[f](x_0, r) := \frac{1}{r}\int_{-\infty}^{+\infty} f(x)\psi\left(\frac{x - x_0}{r}\right) dx;$$
2. Sum along the local maxima lines $\mathcal{L}(r)$ at scale r:
$$Z_q(r) = \sum_{l\in\mathcal{L}(r)} \left(\sup_{(x,\tilde{r})\in l} |T_\psi[f](x, \tilde{r})|\right)^q;$$
3. Find the scaling relation $Z_q(r) \sim r^{\tau(q)}$.

Consider the set of extrema $L(r)$ defined by

$$L(r) := \left\{x,\ \frac{\partial}{\partial x}\left(x \mapsto |T_\psi\left[f\right](x, r)|\right) = 0\right\}. \tag{40}$$

Then, the set $\{(x, r),\ x \in L(r)\}$ is formed of connected curves called *maxima lines*. The set of maxima lines $\mathcal{L}(r)$ is then obtained as the set of all maxima lines defined for all $r' \leq r$. Explicitly,

$$\mathcal{L}(r) := \left\{\left(x(r'), r'\right),\ \forall 0 \leq r' \leq r, x(r') \in L(r')\right\}. \tag{41}$$

Analyzing wavelets can be obtained from several ways. A classical one is to use the successive derivatives of the Gaussian function $\exp(-x^2/2)$. Indeed, the derivative of order n is orthogonal to polynomials of order up to n and of zero mean if n is greater than 1. See top panel of figure II.6 for a representation of these wavelets for order 0 to 5.

Another possible way is to process convolutions of the unit box over Dirac type distributions. On the bottom panel of figure II.6, three successive convolutions of three variants of Dirac distributions are represented. The plot *Dij* is obtained from the Dirac distribution denoted *Dirac i* by applying j number of convolution. Note that only the last two Dirac distributions produce zero mean wavelets and that the unit box has been centered on 0 for aesthetic preferences.

WTMM can be easily extended to n dimensions by considering the wavelets formed by the partial derivatives of a function ϕ such as the Gaussian function $X \to \exp(-|X|^2/2)$, where $X = (x_1, \cdots, x_n)$. The wavelet transform is then replaced by the higher dimensional version

$$T_\psi[f](X_0, r) := \nabla T_\phi[f](X_0, r). \tag{42}$$

More details on the two-dimensional case and examples are provided by Arneodo et al. (2002).

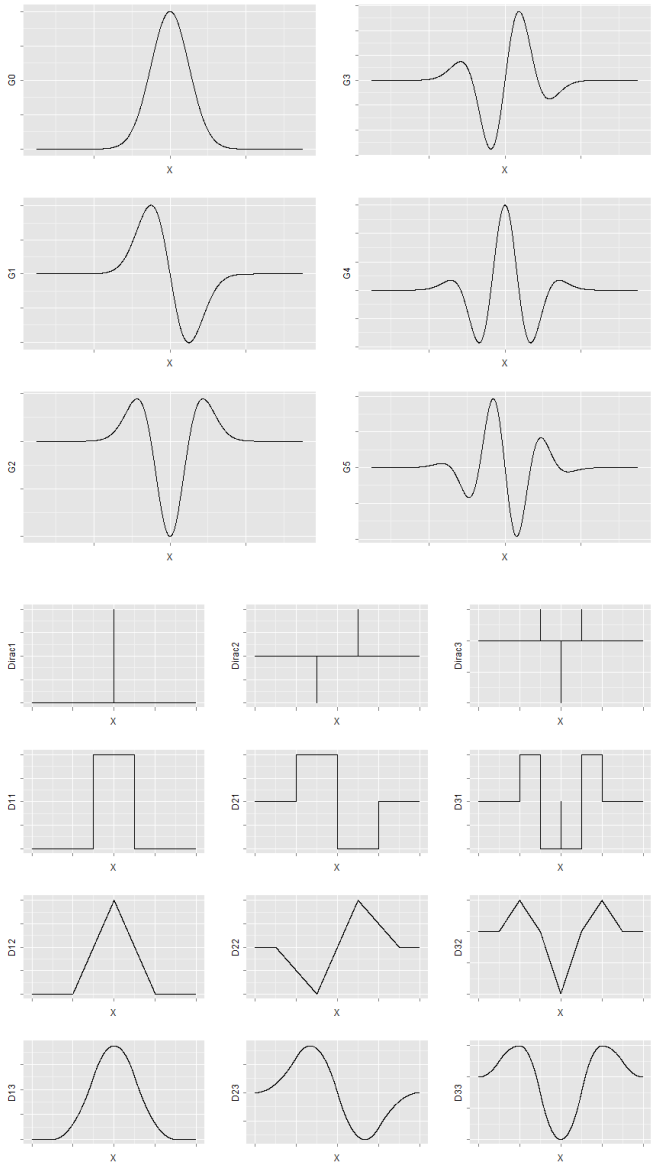

FIGURE II.6. **Analyzing wavelets.** Top: obtained from derivatives of the Gaussian function $\exp(-x^2/2)$. Bottom: obtained from convolutions of the unit box over Dirac type distributions.

Despite its apparent complexity, the WTMM method offers a unique interface allowing to directly use functions representing continuous phenomena as data instead of fully defined mathematical measures. Heuristically, the wavelet transform does transform functions into measures. Indeed, consider the Borel set $\mathcal{B}^n$ over $\mathbb{R}^n$ and a nonnegative integrable function $f : \mathbb{R}^n \to \mathbb{R}$.

Define $\mu : \mathcal{B}^n \to \bar{\mathbb{R}}$, such that $\forall a_1, \cdots, a_n, b_1, \cdots, b_n \in \mathbb{R}$,

$$\mu(]a_1, b_1] \times \cdots \times]a_n, b_n]) := \int_{a_1}^{b_1} \cdots \int_{a_n}^{b_n} f(x)dx. \tag{43}$$

Then μ is a measure. More generally, any increasing right continuous function F (uniquely) defines a measure by considering $\mu(]a, b]) = F(b) - F(a)$. Applying the wavelet transform to a function, explicitly, defining T_ψ such that

$$T_\psi[f](x_0, a) = \frac{1}{a} \int_{-\infty}^{+\infty} f(x)\psi\left(\frac{x - x_0}{a}\right) dx, \tag{44}$$

is heuristically equivalent to evaluating $\mu(W)$ for the above measure, where W is an element of the (heuristic) Σ-algebra created by the wavelets. In particular, if one considers the unit box as the wavelet and normalizes correctly, then T_ψ is formally equivalent to the above measure. Note that the integrability of f in the definition of μ is also required to apply the wavelet transform, so no information is lost by this hypothesis. Note that MDFA accomplishes the same kind of transformation into a measure by dividing the original segment into smaller segments and summing on each of them, which is the discrete equivalent of the measure μ defined above.

However, the ability to work directly with functions is more suitable for nonconservative phenomena, or if one wants to integrate the multifractal analysis in the equations the studied functions are a solution of. The simplicity of box-counting techniques and the adaptability offered by their many variants should nonetheless make those preferable for "static" measures.

A word must be said of another wavelet-based approach called *Wavelet Leaders* (Lashermes et al., 2005; Jaffard et al., 2007). Assuming r is decreased to 0 by the way of a dyadic partition of the space. Then, the wavelet leaders method replaces for each point x_0 the wavelet coefficient $T_\psi(x_0, r)$ by the supremal coefficient within a neighbourhood formed by a triplet of dyadic intervals around the point. It allows to gain more stability for $q < 0$ and to take into account "chirp" singularities, that is singularities that have a parasite short-range oscillatory noise.

4. Our choice of methodology

The different methodologies are tested first on a canonical multifractal example, the binomial cascade of probability $p = 0.6$ introduced in figure II.4. They are then tested on the London house transactions dataset to take into account the particular needs for our type of data.

We consider both the theoretical binomial cascade[2] and a particular realization of a random walk through it. In both cases, the iterative process is stopped after the 20^{th} step for which over a million sub-intervals have already been created. This is done to ensure a reasonable run time and use of memory, and because it is comparable to the size of many encountered data types such as pixels of an HD image or data collected from a city-size human settlement. Unfortunately, it also means that the studied cascades are not equivalent to that produced the spectrum of figure II.4, for which the iterative process is repeated an infinite number of times. As such the resulting spectra are expected to be similar, but not necessarily identical to the theoretical curve of figure II.4 depending on the sensitivity of the chosen multifractal method. The chosen range of q for the moment method goes from -20 to 20.

The results of the standard moment method and its variants, the gliding box and the multiplier methods, are illustrated in figure II.7. In the theoretical case on the top, the range of α is a lot narrower than what is expected based on the reference curve (figure II.4). The variants help improve the situation, but not by much. This problem is due to the fact that the iterative process was stopped too soon. The top figure of figure II.8 evidences that stopping the iterative process at step 25 results in a wider spectrum (circles) than stopping it at step 10 (triangles). Aside from this problem, the resulting spectrum is similar to the reference one and a simple rescaling of the range of α is enough to make both spectra harmonious. For the particular realization of the cascade on the bottom of figure II.7, the accuracy of the standard and gliding box moment methods deteriorates rapidly for negative q. The multiplier method gives the best results overall. To keep the curve above zero, the range of q had to be restricted to $q \geq -4$ for the first two variants and to $17.5 \geq q \geq -10$ for the multiplier variant.

Results of the histogram method applied to the binomial cascades can be found in figure II.9. Unfortunately, for such a small range of scaling, the histogram method is not well adapted and the resulting spectra are not smooth. The error generated by the method makes results difficult to interpret in this case. As a matter of fact, Meneveau and Sreenivasan (1989) have applied the histogram method for a binomial measure, a period doubling attractor for a specific logistic map and the dissipation field of turbulent kinetic energy in turbulence flows. They found good agreement with the results obtained from the moment method for the first two cases but it was evidenced that

[2]That is the result of averaging an infinite number of random walks through the iterative process defining the cascade.

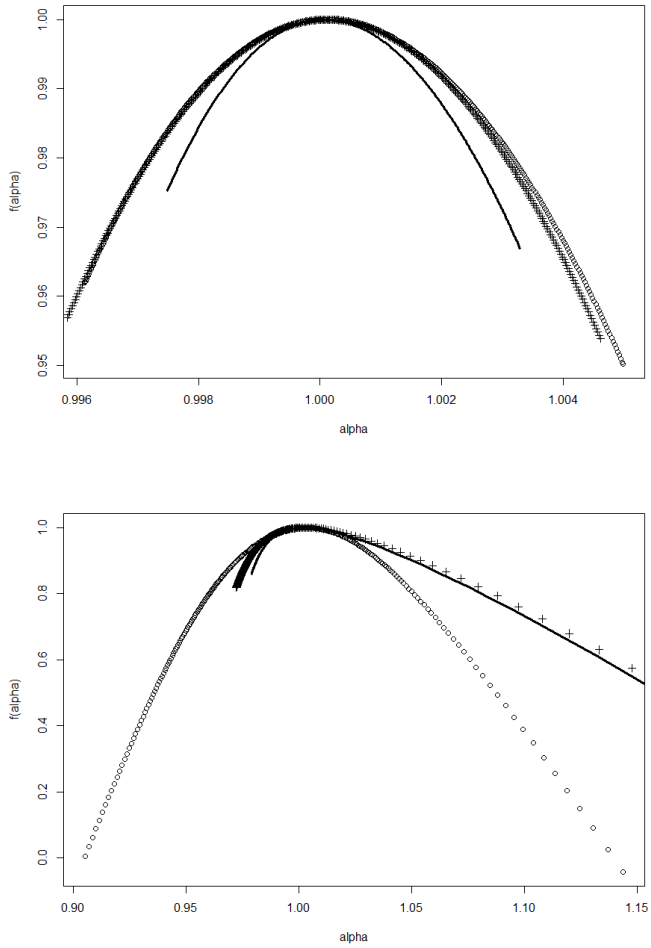

FIGURE II.7. **Moment method and variants applied to multifractal binomial cascades.** The standard moment method (plain line), the gliding box method (circles), and the multiplier method (crosses) are applied to the theoretical cascade on the top and to a particular random walk through the cascade on the bottom.

errors are generated by the histogram method for measures with small scaling ranges such as the third case. In fact it was evaluated that the exponent found by this method is only accurate up to order $\log(L/r)^{-2}$, where L represents a characteristic value intrinsic to the problem (a translation of the unknown prefactor). It was recommended to use this method only for measures such that the largest obtainable scale is at least 10^3 times bigger than the smallest measurable scale. The method has however the advantage of being faster than the moment method and gives a range of α closer to the reference in this particular case.

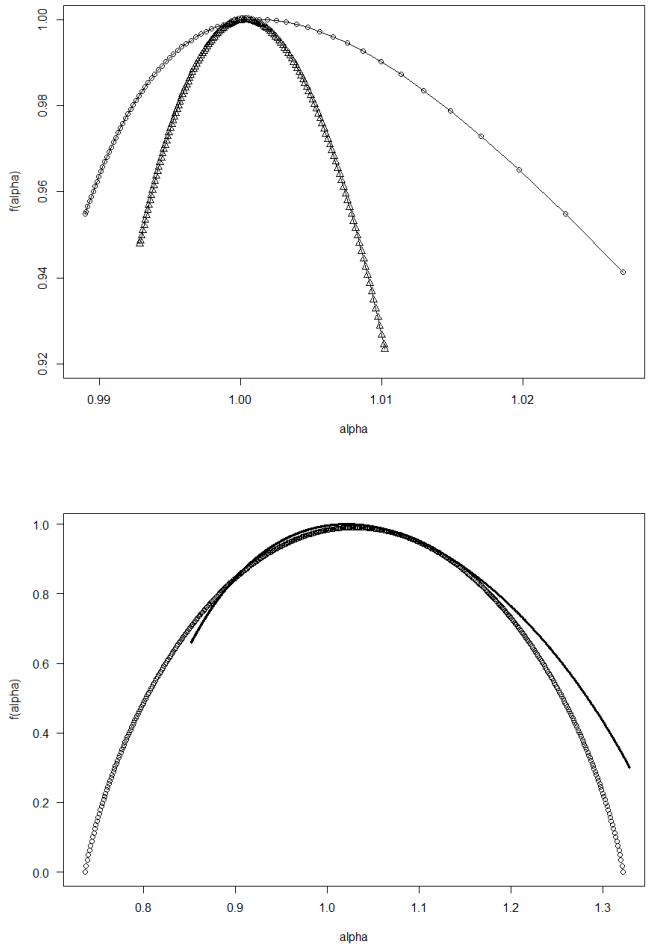

FIGURE II.8. **Influence of the number of iterations on the spectrum.** On the top, the spectrum made of triangles is obtained for 10 repetitions of the iterative process generating the cascade, while the spectrum made of circles is obtained for 20 repetitions. Increasing the number of iterations makes the spectrum larger and therefore closer to the theoretical curve. On the bottom, a rescaling of the range of alpha on the curve resulting from the moment method (plain line) is enough to make it harmonious with the reference curve (circles).

In figure II.10, MDFA is applied to the binomial cascades. When the values of s are chosen as powers of 2 in the theoretical case, the N_s intervals are only translated copies of themselves, resulting in a completely flat spectrum (on the top). MDFA is particularly well suited for data such as the random realization (on the bottom) and gives the closest results to what is expected from the mathematical study, with only a slight offset to the left

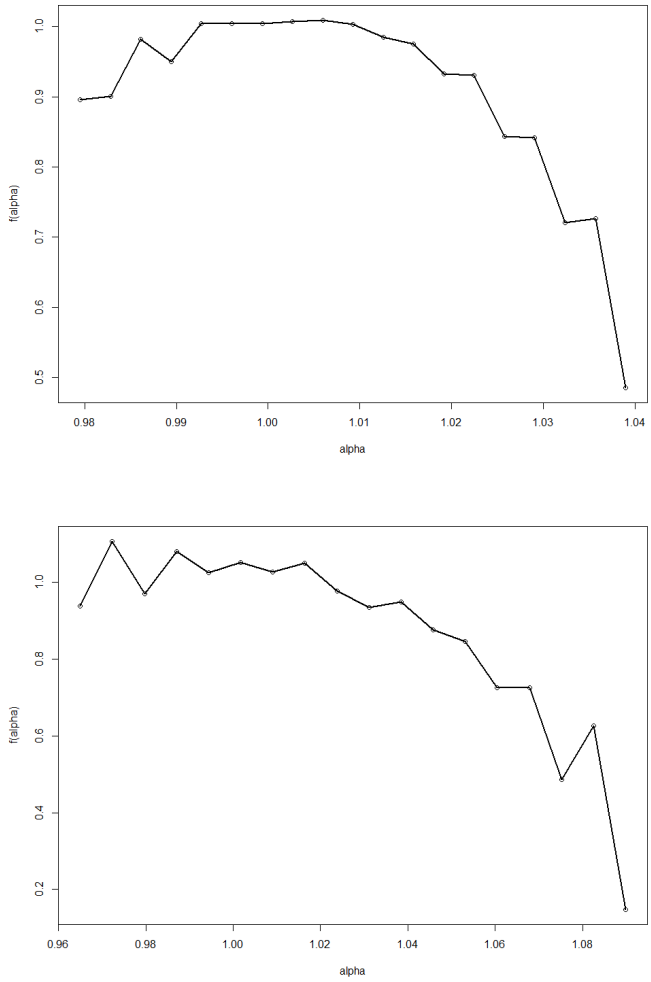

FIGURE II.9. **Histogram method applied to binomial cascades.** On the top, a theoretical binomial cascade of parameter $p = 0.6$ and on the bottom a particular realization of it.

of the range of α which is explained by the fact that the iteration process generating the cascade was stopped at a relatively low level of iterations.

Since wavelet-based methods are primarily meant to be used on continuous phenomena and time-series, no application to binomial cascades are given. The "chirp" singularities in particular are irrelevant to our data whose scale is too broad to posses such a fine noise. As a result, the WTMM and Wavelet Leaders methods were discarded.

The standard moment method applied to real data sometimes seems to fail for α values greater than 1 or 2 (e.g. Murcio et al., 2015; Hu et al., 2012; Cheng, 1999*a*). This can be explained by the following observation. Assume

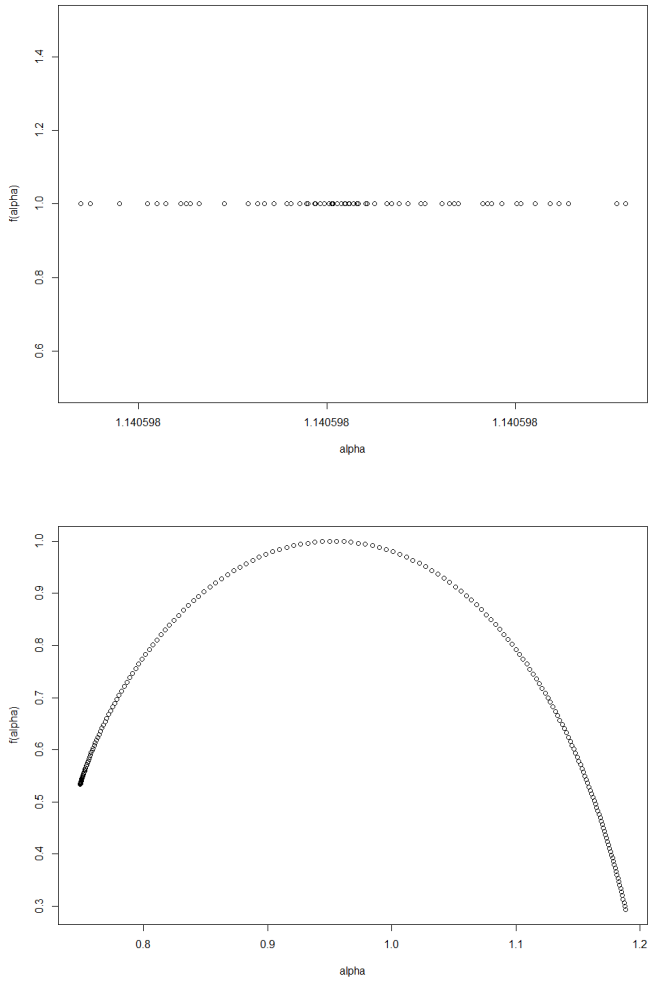

FIGURE II.10. **MDFA applied to binomial cascades.** On the top, a theoretical binomial cascade of parameter $p = 0.6$ and on the bottom a particular realization of it.

that a non-negative signal ϕ is defined on a one-dimensional space, say $\mathbb{R}$. We can create a measure μ from this signal by defining for any $a < b \in \mathbb{R}$

$$\mu([a;b)) = \int_a^b \phi(x)dx. \tag{45}$$

If the signal ϕ is of the form $r^\beta + k$ for some β and a real constant $k > 0$. Then, once integrated, the measure will be either of the form $r^\alpha + k * r$ or $r^\alpha + k * r^2$ for one-dimensional or two-dimensional signals respectively. The noise introduced by k is therefore negligible for α values below 1 or 2 (resp.) when $r \to 0$, while the measure is negligible compared to the noise for α values greater than 1 or 2 (resp.) when $r \to 0$.

In contrast, the multiplier variant assumes by construction that the signal would actually reach 0 (i.e. that the noise k does not exist even when $\alpha > 1, 2$, corresponding to negative q values), and computes an approximation of the α values from the growth of the signal around the point despite the noise. This process could be thought of as "calculating the best multifractal fit" for the measure. The relevance of the spectrum resulting from the multiplier method for α above 1 or 2 would depend on how close the data is to a true multifractal.

The methods have been tested against the London house transaction prices for the year 1995. A grid of size 200×200 (corresponding to a rectangular grid unit of 450 meters by 300 meters) was used to sort the data. The basic moment method (circles), MDFA (plus symbols), and multiplier method in conjunction with gliding boxes aggregation (cross symbols and thick line) are plotted in figure II.11. All the methods agree for α values below the point for which $f(\alpha) = \alpha$. After this point is reached, the moment and MDFA methods fail, while the multiplier method remains stable. This is due to the noise effect explained above. After subtracting the minimum price to all values, the moment method (red line and triangles) is able to pass the previous failing point. It also produces a right-part to the spectrum whose curvature corresponds to a translation of the multiplier method (cross symbols). As expected from the discussion above, only the multiplier method was able to produce convincing results.

The green lines in figure II.11 are "control" lines. It is expected that the multifractal spectrum will touch the line $y = x$ on exactly one point, and that it will not go above the $y = 2$ line. As a matter of fact, the highest point of the spectrum should be the fractal dimension of the space occupied by the measure. By construction, the multiplier methods forces this dimension to be equal to the euclidean dimension of the embedding space. For that reason, we advocate for applying a rescaling to the spectrum that ensures that the point $f(\alpha) = \alpha$ remains identical, and such that the highest point of the spectrum is the correct fractal dimension. This is done by changing equations 31 and 32 to

$$\tau(q) + d_0 \approx -\frac{d_0}{d} \frac{\log(1/N \sum_i M_i^q)}{\log(r_k/r_0)}, \tag{46}$$

$$\alpha(q) = \frac{d_0}{d} \frac{\sum_i M_i^q \log(M_i)}{\sum_i M_i^q \log(r_k/r_0)}, \tag{47}$$

where d_0 is the fractal dimension of the space covered by the measure. Such

In all subsequent analyses, boxes are defined as Moore neighborhoods of radius r around each point such that a full box can be included inside the study area. In practice, this means that points too close to the border to

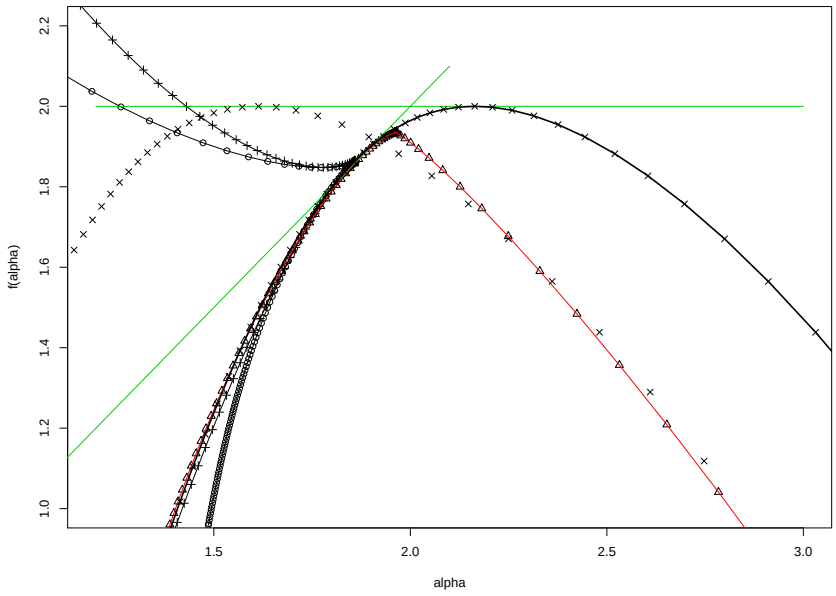

FIGURE II.11. **Multifractal methods applied to real data.** London house transaction prices for the year 1995 were sorted in a grid of 200×200 pixels. The basic moment method (circles), MDFA (plus symbols), multiplier method in conjunction with gliding boxes aggregation (cros symbols and thick line), a translation of it (cross symbols), and the moment method on simplified data (triangles and red line) are plotted. The green lines are control lines.

fit a box of maximal size are ignored in the calculations. The values $\mu_i(r)$ are then the sum of all the lot price whose centroid falls inside each box i. The chosen radius r_0 is the minimum allowed by the resolution (i.e. 1 pixel), and we average the results over several r_k to limit the effect of local inaccuracies in the data. To test the scale invariance of the datasets, we use several series of r_k: $\{1, 2, 4\}$, $\{1, 2, 8\}$ and $\{1, 4, 16\}$. We do not use radii above 16 to avoid removing too much of the data when applying the gliding box technique and because the behaviour far away from the centre of the box has no consequences on the limit for $r \to 0$. If the spectra resulting from different series do not match, then we discard the dataset. The results shown in the figures of chapter IV are the curves obtained for the series $\{1, 2, 8\}$. The q range is defined as all values such that the resulting $f(\alpha)$ is non-negative.

In summary, the main advantage of the multiplier method is that it allows to compute a spectrum even in the presence of underlying large-scale

structures and flat noises. These anomalies in the data are usually responsible for the failing of the more rigorous methods, as identified by Huang et al. (2010, 2011) and Salat et al. (2018). In particular, the method is able to produce a spectrum even for negative q values. The main drawback is that the method assumes the multifractality of the data *a priori*, and therefore requires preliminary scale invariance checks. It also forces some arbitrary rescaling choices, and there is no easy way to control the error induced. However, it is well adapted to our context. Indeed, inequality and segregation are subjective notions whose definitions and traditional measurement methods are riddled with arbitrary choices. Meanwhile, the multifractal multiplier method focuses on describing the heterogeneity of the spatial patterns and will produce directly comparable results as long as the method is applied consistently over the different datasets. As a matter of fact, we prove in chapter V that the method provides more reliable and scale resilient results than the traditional segregation indices.

An interesting information can be added to the spectrum by using the generalized dimension defined by the equation $D(q) := \tau(q)/(q-1)$. Three values in particular relate to well known dimensions: $D(0)$, $D(1)$ and $D(2)$. The first one, $D(0)$, is the fractal dimension of the physical space supporting the measure (the spectrum maximum height). The dimension $D(1)$ is the information (or entropy) dimension, it relates to Shannon's entropy and provides a measure of the density evenness in the data. Finally, $D(2)$ is the correlation dimension, which provides a measure of scattering in the data. By definition, the full range of $D(q)$ is the same as the full range of α. The $D(0)$ dimension can be computed directly using box-counting, while the $D(1)$ and $D(2)$ values can be deduced from the direct expressions

$$D(1) = \lim_{r \to 0} \frac{\sum_i \mu_i(r) \log(\mu_i(r))}{\log(r)}, \tag{48}$$

$$D(2) = \lim_{r \to 0} \frac{\log(\sum_i \mu_i(r)^2)}{\log(r)}. \tag{49}$$

We have produced these three values in tables for the first studied datasets to confirm the validity of the results. Since the information they contain is fully covered by the spectrum, and since the D_q values are particularly unstable around 1, they will not be reported thereafter.

In conclusion, the histogram method is only used for preliminary test runs, and the basic moment method (including its direct variant) and MDFA are only applied to corroborate the results from the multiplier method. The multiplier method is used together with the gliding-box technique to maximize the number of data points. We justify further this choice in the specific urban context in the next chapter. The spectrum rescaling described above

is applied to the results for better interpretative value. In chapter IV, only the final results from the chosen methodology are shown. The method has been applied as consistently as possible to maximize the comparability of the results.

CHAPTER III

Applying multifractality to study urban inequality

We present multifractal theory from an interpretative perspective and illustrate visually the meaning of the main variables. The purpose is to explain how multifractal analysis can be adapted to cities and used to gain new insights in regards to urban inequality. We address some of the limits arising from this particular context and emphasize the role of the multifractal methodology as a comparative and potentially predictive tool. We present the advantages of undertaking multi-directional comparisons, that is through time, between different cities, between several neighbourhoods inside one city, with models and also between different inequality variables for a single city.

From this discussion, the epistemology of our methodology should appear clearly. In particular, we will justify the selection of a number of measures to study urban inequality. For each measure, we will explain how it is related to studying inequality, present the corresponding available datasets, and indicate how they were processed to fit with the requirements of the multifractal framework. Some parts of this chapter are adapted from Salat et al. (2018).

1. Heuristics and spectrum interpretation in terms of inequality

Recall from the previous chapter that multifractal theory can be used to study the heterogeneity and irregularity of measures defined on sets that are too irregular for classical geometric tools, when those measures present two separate scaling properties. Consider a measure μ defined on a set A[1]. It is required that

1. locally around any point x of the set A, the measure is scaling with a local exponent α_x;
2. the set formed by all points around which the measure scales with the same local exponent α_x is a fractal set of dimension $f(\alpha_x)$.

[1] A mathematical measure on a set can be understood as a way of assigning a size to every subset of that set, with the minimal conditions necessary to extend the intuitive notion of *area*. Formally, μ is a function from the parts of A to $\mathbb{R}^+$, such that $\mu(\emptyset) = 0$, and if $\{B_i\}$ is a countable collection of pairwise disjoint sets in A, then $\mu(\cup B_i) = \sum \mu(B_i)$.

Since the canonical Hausdorff dimension is impractical in most case studies, we will define a *fractal set* as any set such that the more flexible box-counting dimension can be computed. Both dimensions match for self-similar sets, but the box-counting dimension may be less accurate, for example when the studied set is a dense subset of its environment. It will nonetheless adequately suit our needs. We will also consider sets with an integer dimension as particular cases of fractality, rather than as non-fractal sets.

The curve $f(\alpha)$ against α is the *multifractal spectrum*. It gives, roughly speaking, the "fractal dimension" $f(\alpha)$ of sets formed by points where the measure scales locally with the same exponent α. In order to get a heuristic idea of what the α values represent, assume that we want to study the multifractality of a non-negative signal ϕ defined on a one-dimensional space, say $\mathbb{R}$. We can create a measure μ from this signal by defining for any $a < b \in \mathbb{R}$

$$\mu([a;b)) = \int_a^b \phi(x)dx. \tag{50}$$

In particular, the first scaling rule $\mu([0,r)) \propto r^\alpha$ translates into $\phi(x) \propto x^{\alpha-1}$ on the interval $[0,r)$. Assuming there is a reflectional symmetry around 0, this formalization allows us to illustrate the typical limiting behaviour of a multifractal signal around a point (here arbitrarily represented by 0) corresponding to some particular α when $r \to 0$ (see figure III.1(a)). Note that the vertical scaling is arbitrary in this example.

If we were to consider instead a perfectly isotropic two-dimensional signal, then the cross-cut along any particular direction would be the same as the curves above at the condition of adding 1 to the corresponding α. A representation of such a signal for particular α values can be found in figure III.1(b). The real signal does not have to be isotropic, for example "bumps" on one side of a circle of radius r_0 can be compensated by "holes" on the other side of the same circle. Note that α values represent the rate at which a signal, and more generally any measure considered, grows around a point in contrast to the actual value of the measure at the point.

We use for $f(\alpha)$ the box-counting dimension of the set formed by all squares in a grid whose measure shares the same local strength α. This is illustrated in figure III.2, using the land price distribution for Kyoto in 1912 as an example. On the top left, the actual land price distribution is represented in a blue continuous logarithmic scale applied over a 512x512 grid. In the three other images, the 4x4 squares corresponding respectively to a strength of $\alpha = 3$, $\alpha = 6$, and $\alpha \geq 7$ (counting clockwise) are highlighted in red. The values $f(\alpha = 3)$, $f(\alpha = 6)$, and $f(\alpha \geq 7)$ are the box-counting dimension of each highlighted zone. The final aim would be to infer from the

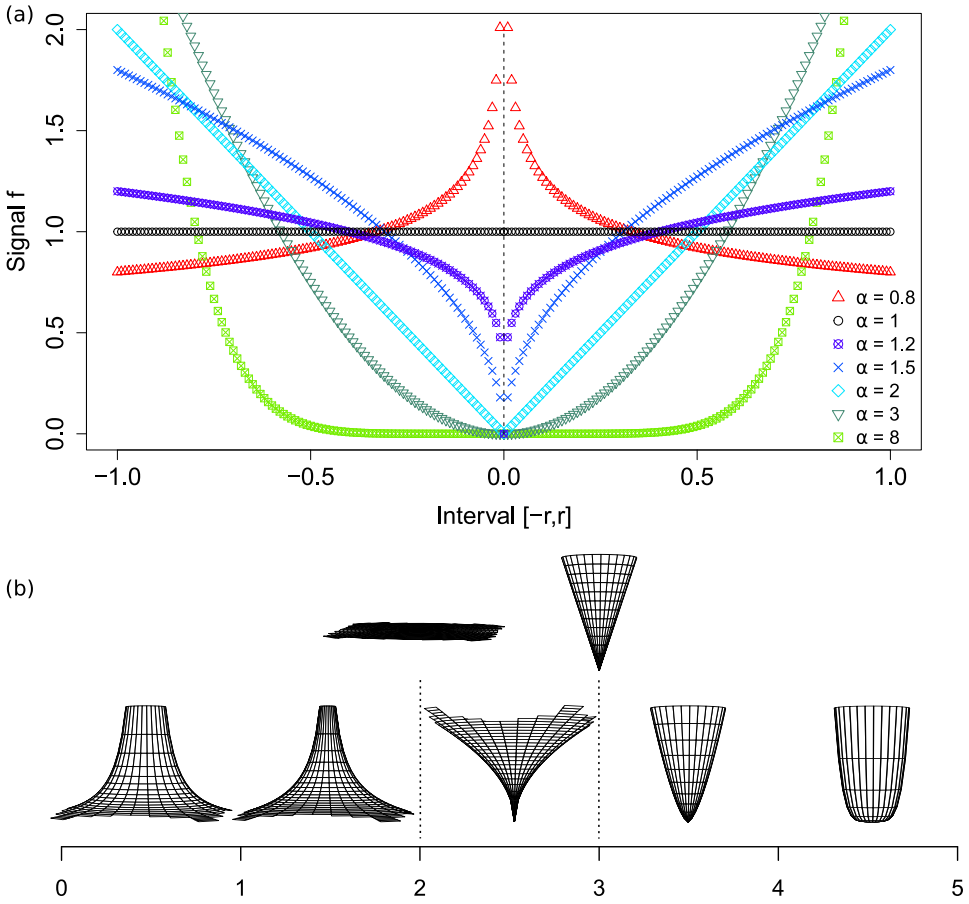

FIGURE III.1. **Meaning of the α values.** (a) Idealized local behaviour of a one-dimensional signal around a point of strength α. (b) Idealized behaviour of a two-dimensional signal around a point whose strength α is indicated on the scale below.

data the α and $f(\alpha)$ values when the size of the neighbourhoods approaches 0, not 4x4. As a result, the α values in this illustration are overestimated.

The link to inequality and segregation stems from several characteristics of the spectrum. The most obvious one is its width. The range of α values is more representative of the variety of neighbourhoods than it is of the spread of the variable distribution. For example, expensive mansions surrounded by low-cost houses will be represented by a very low α value. If the group of mansions is reduced to just one odd isolated manor, then the α value will be moderately low. In contrast, if an urban planner decides to erect modern social housing in the middle of traditional detached houses, then it will result in a high α value. Meanwhile, intermediary α values are reached when the houses are all locally similar. The range of α values therefore represents all the different "types" of neighbourhoods in the city. A narrow spectrum

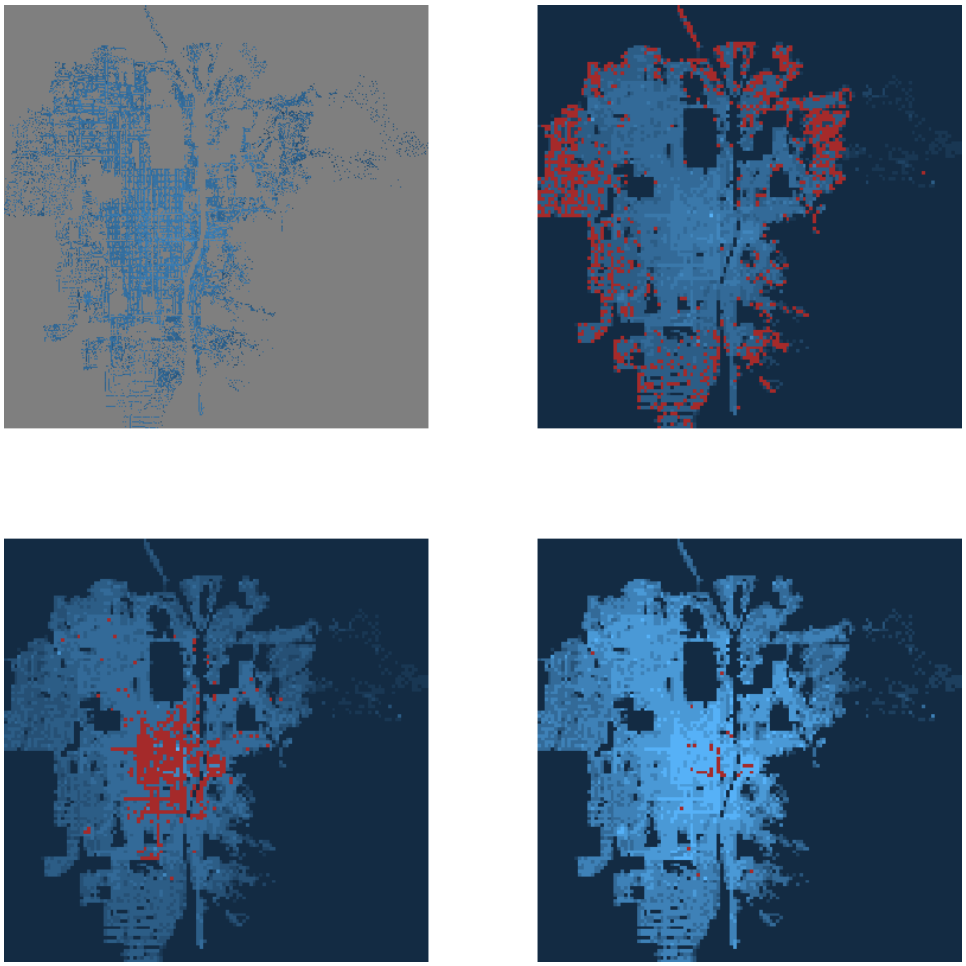

FIGURE III.2. **Meaning of the $f(\alpha)$ values.** Top left: real land price distribution for Kyoto in 1912 in a log-scale. The other figures represent the corresponding α distribution with: top right: $\alpha = 3$ highlighted in red; bottom left: $\alpha = 6$ highlighted in red; and bottom right: $\alpha \geq 7$ highlighted in red. For each α value, the dimension $f(\alpha)$ is akin to the box-counting dimension of the highlighted zone.

means local homogeneity everywhere, while a large spectrum indicates a lot of heterogeneity.

Recall that segregation is defined as "the degree to which two or more groups live separately from one another in different parts of the urban environment" (Massey and Denton, 1988). Assume that the α distribution of the spectrum of a price distribution is narrow. Since lower and higher α values mean sharper growth, while values around 2 (in the case of 2-dimensional measures) are a sign of local homogeneity (with only a few isolated singularities), it means that the prices are clustered into groups of locally similar α values (for which the $f(\alpha)$ dimension will be close to 2). In this case,

the lower and higher α values represent the sharp edges of the clusters (for which the $f(\alpha)$ dimension will be closer to 1). As a result, segregation is high. Note however that if the spread of prices is limited, then there is still no segregation (and the local homogeneity is the result of the presence of only one economic group).

Moreover, the $f(\alpha)$ values represent in a sense the spatial "density" of each type of α value. As such, in reference to Massey and Denton (1988), high $f(\alpha)$ values mean concentration and clustering, while low $f(\alpha)$ values mean dispersion and exposure. Taking the example of income, the left part of the spectrum represents the "richer" living in the middle of the "poorer", while the right part of the spectrum represents the "poorer" living in the middle of the "poorer". A "round" shape for one part of the spectrum would then indicate high exposure of the economic group it refers to. A particular interest should therefore be given to the vertical asymmetries between the left part and the right part of the spectrum. Beware that a generally low $f(\alpha)$ value distribution for the entire city is more a sign of low density in the city rather than low exposure everywhere, although one may argue that the former implies the latter. These considerations will be easier to grasp for the reader after reading section 2.2 of chapter V where they will be illustrated directly on an example drawn from the results of the multifractal analyses.

In addition to these spatial descriptions of the studied variable, multifractal analysis is best used for making comparisons. It could be argued that full homogeneity of house prices is a favourable sign of equality. However, if there is no evidence that such an homogeneity could also be imposed on income, then it is perhaps more beneficial to match the spectrum of house prices with the spectrum of income rather than to create a situation where all houses are equally unaffordable to most.

2. Scope for cities and limitations

Contrary to the notion of monofractality that can be easily extended to sets that are irregular in a loose sense, and even to non geometric objects, such as homogeneous function[2], the notion of multifractality is quite rigid. Most practical techniques usually rely on a strict compliance to the two rules mentioned in the previous section. In particular, we showed in the previous chapter that the α values are not entirely invariant through vertical translation of the measure. Indeed, if the signal ϕ defined previously is of the form $r^\beta + k$ for some β and a real constant $k > 0$. Then, once integrated, the measure will be either of the form $r^\alpha + k * r$ or $r^\alpha + k * r^2$ for one-dimensional or two-dimensional signals respectively. The noise introduced

[2]Functions that have a multiplicative scaling behaviour.

by k is therefore negligible for α values below 1 or 2 (resp.) when $r \to 0$, while the measure is negligible compared to the noise for α values greater than 1 or 2 (resp.) when $r \to 0$.

We explained that for this reason, the standard moment method applied to real data may fail for α values greater than 1 or 2 (Murcio et al., 2015; Hu et al., 2012; Cheng, 1999*a*). In contrast, the multiplier variant ignores the noise and computes an approximation of the α values from the growth of the signal around the point. This process is akin to "calculating the best multifractal fit" for the measure. It is difficult to evaluate precisely the error created by the choice of this particular multifractal method. However, urban systems are in essence extremely chaotic, so that strict scaling laws are not to be expected in relevant datasets. For that reason, we have chosen to use the results from this more forgiving multiplier variant, but we still compare them with the stricter methods and only use them if they match on a significant portion of the spectrum (classically, the part that lies below 2 for the reasons mentioned above).

In addition, we abide by the idea developed by Batty (2018) that models should be useful rather than truthful. Batty argues against the real predictive value of theories and models for social complex systems, and encourages restricting their use to "structuring and focussing debate". Rather than seeking the most truthful description of an overly noisy phenomenon, we aim at finding a useful improvement of the current inequality analysis. To that end, we compare extensively the multifractal methodology to the results from classic inequality and segregation measures in chapter V. We find that the methodology recovers the main results, while often conforming better to intuition in particular cases. It also solves many technical difficulties encountered by the classical segregation measures, such as the reliance on arbitrary administrative boundaries or the need to prioritize arbitrarily either the spread or the distributional shape of the inequality variable.

The real power of multifractal analysis resides in its capacity to detect change and hence compare spaces at different points in time, or to compare different neighbourhoods. There are many combinations of objects that can be compared. Indeed, we can study the temporal evolution of a single city (ie compare a single city at different time intervals), we can compare a city with another city (intercity comparison), or compare several neighbourhoods inside one city (intracity comparison), or compare a city to some abstract models of urban development, or compare a model with another model, and even compare an inequality measure to another inequality measure. We have chosen several cities (London, Paris, New York and Kyoto) representing the epitome of economically efficient urban developments, and for which

quality datasets can be easily obtained, and some static basic models (uniformly random, polycentric and Diffusion-Limited Aggregation), to serve as a comparison basis for an initial assessment of inequality in modern urban development. Obviously, it is not realistic to make every possible combination of comparisons, so we focus on exploiting the most promising features for each city or model as evidenced in the next section.

The input for multifractal analysis needs to be a formal mathematical measure. As such, densities and categorical variables cannot be used directly. Some non-measure distributions, such as betweenness centrality for nodes in a network, could be interpreted as a measure representing an idea of point "potential". However, claiming that these potentials can be summed over several points is a risky assumption. In the next part, we justify the choice of five urban parameters as inequality indicators, and explain how they have been transformed into satisfyingly rigorous measures. For each of the newly formed measures, we present the datasets they have been applied to.

3. Urban measures selected for analysis

In accordance with Dalton (1920) and Sen (1997), we believe that inequality measures should aim at being a good translation of economic welfare, rather than being restricted to the analysis of household income only. As such, we explore four directions that could translate household economic welfare: real estate, energy consumption, income and accessibility to a diverse neighbouring urban environment.

According to (Tannier et al., 2016), the spatial differentiation in cities results from three main processes: the competition for economically advantageous space, cooperation processes, and processes by which individuals try to minimize the energy used for exchanges and movements[3]. As a result, individuals tend to cluster with other individuals belonging to the same social groups. This is known as the *peer effect*: individuals identify to certain social groups, then "collective references lead individuals above all to reside in the same place, frequent the same places and use the same means of transports as other members of the social group(s) they belong to" (Tannier et al., 2016).

Real estate, energy, income and accessibility spatial distributions can be seen as the outcome of these processes. In turn, these distributions help defining the opportunities and social identifiers for future generations. In this thesis, we do not analyse the processes themselves, but only their consequences in terms of individual economic welfare.

[3]In this case, the energy cost can result from physical distance, but also from social or cultural distance for example.

3.1. Real estate. Access to quality housing is an obvious aspect of economic welfare. From a functional perspective, housing location determines the number and types of jobs accessible and, together with accommodation quality, can have direct consequences on health (through air quality for example) and perceived happiness. In addition, according to Fielding (2004), housing is traditionally seen as an important sign of social status in the West, while the functional aspects prevail in the Japanese culture. For that reason, we expect house prices to reflect segregation in western cities, and be more evenly distributed in Japan. We have at our disposal datasets in London, Kyoto, New York and Paris to study both the inequality and segregation dimensions of house prices.

A real estate measure needs to be counted on a suitable base unit of land. Different units can be chosen, inferring different interpretations. To describe the spatial distribution of land value, the unit could be each square meter of land. Note that this is different from counting the average square meter price: the price is counted additively for each square meter, so that the price of two square meters of land combined is equal to the sum of the prices for each square meter. To describe property value instead of land value, the unit should be based on floor space (one square meter times the number of stories for example). Indeed, considering only house price per square meter would miscalculate the total housing value carried by the land. To study housing inequality, each accommodation can be considered as a unit of its own, independently of its size. The results would then give information on the affordability of suitable housing assets and on the spatial repartition of each price category. From the contrasting point of view of policy makers, one may want to choose a set number of people as the base unit and try to calculate the cost of accommodating that number of people.

The choice of a unit, however, may be constrained by the data available. For example, for London, the HM Land Registry (Data, HMLR:1995-16) provides a highly detailed dataset containing all the housing transactions that have happened in Greater London since 1995. For a highly dynamical market such as London, we can assume that houses do not stay unsold for long periods, so that the unit defined by each transaction represents adequately what was available in that year. In contrast, for Kyoto a digitalization of a cadastral map first published in 1912 (first year of Taishō era) was made available by Yano et al. (2007). At the smallest level, all land is divided into lots registered to a single owner for which the tax assessed price is known. Taking each lot as the unit represents accurately all existing residential land assets in the city, but we cannot distinguish which land plots were actually available for sale.

Other datasets include a land tax assessed road valuation around 2012 for Kyoto, as provided by the official Open Data website maintained by Kyoto City (Data, KC:2012*a*). After transformation, those values can be seen as approximations comparable to the 1912 lot values. The PLUTO[4] database, from NYC Planning, provides all assessed tax values for land prices in New York at 'Borough Block Lot' (BBL) level since 2002 (Data, NY:2002-18). These prices are quite comparable with the data for Kyoto. In addition, a second dataset containing the actual transactions, obtained from the NYC Open Data website (Data, NY:Sales), can be used for comparison with the London dataset. Finally, a dataset obtained from the Urban Morphology Institute in Paris, provides the average square meter prices at 'aggregated units for statistical information' (IRIS) level for Paris in 2014. IRIS were implemented to gather statistics throughout France and aim at subdividing the territory into units containing around 2000 people. Choosing IRIS as the base unit meets the policy makers' perspective mentioned earlier of analysing the cost of accommodating a set number of people. Because square meter prices are a density that cannot be used directly, it is necessary to multiply the prices by the population count inside each IRIS.

Based on the characteristics of each dataset, we decide to use the data for Paris solely for comparison with other variables, such as the number of jobs and average income. In contrast, the data for London, Kyoto and New York is also used for intercity (and even intracity comparisons for New York) and for comparisons through time. Due to the high quality of the Kyoto data, it is further used for comparisons with static models. These models are shuffles of the Kyoto land prices representing the null (fully random) model, the polycentric model typical of modern cities, and a maximally multifractal case using Diffusion-Limited Aggregation (DLA) models. They are presented in full details in the next chapter.

3.2. Income. Income has been the most studied variable in relation to inequality ever since the notion was formalized (see notably Pigou, 1912; Gini, 1912; Dalton, 1920; Atkinson, 1983; Sen, 1997; Atkinson, 2015). To transform income into a spatial measure, we need to consider the total income carried by a unit of land, or alternatively, received by a fixed number of people. In simpler terms, the average income needs to be known and multiplied by the number of people considered (either directly or inside the land unit considered). This is more restrictive than it seems, since data is often presented with median values or with a limited number of income categories that cannot be used to determine the average value. Moreover, the sampling

[4]Primary Land Use Tax Lot Output

polling methods usually applied to gather the data prevent reaching a fine enough resolution that satisfies multifractal analysis.

The estimated unequivalised mean household income at Lower Layer Super Output Area (LSOA) level was obtained for London from the Greater London Authority (GLA) (Data, LonIncome:2002-13). For New York, the best data found was taken from the Census FactFinder and includes the 2010 population count and the estimated mean household income at Census Tract (CT) level (Data, NYIncome:2010). For Paris, the estimated average income and population count in 2014 at IRIS level was obtained from INSEE[5] (Data, ParIncome:2014*a*).

These three datasets share a common resolution, a common time period, and a common "official" estimations quality. They are therefore highly suitable for intercity comparisons. In addition, these datasets have good comparative value respectively with the house transactions dataset for London (aggregated at the LSOA level), the BBL transaction dataset for New York (aggregated at the CT level), and the square meter price dataset for Paris described in the real estate section. This allows good inter-measure comparisons. Finally, the London dataset covers over 13 years, including the 2008 financial crisis, and is therefore suitable for a temporal analysis.

3.3. Energy consumption. Energy consumption represents the intensity of activity of the professional sector and can be considered a proxy for land development (Garrett, 2011; Kasperowicz, 2014). At the household level, there is a connection between energy consumption and standard of living (Dzioubinski and Chipman, 1999). Joyeux and Ripple (2007) found out that residential energy consumption is not explained by income alone, so that measures of standard of living should take into account both parameters. Energy consumption being additive (at the condition of converting energy from all sources into a common normalized unit, such as kW), there is no particular difficulty in transforming it into a measure.

Primary spatial data on energy consumption proved difficult to obtain. For New York, Howard et al. (2012) propose a methodology to estimate energy consumption from land use. It is based on the land use description from the PLUTO database described above (Data, NY:2002-18), coupled with data from the New York City Mayor's Office gathering the annual electricity, natural gas, steam and fuel oil consumption for 191 zip codes. This approach contains several accuracy issues, described in detail in chapter IV, limiting the value of the results. In addition, the assessed tax values

[5]Institut National de la Statistique et des Etudes Economiques

used for land prices being also estimated from land use, it is unlikely that the results of the two analysis will be significantly different.

Furthermore, for London, a dataset based on the energy certificates that are created when a house was sold between 2008 and 2016 is available from the Ministry of Housing, Communities & Local Government (Data, LonEnergy:2008-16). It contains in particular a field corresponding to the estimated consumption, and the expected consumption if the property is improved. We are not able to directly compare it with the New York dataset since it only reports the domestic consumption, while for New York the domestic consumption is considered homogeneous. It complements nonetheless the different measures to be compared inside London.

3.4. Diversity of accessible activities. We want to find a measure that represents the quality of life in terms of diversity of professional, leisure and social opportunities. Instead of counting the total number of jobs or amenities reasonably reachable, here we want to describe the accessibility to amenities through the actual composition of the surrounding neighbourhood at different scales. The rationale is that the types and proportions of each activity shape the potential lifestyle of an individual. For example, if a neighbourhood has low racial segregation but is deprived of leisure facilities favouring social interactions, its population may feel more isolated than in a neighbourhood where the segregation is high, but where interactions are encouraged. To be able to differentiate between each type of activities and to be able to calculate their respective proportion, we intend to use detailed land use data.

Land use cannot be integrated directly as a measure as it is by essence categorical. In the description of the previous inequality factors, we have already alluded to ways of transforming land use into a measure through the way tax assessed value was assigned and through the way energy consumption was estimated. We want however to translate a different perception of land use, which is the diversity of activity accessible at different scales from an individual perspective, assuming for simplicity that the different types of activities are equipollent. To do that, Barner et al. (2018) propose a methodology based on Shannon's entropy formula that takes into account the multiscale diversity of activity. A phase space is created whose coordinates are represented by a matrix, called *state matrix*, where the rows represent the proportion of each activity at a scale defined by the column index. The probability distribution $\{p_i\}_i$ corresponding to the frequency of each state in the discretized phase space is then used as the variable of the entropy

formula, resulting in the entropy H defined by

$$H := -\sum_i p_i \log(p_i). \tag{51}$$

This method gives one global entropy value H for the system. However, we can create a local version of it by considering the local "contribution" to the entropy at any given point x given by $\log(1/p_x)$ where p_x is the frequency in the phase space of the state corresponding to the point considered. This local contribution defines an adequate mathematical measure. Alternatively, we can use the probability distribution $\{p_i\}_i$ directly, as it is by definition a measure normalised to be equal to 1 for the entire system.

This approach is difficult to interpret. Choosing the $\{\log(1/p_i)\}_i$ distribution can be understood as computing the diversity that each local situation adds to the city in its whole. Inversely, choosing the $\{p_i\}_i$ distribution measures how similar each local situation is compared to the other situations (how homogeneous the city is). A highly diverse city is probably preferable when coupled with an efficient transportation system, while a locally homogeneous city is more equalitarian when transportation is lacking. Alternatively, we could include the efficiency of the transportation system in the choice of the multiple scales defining the state matrix and aim for homogeneity. For now, we hope to find multifractality in these new, not yet fully refined, measures.

As mentioned in the energy section, the PLUTO database presents highly detailed land use data for New York (Data, NY:2002-18). Although irregular, the description is detailed enough to create six broad working categories (residential, office, store, education, health and other) to test the methodology. Other datasets exist for London and Kyoto, but were discarded due to the New York results not presenting the same level of interest as those obtained for the other measures.

In summary, we have chosen to apply the multiplier multifractal moment method to calculate the "best multifractal fit" of four inequality measures (real estate, energy consumption, income and diversity of activity) in four cities (London, Paris, New York, Kyoto and a few basic models (uniform, polycentric and DLA). These case studies will be presented in the next chapter and will operate the comparisons that are represented in the diagram of figure III.3, based on the datasets summarized in table III.1. The scientific soundness of the methodology will be ascertained in the following chapter based on the obtained results by comparing them to the classic inequality and segregation indicators.

TABLE III.1. **Summary of all datasets.** PC means post-code, BBL means Borough-Block-Lot, IRIS means "Ilots Regroupés pour l'Information Statistique", LSOA means Lower Layer Output Area and CT means Census Tract.

Land/house prices				
CITY	TYPE	DATES	SCALE	ORIGIN
London	Transactions	1995-2016	PC	HM Land Registry
New York	Transactions	2003-2015	BBL	NYCOpenData
New York	Tax estimations	2002-2016	BBL	PLUTO
Kyoto	Tax estimations	1912-2012	Lot	KCOpenData
Paris	Prices (sqm)	2014	IRIS	UMI
Energy consumption				
CITY	TYPE	DATES	SCALE	ORIGIN
New York	Estimations	2009	BBL	PLUTO
London	Certificates	2008-16	PC	HCLG
Income & Job accessibility				
CITY	TYPE	DATES	SCALE	ORIGIN
London	Mean estimations	2001-2013	LSOA	GLA
New York	Mean estimations	2010	CT	Census FF
Paris	Mean estimations	2014	IRIS	UMI
Paris	# Jobs access.	2014	IRIS	UMI
Land use				
CITY	TYPE	DATES	SCALE	ORIGIN
New York	> 200 Categories	2002-2016	BBL	PLUTO

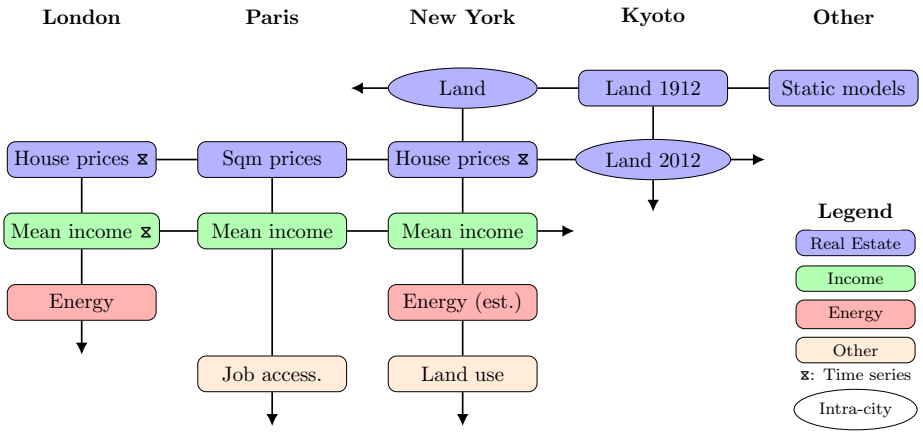

FIGURE III.3. **Summary of all comparative analyses.** Dataset on a same arrow are compared. An hourglass indicates a time series and an elliptical box means that several boroughs of the city are compared to one another.

CHAPTER IV

Case studies: London, New-York, Paris and Kyoto

In this chapter, our selected multifractal methodology, the multiplier method with a vertical rescaling, is applied to several urban measures in real case situations. Due to the high quality of available datasets for real estate and due to the particularly interesting results that stem from those, the real estate dimension of inequality will nourish the largest part of the results. Additional results on income, job accessibility, energy consumption and diversity of land use are also presented. The first section is devoted to a more in depth presentation of all the datasets. The second section gathers and compares the results from real estate and income distributions across Kyoto, New York, Paris and London. The third section is focused on comparing several measures inside a same city. We will in particular evidence that income alone is not enough to characterize inequality and that real estate and energy consumption should also be considered.

Throughout the chapter, we will prove that many urban measures indeed possess multifractal characteristics, and that the method is able to differentiate efficiently between different situations and to provide useful information. We will show in particular that multifractality is particularly adequate to study the spatial dimension of the measures rather than their distributional characteristics. We will also confirm that there is a trend of cities evolving from multifractality towards monofractality, and that income alone is not enough to characterize inequality.

The functions and codes in the R language used for the main analyses are available in the following repository: Codes (2018) (see references).

1. Datasets

We present the different datasets used to conduct the analysis, and explain the technical decisions taken to make them suitable for comparison post analysis. The richness and quality of the real estate data is reflected by the particularly detailed way in which we display them. Although some of the raw datasets used for the analysis contain personal information, the data was treated anonymously and no personal information is disclosed in this chapter. The maps shown are aggregated to larger scales and the results

only provide information for the city as a whole. All the data has been converted into grids. Each cell of the grid contains the sum of the measures of all the geographic areas considered whose centroid fall inside the cell. The grid is then processed as described in section 4 of Chapter II. A summary of all grid resolutions and equivalent distance in meters is given in table IV.5.

1.1. Real estate. For London, the HM Land Registry provides a highly detailed dataset containing all the housing transactions that have happened in Greater London since 1995 (Data, HMLR:1995-16). Although the transactions are given individually with full address and date of transaction, they are aggregated by Postcode (PC) and year using a sum. The resulting measure represents the total housing market value for each PC. Considering that London is a highly dynamical market, we can assume that houses do not stay unsold for long periods, so that the actual transactions are a truthful representation of what was available for each year at each PC. The distribution for the year 2016 (aggregated by LSOA) can be seen in figure IV.1.

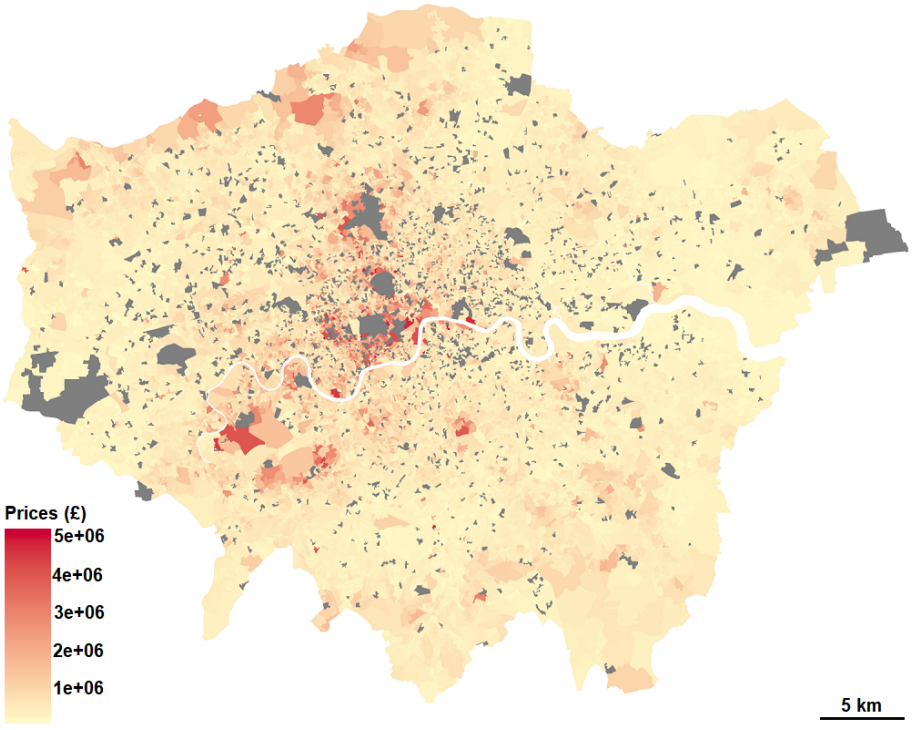

FIGURE IV.1. **London house transactions in 2016.** Prices are represented from red (most expensive) to yellow (least expensive). Gray indicates unavailable data.

In figure IV.2, the distributions from 1995 to 2017 are presented in a common price scale. Note that 2017 is incomplete, and was not used for the analysis. It is noticeable that in the 90s the eastern parts of London were

not considered attractive, which is evidenced by a lot of grey indicating no transactions in the corresponding LSOAs. As prices became more and more unaffordable, the city expands to previously neglected zones. The influence of the 2008 crisis is obvious, with the appearance of dispersed grey areas (particularly in 2009) indicating a shaken market.

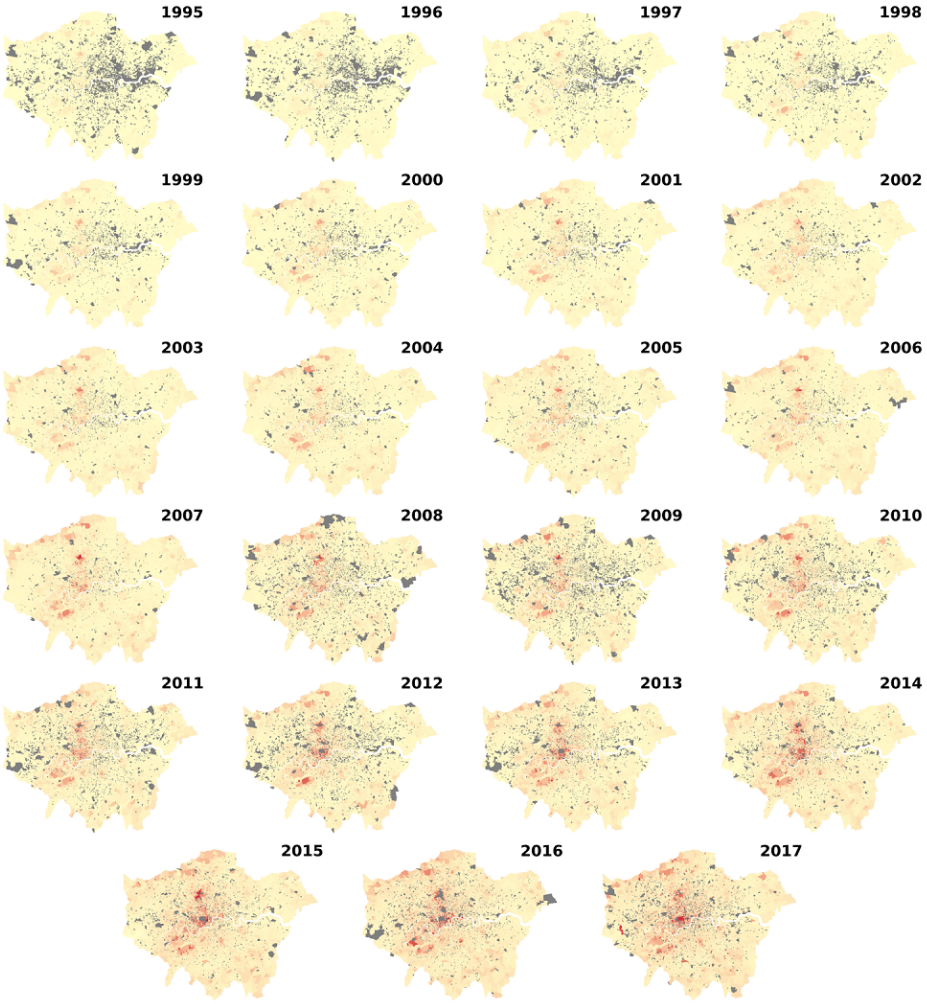

FIGURE IV.2. **London house transaction distributions from 1995 to 2017.** The price scale is common for all years and identical to figure IV.1.

The lowest price paid is consistently kept at around £50k throughout the years, while the average and maximum price paid increase every year, with the exception of 2009. See figure IV.3 for more details. The maximum price paid has increased exponentially in the few recent years. It is to be noted that transactions cover any sell made to a private buyer at one registered address. As a result, privately buying a multi-flat building as investment

counts as one transaction. The typical number of values, range, mean and standard deviation for these sets is given in table IV.2.

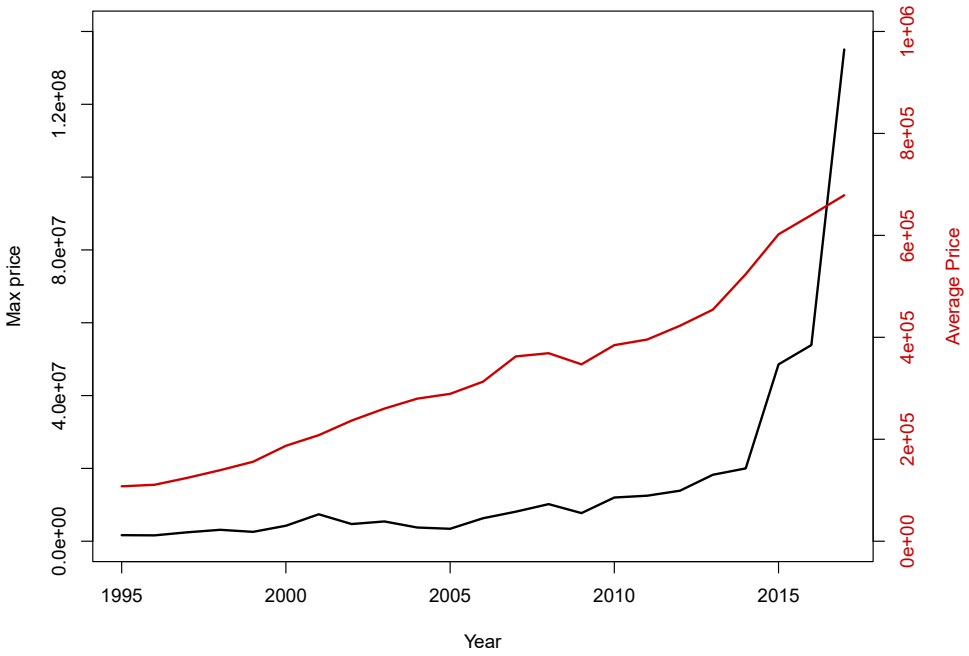

FIGURE IV.3. **London average and maximum price paid from 1995 to 2017.** The scale for the maximum price paid is indicated on the left while the scale for the average price paid is indicated on the right. Prices are in GBP.

For Kyoto, two datasets were made available by Yano et al. (2007, 2008, 2009, 2011). The first one is a digitalization of a cadastral map first published in 1912. All land is divided into lots registered to a single owner for which tax assessed price, category, and area are known. We used the total price of each lot marked as residential (82% of all lots) as the base unit for the analysis. Assuming that the land lots are not meant to be divided, it represents accurately all existing residential land assets in the city. The values are paired with the centroids of their corresponding lots. The data is then processed as a matrix representing a grid overlay over the Kyoto map.

A second dataset consists in land tax assessed value by road valuation around 2012, as provided by the official Open Data website maintained by Kyoto City (Data, KC:2012*a*). The price is given as mean land price per square meter along each road segment, where a road segment is defined as any part of a road included between two street intersections (or dead ends). Most road segments are edges of a block, and some are smaller intra-block streets. Making the unavoidable assumption that the difference in depth between different residential buildings is negligible compared to the length of the roads segment, we have multiplied the mean price along each segment

by the length of said segment. The result are values proportionate to the sum of all land lot prices along each segment. Since multifractals are invariant under a linear transformation, those values can be seen as approximations comparable to 1912 lot values (although at a broader scale). Both the full extent of modern Kyoto and its intersection with the extent of 1912 Kyoto will be considered.

To be able to compare accurately Kyoto in 1912 and in 2012, it would have been preferable to use the same resolution in both cases. Unfortunately, the road valuation data for 2012 creates undesired "gaps" between data points when plotted at the resolution used in the 1912 case. Those gaps do not describe real land value well, as price lots should be contiguous or almost contiguous, with only big natural obstacles (such as the Kamo river for Kyoto) representing an actual empty space. To tackle this problem, the resolution used for present Kyoto has been reduced by 4 to obtain a relatively compact grid. A first map was created representing the full extent of the present city at a resolution of 256x256, the same resolution that was used for the 1912 extent of the city, despite the new city being roughly four times bigger than the old city. A second map was created to represent the evolution of the old city alone. It comprises only the roads that are fully included in the boundaries of the 1912 city. This map is at a resolution of 128x128, i.e. four times lower than for the 1912 map, despite the geographical extent being identical. The study areas for each case are illustrated in figure IV.4. Refer to table IV.2 for a statistical description and to figure IV.9(b & c) for an histogram of the distributions.

For New York, the Department of City Planning has released the PLUTO database, which provides all yearly assessed tax values for land prices at 'Borough Block Lot' (BBL) level since 2002, except for the year 2008 (Data, NY:2002-18). The prices are divided into prices for land alone and prices for land and built assets bundled together. The prices for land alone are similar to those for the lots defined for Kyoto, although the BBL scale is somewhat intermediary between the smaller 1912 lots and the bigger 2012 blocks. However, since multifractal analysis is scale invariant, this difference in scale does not diminish the high comparative value with Kyoto's land prices. The dataset for the year 2016 is represented in a logarithmic scale in figure IV.5.

According to the documentation, the land tax assessed prices appearing in the PLUTO database for New York are estimated by the Department of Finance from the market value as if the land was vacant and unimproved. The prices are then multiplied by a percentage for the property's tax class, itself depending on its use. Since the lot shapes and sizes have known little

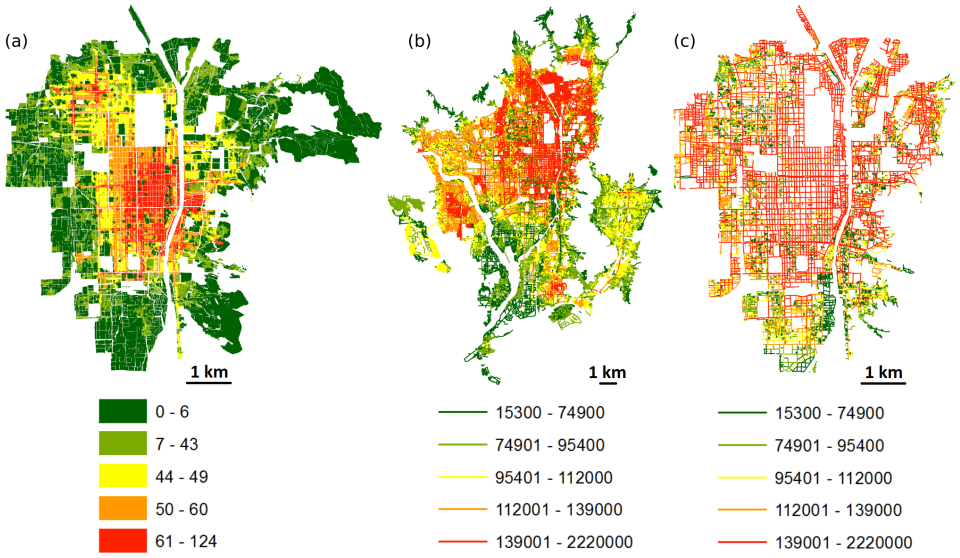

FIGURE IV.4. **Kyoto land price dataset.** (a) Kyoto, 1912 extent; (b) Kyoto, 2012 extent; (c) 2012 Kyoto cropped to the 1912 extent. All prices are expressed in Yen (1 Yen of 1912 is worth approximately 2000 Yens of 2012).

change, especially in Manhattan, since the last development works of the early twentieth century, it can be hypothesized that today's prices are still in good distributional correspondence with what they were then. As a matter of fact, between 2002, when the PLUTO data was first gathered, and 2016, only marginal adjustments were made from one year to another. Those adjustments are reported in table IV.1. Note that the period from 2008 to 2010 is disrupted due to a reworking of the database.

In addition, a second dataset containing the actual transactions with full address, obtained from the NYC Open Data website (Data, NY:Sales), was used for comparison with the London dataset. Similarly, the values have been aggregated to the BBL level. In figure IV.6 pannel (a), we can see the max and mean price paid per transaction. Each year, between 20% and 35% of the transactions are recorded as free, in addition to many transactions occurring at symbolic prices. These are transfers of ownership without money involved, such as inheritance. The total volume and portion of free transactions are shown in panel (b). The effect of the 2008 crisis is clearly visible with a sudden decrease in prices, a gradual decrease in transaction volume, while the portion of free transactions increases significantly. The map corresponding to the transactions averaged at CT level for the year 2015 can be seen in figure IV.7. The visual differences from one year to another being minimal, we do not show the map for the other years. As before, more details can be found in table IV.2 and in figure IV.9(d & e).

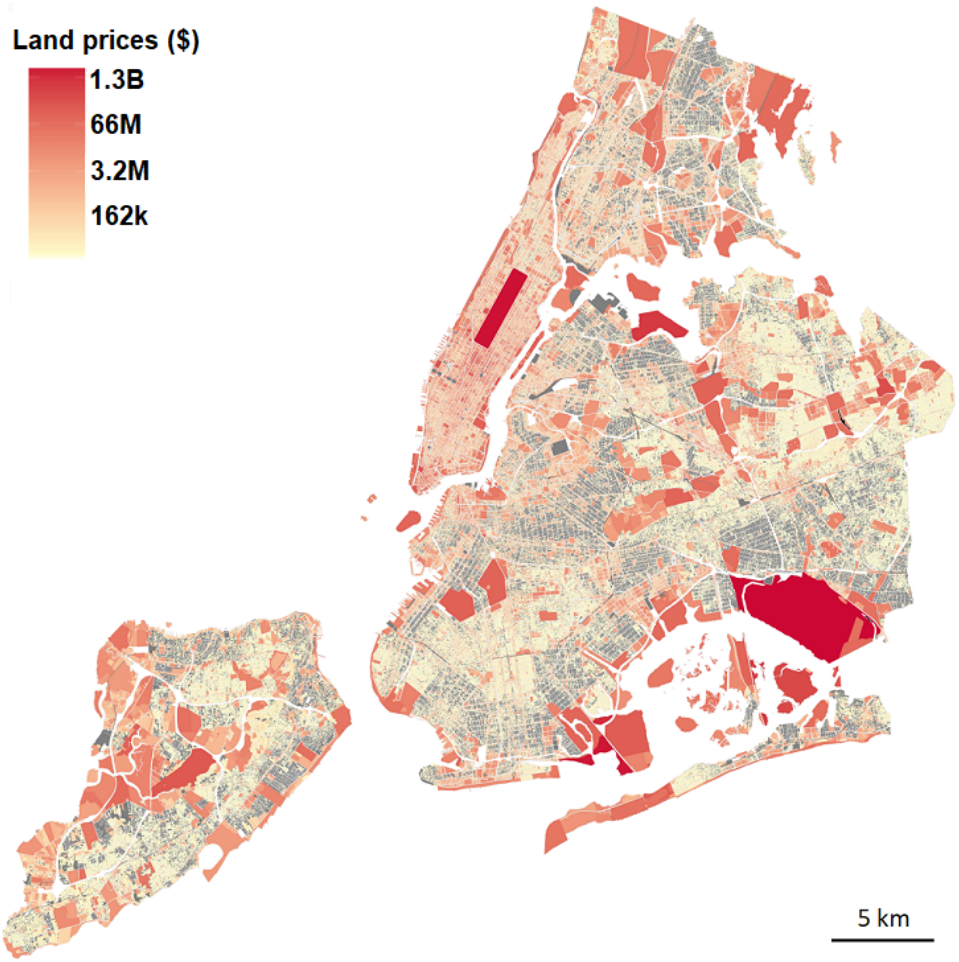

FIGURE IV.5. **New York land price 2016 dataset.** Prices are represented with a logarithmic scale from red (most expensive) to yellow (least expensive). Gray indicates unavailable data.

For Paris, a dataset obtained from the UMI[1], based on data from INSEE[2] and estate agencies public data, provides the average square meter prices at 'aggregated units for statistical information' (IRIS) level in 2014. IRIS were implemented to gather statistics throughout France and aim at subdividing the territory into units containing around 2000 people. Although their definition varies widely in the countryside and small towns, they are quite regular inside Paris with 5262 IRIS for a population of around 10 millions, and an average size of 2.29 square kilometres. Because square meter prices are a density that cannot be used directly, it is necessary to multiply the prices by the population count inside each IRIS. In a sense it forces to make

[1]Urban Morphology Institute
[2]Institut National de la Statistique et des Etudes Economiques

TABLE IV.1. **Yearly change in land tax assessed value in Manhattan from 2003 to 2016.** #LC is the percentage of lots changed, MAC is the mean absolute change, and TC is the total change of the mean. Data is missing for year 2008, and year 2009 has been omitted as a result. Note that year 2010 yields a unusually high MAC due to lot renaming.

Year	#LC	MAC	TC
2003	26.7%	5.7%	3.9%
2004	67.1%	14.6%	-5.0%
2005	62.0%	26.4%	4.7%
2006	52.8%	8.8%	1.8%
2007	51.4%	17.8%	1.4%
2010	50.1%	50.9%	3.4%
2011	53.2%	11.9%	1.0%
2012	42.9%	20.0%	0.6%
2013	43.4%	6.6%	0.1%
2014	44.8%	6.4%	0.4%
2015	44.2%	9.2%	1.0%
2016	44.6%	8.8%	0.6%

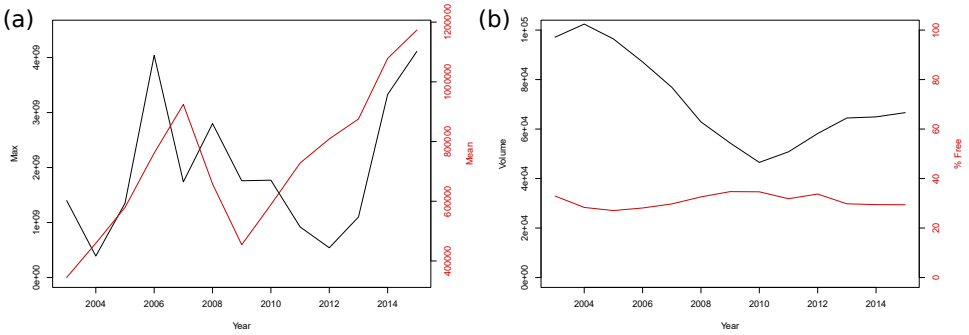

FIGURE IV.6. **House transactions from 2003 to 2015 in Ney York.** (a) Evolution of the max and mean sale price. (b) Evolution of the number of transactions and percentage of transactions that were given for free (note that these exclude transactions at a symbolic rate).

the factually wrong assumption that the average accommodation size is the same across all IRIS. The assumption is not unreasonable, however, since according to INSEE, the standard deviation of the average accommodation size by department is only 2.89 for an average of 32.575. Additionally, this hypothesis can be thought of as an interesting equality ideal. Only 5000 data points is in the low limits of multifractal analysis requirements, and compares poorly with the much finer scale of the other datasets. Moreover, the nature of the data for Paris is quite different from the rest. This data

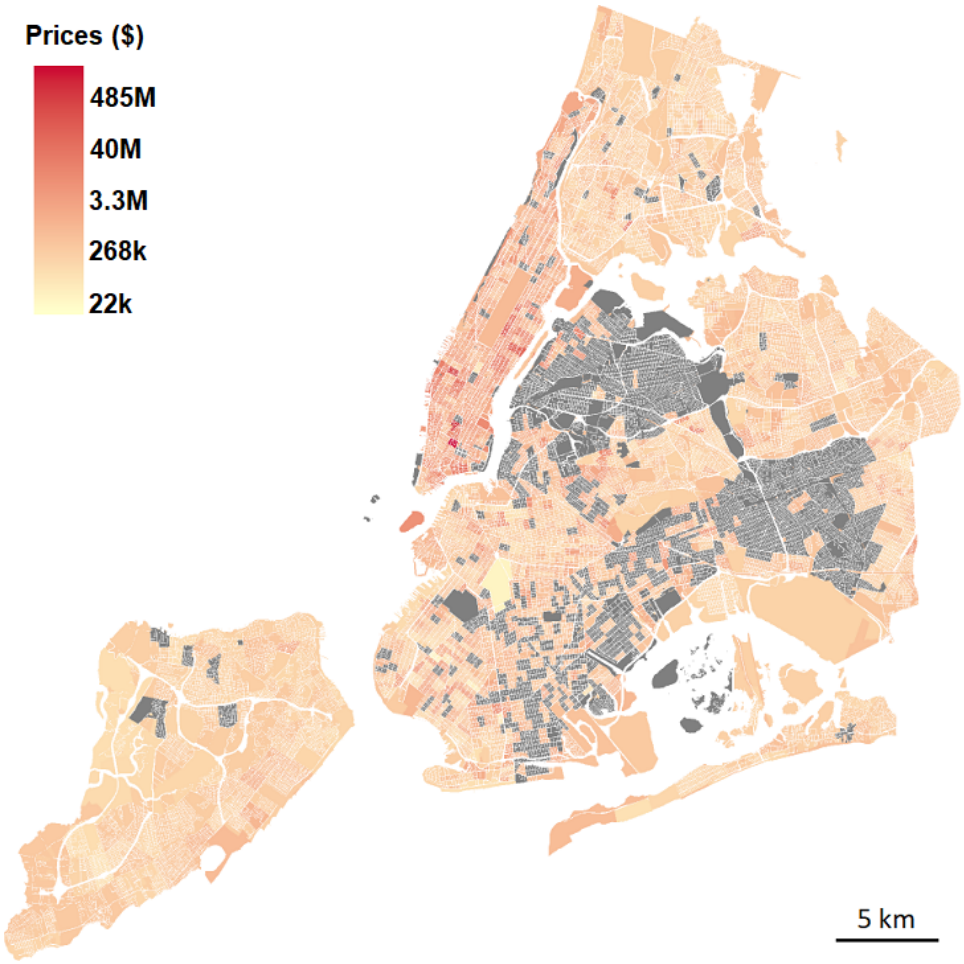

FIGURE IV.7. **New York transactions 2015 dataset.** Prices are represented with a logarithmic scale from red (most expensive) to yellow (least expensive). Gray indicates unavailable data or transactions below 100$.

comes handy, however, when it is related to the INSEE census variables, such as number of jobs and average income, also at IRIS level. Both the true prices per square meter and the prices per square meters multiplied by the population count are represented in figure IV.8.

In the calculations below, since the IRIS are represented by their centroids, we have discarded all IRIS of size greater than 3km^2 for which the centroid is not a good approximation of their geometry (accounting for 23% of all IRIS). The dataset remains quite sparse even after this process, as indicated by a low (mono)fractal dimension.

The data characteristics are summarized in table IV.2. The price distributions can be seen in figure IV.9. They are all akin to either a log-normal distribution, or two intertwined log-normal distributions.

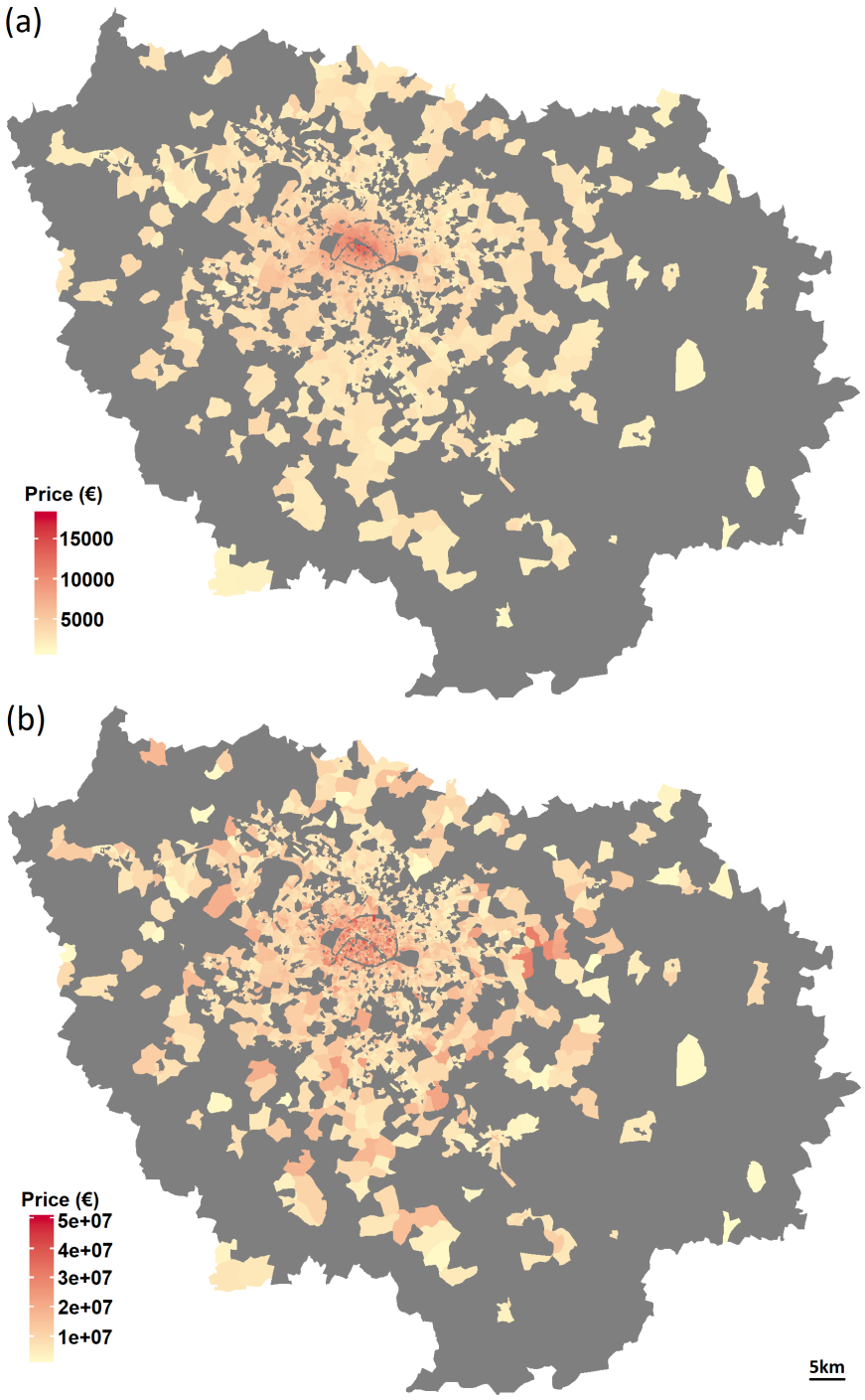

FIGURE IV.8. **Paris housing price in 2014.** Prices are represented from red (most expensive) to yellow (least expensive). Gray indicates unavailable data. (a) True prices per square meter. (b) Prices per square meter multiplied by the population count in each IRIS.

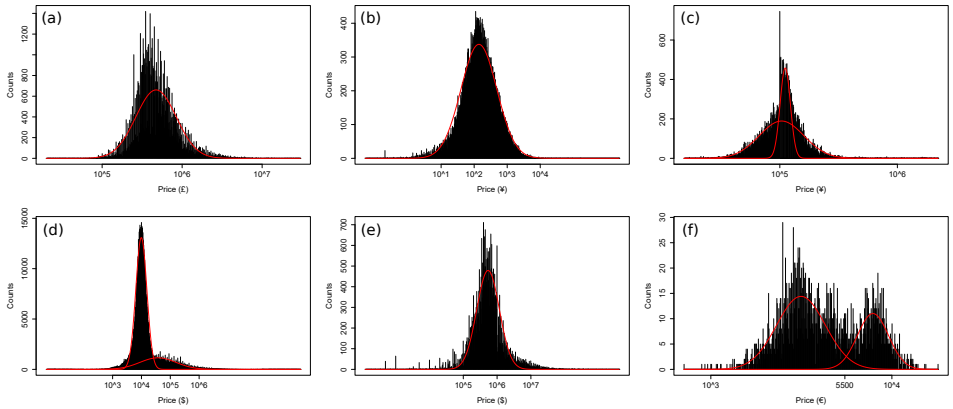

FIGURE IV.9. **Price distributions.** (a) London transactions, 2016. (b) Kyoto tax assessed land prices, 1912. (c) Kyoto road valuations, 2012. (d) New York tax assessed land prices, 2016. (e) New York transactions, 2015. (f) Paris Sqm price, 2014.

TABLE IV.2. **Summary of data characteristics for Real Estate.** All prices are indicated in their original currency, without taking inflation into account. For datasets covering multiple years, the typical number of values for one year is given. # stands for number of values, Sd stands for standard deviation.

City	Type	#	Min	Max	Average	Sd.
London <2016s	Transactions	132k	30k	55M	291k	400k
Kyoto 1912	Land Tax	53k	0.05	2.45M	345	11k
Kyoto 2012	Road valuation	42k	15k	2.22M	116k	93k
New York 2000s	Land Tax	83k	5	3.21B	108k	6.0M
Manhattan 2000s	Land Tax	43k	110	2.86B	1.18M	15M
New York 2000s	Transactions	50k	0	400M	1.04M	14M
Paris 2014	Sqm prices	2.5k	710	18k	3.8k	3.1k

We expect that the ranking in width of the spectra will be consistent with the ranking in Gini coefficients for the different cities. The Gini coefficient for the Kyoto land price distribution in 1912 is 0.666, although it can be lowered to 0.606 by removing the Imperial palace and the temples. In 2012, it is lowered to 0.479 for the entire city, and to 0.520 for the extent corresponding to the 1912 city. A more extensive comparison of traditional inequality indicators for the evolution of Kyoto and with models based on rearrangements of the land price distribution and the multifractal spectra is proposed in section 2.1 of chapter V. The Gini coefficient for one year of transactions in London is 0.366 on average, with a standard deviation of 0.031, and for one year of transactions in New York, it is 0.771, with a

standard deviation of 0.050. A detailed breakdown of the evolution of these prices is given in section 2.3 of chapter V, together with an analysis around the 2008 financial crisis. The Gini coefficient is intermediary for Paris with 0.481. It is by far the highest for New York with 0.902. Inside New York, the coefficients are similar with 0.840 in Manhattan, 0.808 in the Bronx, 0.834 in Brooklyn, 0.830 in Queens, and 0.739 in Staten Island. We will see in the result section and in chapter V that the spectra are consistent with these coefficients.

1.2. Income. The Greater London Authority (GLA) has released an estimation of the unequivalised mean household income at Lower Layer Super Output Area (LSOA) level (Data, LonIncome:2002-13). The LSOA level aims at separating the population into groups of around 1700 people (with a minimum of 1000). There are a little under 5000 LSOAs in Greater London, which is in the low limits of acceptability for multifractal analysis. The dataset covers two yearly estimates from 2001 to 2013, one taking into account the inflation while the other does not. For New York, the best data found was taken from the Census FactFinder and includes the 2010 population count and the estimated mean household income at Census Tract (CT) level (Data, NYIncome:2010). For Paris, the median income and population count in 2014 at IRIS level was obtained from INSEE (Data, ParIncome:2014*a*). Median income does not hold the same value for this analysis as average income, and we only use it for reference to a scenario where the average and the median income would be equal. The data characteristics are summarised in table IV.3. Corresponding maps are shown in figure IV.10, each with its own income scale from the city's minimum value to the city's maximum value. The distributions are shown in figure IV.11. Similarly to price distributions, all three are close to log-normal distributions.

TABLE IV.3. **Summary of data characteristics for Income.** All income are indicated in their original currency, without taking inflation into account. # stands for number of values, Sd stands for standard deviation.

City	Type	#	Min	Max	Average	Sd.
London 2000s	Average	4.8k	20.7k	183k	43.3k	13.7k
New York 2010	Average	2.2k	11k	436k	84.7k	43.1k
Paris 2014	Median	3.8k	11.8k	89k	34.7k	10.3k
Paris 2014	#Jobs 30m	4.2k	0	2.1M	154k	353k
Paris 2014	#Jobs 45m	4.2k	0	3.2M	513k	839k

It is to be noted that these datasets have good comparative value respectively with the house transactions dataset for London (aggregated at

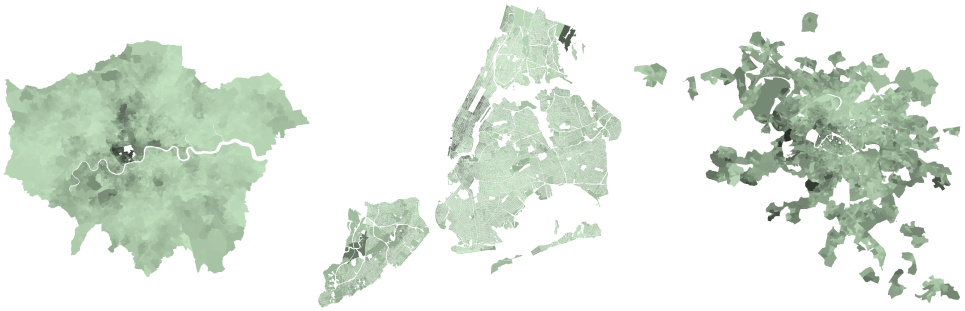

FIGURE IV.10. **Income datasets.** Average income for London (2013), New York (2010), and median income for Paris (2014). Each map is plotted according to its own continuous income scale, from the minimum values (light green) to the maximum values (dark green) reported in table IV.2.

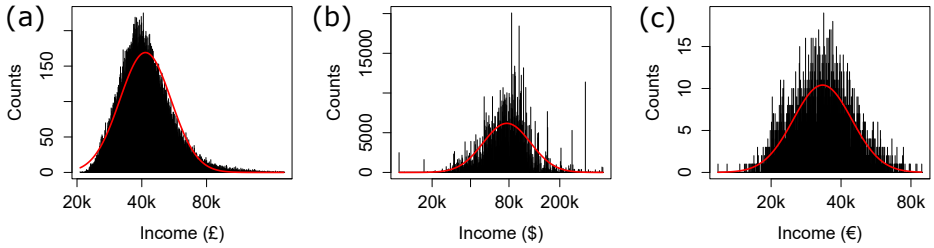

FIGURE IV.11. **Income distributions.** (a) London, 2000s; (b) New York, 2010; (c) Paris, 2014.

the LSOA level), the BBL transaction dataset for New York (aggregated at the CT level), and the square meter rent price dataset for Paris described in the real estate section. Additionally, the London dataset also has some time evolution analysis value, limited by the short time frame (13 years), but interesting nonetheless since it covers the 2008 financial crisis. It is similar in that respect to the house transactions dataset.

For all these datasets, the actual variable we study is the income multiplied by the number of people living in the area. This is to guarantee that the measure is indeed additive, and to represent the total carried income value. The relatively large size of LSOA, IRIS and CT is a severe limitation for a fine analysis of the income distribution itself.

A quick observation of figure IV.11 suggests that the geographical zones where the income is high are in good correspondence with those where the house prices are high. We therefore expect that the spectra for income and real estate will be similar. Furthermore, the Gini coefficient for the income distribution multiplied by the population count in London is 0.155 on average, with very little variation from one year to another[3]. This is a

[3]The standard variation of the set of yearly Gini coefficients is only 0.005.

particularly low number compared to Paris (0.302) and New York (0.479). Inside New York, the Gini coefficient is the highest in Manhattan (0.470), while it is very similar for the other four boroughs (0.356 in Bronx, 0.320 in Brooklyn, 0.342 in Queens and 0.298 is Staten Island). We therefore expect a narrower spectrum for London than for Paris and New York. A more extensive analysis of the datasets with traditional inequality indicator is provided in section 2.2 of chapter V.

In addition to these datasets, we include here some data describing the number of jobs accessible in 30 minutes and 45 minutes from every IRIS in Paris. This data is presented in figure IV.12. It is part of the data also describing square meter prices and median income. Since the number of jobs accessible induces competition within the job market, it has an influence on the potential salary, work conditions and average time to find a job an individual can expect. It is therefore thematically linked to income. We primarily intend to use this dataset to check the potential correlations between house prices and accessibility.

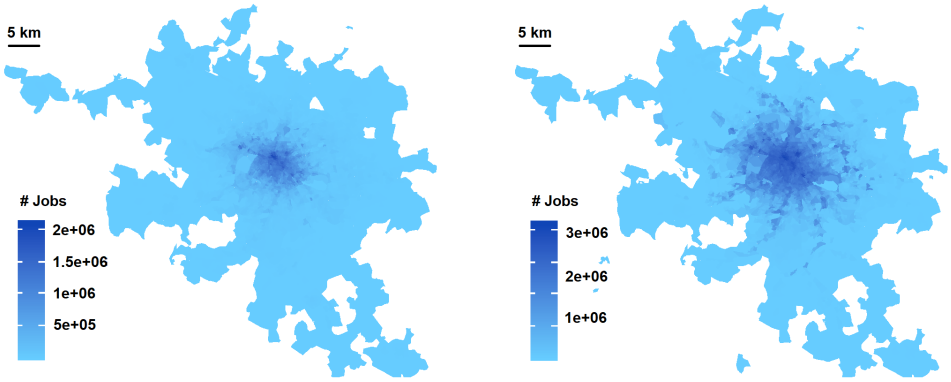

FIGURE IV.12. **Number of jobs accessible in Paris.** (a) Jobs accessible in 30 minutes. (b) Jobs accessible in 45 minutes.

1.3. Energy consumption. For the city of New York, Howard et al. (2012) estimate energy consumption from the land use description from the PLUTO database described above, coupled with data from the New York City Mayor's Office gathering the annual electricity, natural gas, steam and fuel oil consumption for 191 zip codes. The average consumption per type of land use is estimated using a multilinear regression from the values measured for the 191 zip codes. A map of energy estimates is then deduced for all of New York. They chose the year 2009 due to the weather conditions for that year being the closest to the 30 year average values, so as to limit meteorological bias.

This approach contains several issues. First, the land use description in the PLUTO database is irregular. A land use code is first used to sort the lots into 11 broad categories depending on the main social function, then a building class code is used to sort the lots into over 200 more technical categories. For computational simplicity, Howard et al. (2012) reduced the number of categories to a total of 7: residential 1-4 families, other residential, office, store, education, health and warehouse. However, a closer look at the content of the categories enlightens some unresolved overlapping (for example, education, although mainly made of school-type buildings, encompasses at least one store and one warehouse). Another issue is that fuel oil consumption in the Mayor's Office data is only estimated and not measured. Since these limits are due to the nature of the available data, there is no particular solution to avoid them.

Nonetheless, we have reproduced their approach for that same year 2009 on Manhattan using the PLUTO database for land use reference. The other four Boroughs (Bronx, Brooklyn, Queens and Staten Island) are not considered in order to save computational time as they do not add new elements to the discussion. The resolution is identical to the one used for the PLUTO assessed land price to ensure comparability. This dataset is mapped in figure IV.13, the statistical description is given in table IV.4.

For London, the Ministry of Housing, Communities & Local Government has released a dataset containing the energy performance certificate for many domestic buildings in England and Wales (2.2M datapoints Data, LonEnergy:2008-16). Those were established when a sale took place between 2008 and 2016. We make use of the energy consumption field estimating the yearly consumption in kWh/m^2, the estimated potential energy consumption (after improvement suggested by the contractor would be carried out), as well as individual lightning, heating and water heating costs in GBP. The energy consumption is multiplied by the given floor area in square meter, to obtain the total consumption. The statistical summary is presented in table IV.4. This dataset is not comparable to the New York one, since it is focused on domestic use only.

1.4. Diversity of accessible activities. We implement an entropy formula to quantify the diversity of land use. We use the same land use data that allowed us to derive the energy estimates for Manhattan in 2009. The buildings are all sorted into 8 broad categories (residential 4 families or less, residential more than 4 families, office, store, education, health, warehouse, and other). The result can be seen in figure IV.15. In the figure, only the category covering the most space is represented for each lot. For the actual entropy computation, both residential categories were combined and

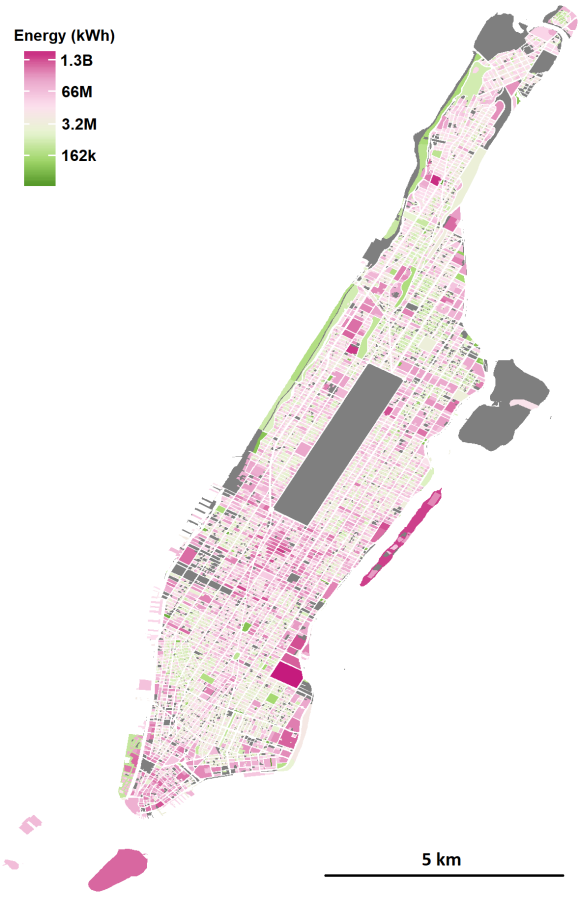

FIGURE IV.13. **Energy consumption estimations in Manhattan.** The scale goes from green (low consumption) to pink (large consumption)

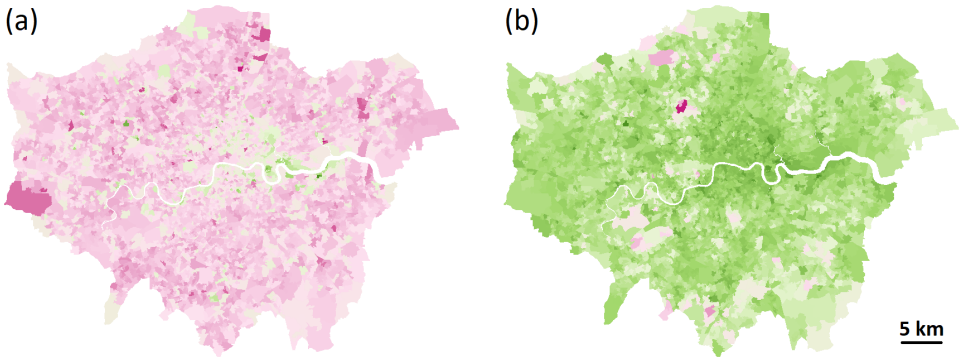

FIGURE IV.14. **Energy consumption estimations in London.** (a) Estimated consumption by square meter from low consumption (1 kWhm^{-2}, green) to high consumption (1000 kWhm^{-2}, pink). (b) Estimated total consumption from low consumption (32 kWh, green) to large consumption (15.8 BWh, pink).

TABLE IV.4. **Summary of data characteristics for Energy.** # stands for number of values, Sd stands for standard deviation.

City	Type	#	Min	Max	Average	Sd.
Manhattan 2009	Electricity (kWh)	44k	0	1.4B	5.6M	28M
Manhattan 2009	Fuel (kWh)	44k	0	2.0B	8.1M	32M
Manhattan 2009	Total (kWh)	44k	0	2.8B	14M	54M
London 2008-16	Sqm energy (kWh)	83k	1	1k	266	130
London 2008-16	Total (kWh)	43k	32	15M	21k	21k

the warehouse category was ignored in order to decrease the total number of categories to a more manageable six.

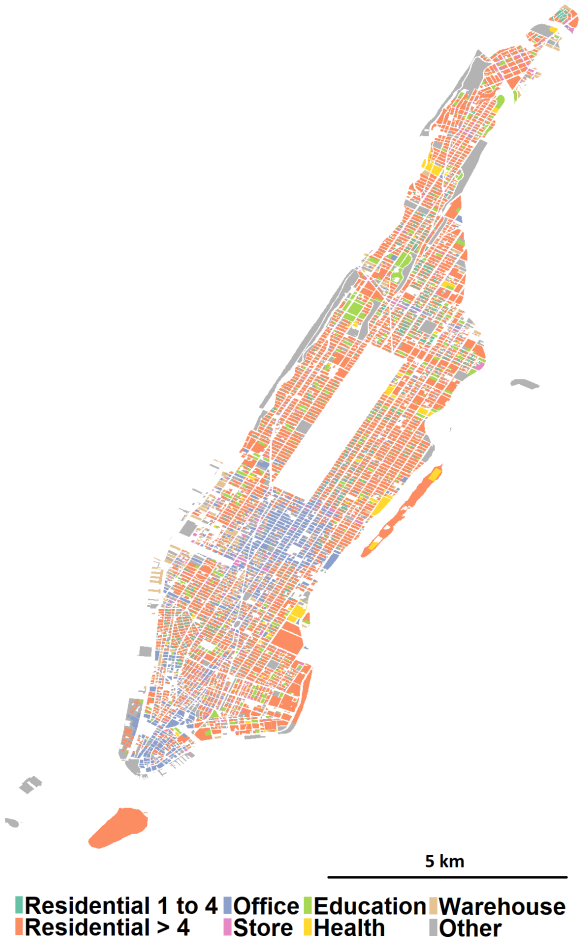

FIGURE IV.15. **Primary land use in Manhattan in 2009.** Non available data is represented in white.

The methodology is based on a working paper by Barner et al. (2018), where more details and applications to London land-use can be found. In

this approach, the data is converted into a grid. For each cell x, we denote x_i^r the proportion of category i in a neighbourhood of radius r around x. Then, assuming we have n categories and N scales, the state of cell x across several scales is fully characterized by the matrix

$$M_x = \begin{bmatrix} x_1^{r_1} & x_2^{r_1} & \dots & x_n^{r_1} \\ x_1^{r_2} & x_2^{r_2} & \dots & x_n^{r_2} \\ \vdots & \vdots & \vdots & \vdots \\ x_1^{r_N} & x_2^{r_N} & \dots & x_n^{r_N} \end{bmatrix}.$$

By definition, the elements of the matrix are all between 0 and 1. We aggregate them into 8 bins. For our study, we consider 3 scales: immediate proximity (200m), proximity (2km), and proximity via transport (6km). Each matrix is therefore made of $6*3 = 18$ elements that take one out of 8 possible values. Each cell is therefore represented by one out of 144 possible matrix states. The total entropy of the system is then given by Shannon's entropy formula

$$H := -\sum_i p_i \log(p_i), \tag{52}$$

where p_i is the probability of state i, i.e. the frequency of cells in state i in the system.

For Manhattan, this formula gives a global entropy of 2.25. For the purpose of multifractal analysis, each point is given a value corresponding to its "local" contribution to the total entropy, i.e. $\log(1/p_x)$, where p_x is the frequency in the matrices space of the state corresponding to the cell considered. Figure IV.16 represents Manhattan entropy map in a grid of size 187×277.

The different grid resolutions that we used for each city are presented in table IV.5. These are the final resolutions chosen to ensure maximum comparability, although others were tested. Kyoto, in particular, has been tested with a resolution twice as precise. The spectra were not significantly changed, which is consistent with multifractality's scale invariance. The resolution for Paris is broader than for the other cities due to the relatively large scale of the IRIS. It is the minimum resolution that allowed a fractal dimension $f(\alpha_0)$ higher than 1.5. The sizes chosen to operate the gliding boxes are 1, 2 and 8 times these resolutions, as discussed in section 4 of chapter II.

2. Comparisons between cities

In this section, we present cross-cities analysis on real estate and income data. We first look at the early 20^{th} century Kyoto and New York

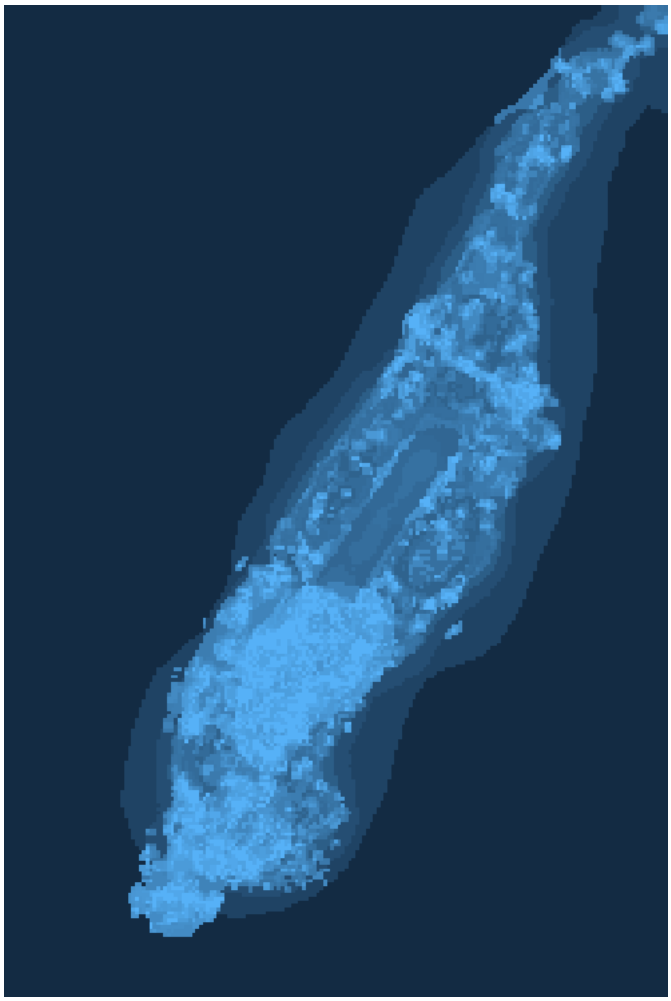

FIGURE IV.16. **Land use entropy map of Manhattan in 2009.** Each pixel represents the local contribution to the total land use entropy of Manhattan. An exact scale is not provided as these values have no tangible meaning and only depend on the frequency of similar pixels.

land assessed tax prices, complemented with some static models based on the Kyoto data. Those models are of two kinds: spatial, including a fully uniform random repartition of the prices taken as a null model, realistic polycentric repartitions, and diffusion-limited aggregation (DLA) repartitions representing "maximal" cases; and distributional, including uniform, normal and Pareto distributions of the prices. The technicalities of building the models are given as and when they appear. Next, we study early 21^{st} century real estate in London, New York, Kyoto and Paris and compare the results with the 20^{th} century data. A particular attention is given to the change in spectrum around the 2008 financial crisis in London and New York. We finally compare London, New York and Paris income distributions.

TABLE IV.5. **Grid resolutions used for analysis for all cities.** The boxes are rectangular shapes of size 1, 2 and 8 times these resolutions. Kyoto inter is the intersection of Kyoto in 2012 and the 1912 extent.

City	Resolution (px)	Resolution (m)
London	200x200	450x300
Kyoto (1912)	256x256	15.5x17.5
Kyoto (2012)	256x256	66x90
Kyoto inter	128x128	31x35
New York	1280x1280	120x120
Manhattan	187x277	200x250
Bronx	208x179	200x250
Brooklyn	251x246	200x250
Queens	353x356	200x250
Staten Island	280x221	200x250
Paris	100x100	700x250

2.1. Real estate in the early 20th century. Starting with the 1912 Kyoto data, a first batch of models is built by changing the spatial pattern while the price distribution is kept identical to the true distribution. Three types of spatial distributions are chosen to supplement the true pattern: uniform, polycentric, and DLA. The first one is used as a null model, the second one as a representation of how modern megacities develop (Odland, 1978; McMillen and Smith, 2003; Louf and Barthelemy, 2013), and the third one as a multifractal reference since it is known to generate strong multifractality (Witten and Sander, 1981; Vicsek et al., 1990; Murcio and Rodríguez-Romo, 2009; Rodríguez-Romo and Murcio, 2014). All these models are plotted in figure IV.17 alongside the true distribution. The latter is represented in the top left image. Next to it is the price distribution drawn uniformly. The four figures on the bottom left are DLA models with either 1 or 3 centres exerting different levels of attraction. Finally, the nine models on the right are polycentric models with different number of centres exerting varying levels of attraction. The true spatial distribution uses a logarithmic overlay of the real price distribution, while all other images use an overlay representing the rank of each point in the price distribution after it has been drawn into the space. All images are represented in a grid of resolution 256×256.

The uniform distribution has been drawn 50 times. To generate the polycentric models, a number of centre coordinates (between 1 and 30) are chosen randomly in the grid. Then, all the cells in the grid are ranked

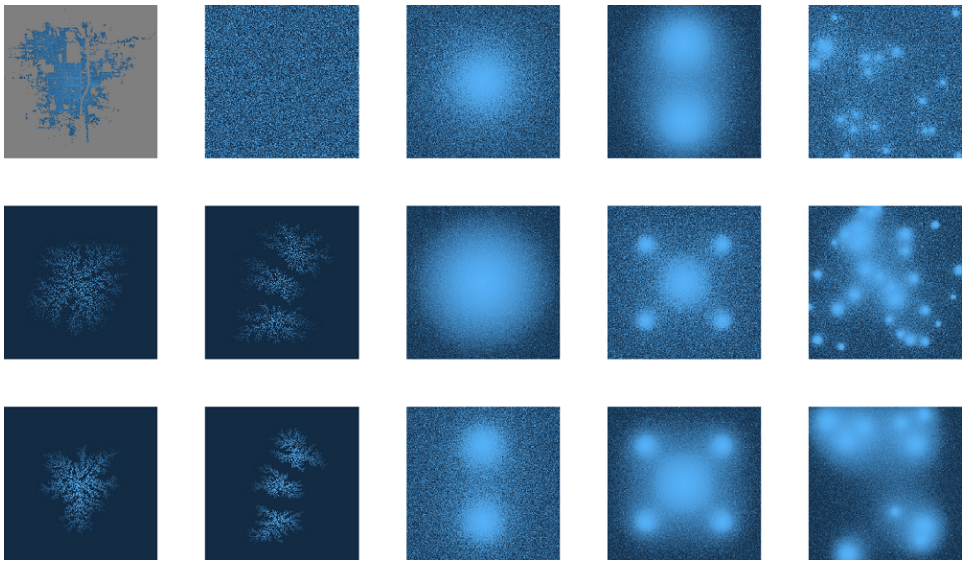

FIGURE IV.17. **Spatial models.** Top left: logarithmic overlay of the real price distribution over the real Kyoto pattern in a grid of resolution 256x256. Next to it: corresponding rank distribution drawn uniformly. Four on the bottom left: rank distribution overlayed over four DLA models with 1 or 3 centres and different levels of attraction. Nine on the right: rank distribution overlayed over nine polycentric models with different number of centres and levels of attraction.

according to the formula

$$s_i = \sum_k b_k / d_{ik}^{\gamma}, \tag{53}$$

where s_i represents the strength of cell i, b_k a weight given to centre k, d_{ik} the distance between point i and centre k, and γ a global "attractivity" parameter. Similarly, the DLA models are generated by first choosing randomly either one or three "anchor" coordinates in the grid. Then, the cells are ranked by introducing "particles" carrying a rank tag (lowest ranks first) into the system. Each particle operates a random walk until it encounters an anchor or a cluster of particles attached to an anchor, and attaches to it with a probability of either 1 or 0.5.

Once all the cells in the grid have been ranked (ties are resolved by a random draw), the prices are mapped over the points by rank order, so that the most expensive prices are closer to the centres or anchors. A noise is previously introduced in the ranked price distribution, by redrawing the price ranks according to a probability distribution

$$r_i^p / \sum r_i^p, \tag{54}$$

where r_i is the current rank in the distribution, and p is a power set to 2 for the polycentric models, and either 1 or 8 for the DLA models.

The spectra resulting from the first batch of models plotted against the true Kyoto distribution can be seen in the top of figure IV.18. On the bottom, the local idealized shapes corresponding to the α values are represented for reference. We have in total: the five most relevant polycentric models (referred to as $C-$ in the legend, where $-$ is the number of centres), fifty iterations of the uniform draw (U in the legend), and two fully ranked one-centre DLA models with normal and halved centre attraction weights and fifty iterations of each DLA model with a noise added to it (respectively Dr, $D.5r$, Dn, and $D.5n$). We can immediately observe that the real distribution (red circles) seems to maximize the width of the spectrum, while minimizing its height. Only some of the DLA models with added noise could create a wider right-spectrum and remain close on the left side. Polycentric models generate fairly weak multifractality, especially considering that the multiplier method tends to artificially widen the spectrum in weak cases. The uniform distribution lays between the polycentric and DLA distributions.

A second batch of models is built by changing the price distribution while the spatial pattern is kept identical. Three distributions are considered: uniform, truncated normal, and Pareto. The uniform distribution is taken as a null model, while the normal and Pareto distributions are the most recurrent distributions observed in urban science (in particular, the Pareto distribution is usually associated to the distribution of wealth). The true distribution is log-normal. To create the distributions, range, mean and standard deviation can be adjusted. Since it is by construction impossible to match all three parameters for each distribution, priority was given to matching the range with the true distribution. When the exceptionally high priced imperial palace is removed, this range consists of values between 0 and 10000 yens. These three distributions are plotted in figure IV.19. In addition to the price distributions being laid over the true spatial pattern, they have also been laid over the uniform spatial distribution for reference.

The results of the second batch of models are represented in figure IV.20. In the first case, overlaying over the true spatial distribution, there is almost no difference in the left part of the spectra, while the right part are very similar, with Pareto distribution giving the widest spectrum. Meanwhile, as can be inferred from figure IV.18, changing the spatial distribution has noticeable consequences on the curves. However, the price distribution does have an impact on the spectrum, as evidenced by the second case, where all four price distributions have been drawn randomly in space. The uniform and truncated normal distributions present almost no multifractality, the very

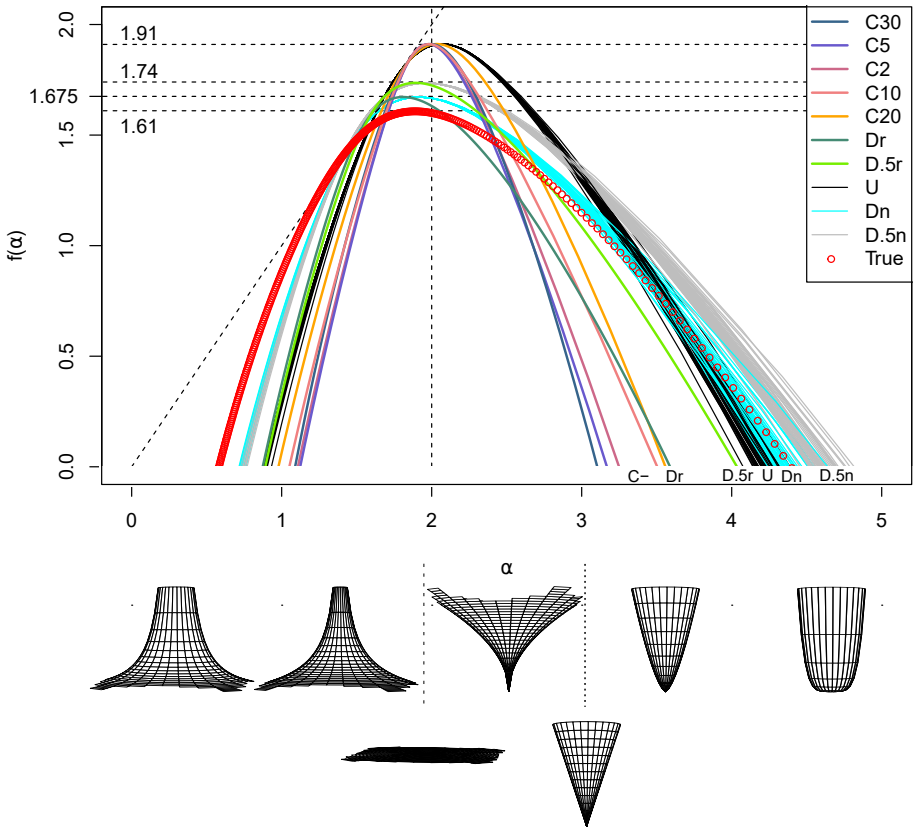

FIGURE IV.18. **Spectra for 1912 Kyoto price distribution mapped over several spatial models.** The models are polycentric (C-, where - is the number of centres), ranked DLA (Dr), ranked DLA with half centre attraction (D.5r), uniform (U, 50 draws), DLA with a noise (Dn, 50 draws), DLA with half centre attraction and a noise (D.5n, 50 draws), and true distribution (True). The corresponding idealized two-dimensional signal is added below the α axis for reference.

narrow spectrum being identifiable to an artefact of the multiplier method. The Pareto and the real distributions produce more convincing spectra, close to one another.

An analysis was performed over the five boroughs of New York: Manhattan, Brooklyn, the Bronx, Queens, and Staten Island at a common resolution to avoid any bias. The results are reported in figure IV.21. The multifractal spectra are quite similar in width for all five boroughs, except Manhattan. However, since the results provided by the method are more stable for the left part of the spectra, it may be more interesting to notice that Brooklyn has a narrower left spectrum than the other boroughs. This can be explained by a lesser presence of big isolated lots there. In any case, the difference remains very small compared to what have been observed in the previous and

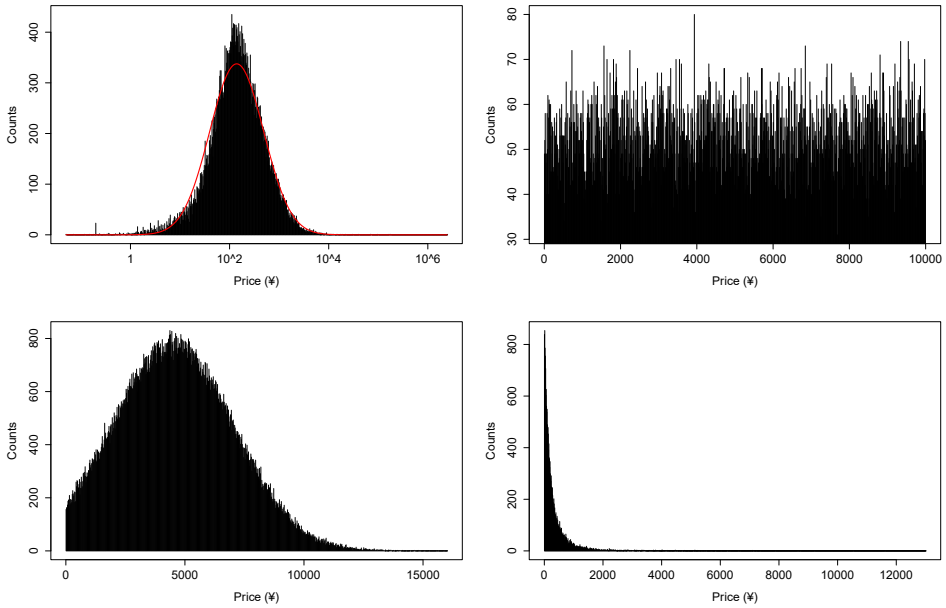

FIGURE IV.19. **1912 price distributions.** Top left: real Kyoto price distribution (note the logarithmic x-axis), top right: uniform distribution, bottom left: truncated normal distribution, bottom right: Pareto distribution.

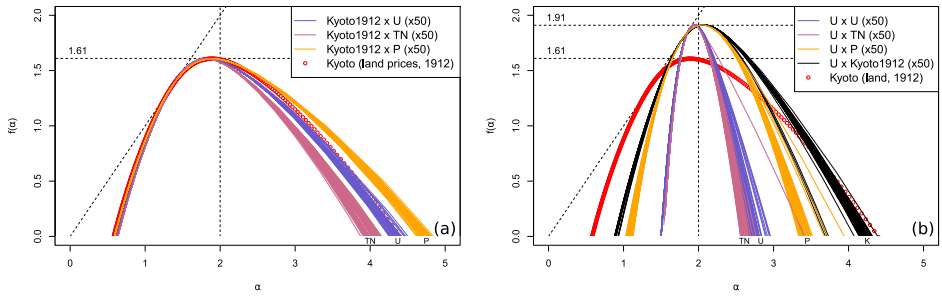

FIGURE IV.20. **Spectra for 1912 Kyoto and price models.** (a) Uniform (U), truncated normal (TN), Pareto (P) and true (red circles) distributions mapped over 1912 Kyoto true spatial distribution. (b) Same distributions and true price distribution (K) uniformly drawn into space.

future comparison. The difference in height between Brooklyn, Queens and the other boroughs is due to more compactness in these two places. The spectrum for all of New York at once appear to be an average of all five boroughs. In the following analyses, we will separate Manhattan from the other boroughs to make comparisons with other cities more significant.

When compared to the 1912 Kyoto land assessed tax value (figure IV.22), the similarity between the two spectra is striking considering how far apart the two cities are. The spectrum for Kyoto fits nicely between the spectrum for Manhattan alone, and the spectrum for all of New York. Once again, the

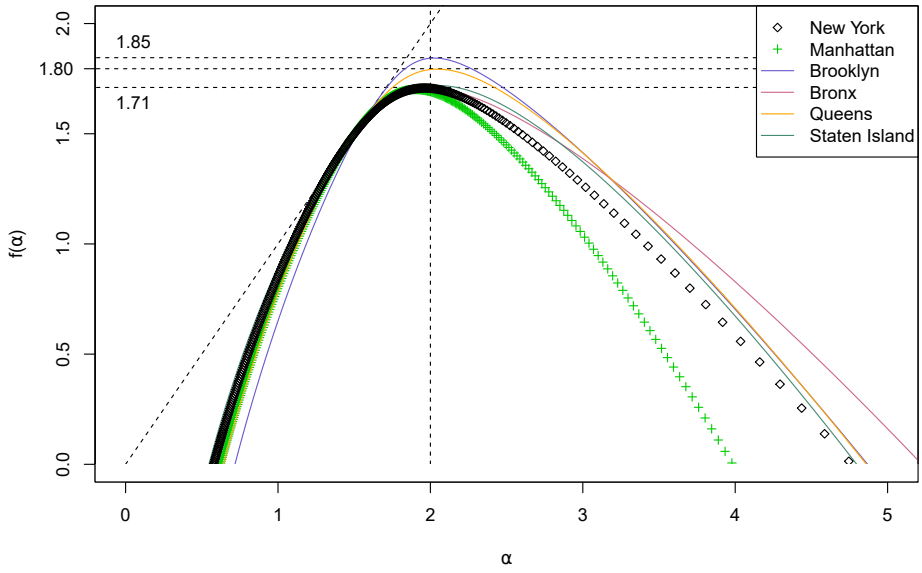

FIGURE IV.21. **Comparison between New York's boroughs.**

slightly higher curve for New York can be explained by a higher compactness in that city. We will now see if the cities evolved in a similar way into the early 21st century.

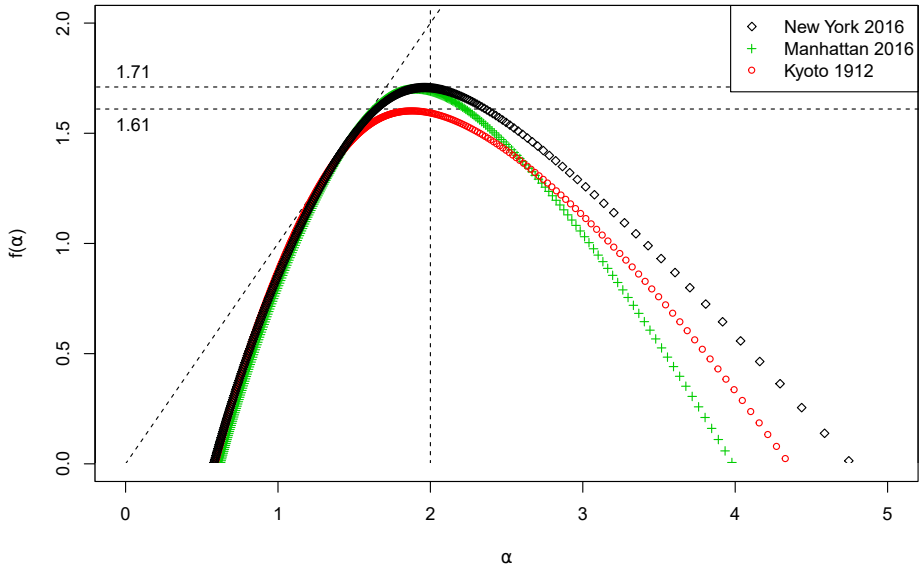

FIGURE IV.22. **Comparison between Kyoto and Manhattan.**

2.2. Real estate in the early 21st century. Considering that the data for present Kyoto is less reliable than the data for 1912, we will not repeat the same analysis on spatial models. Instead, we only reshuffle randomly the price distribution while preserving the actual locations of all road

segment centroids. Fifty iterations of this process produced the spectra that can be seen in figure IV.23(a). Contrary to the 1912 case, the real placement seems to minimize the spectrum width. In figure IV.23(b), the spectrum for the 2012 distribution cropped to the 1912 extent is plotted against the spectrum for the full extent. Only minimal changes are observable, indicating that there is no significant discrepancy in the development of new neighbourhoods compared to how the old city evolved.

The price distribution for 2012 Kyoto is almost log-normal, akin to the price distribution for 1912, although it is less symmetrical and only spans over two orders of magnitude compared to four in the previous case (figure IV.24). Similarly to the previous analysis, we generated 50 iterations of some corresponding uniform, normal and Pareto distributions. The spectra for each distribution can be found mapped over the true spatial pattern in Fig IV.23(c), and uniformly drawn into space in Fig IV.23(d). The results are similar to those obtained for 1912. In the true pattern case on the left, the spectra follow the same ranking in width as for 1912, with only slightly more pronounced differences. In the uniform pattern case on the right, the actual price distribution gives results closer to the uniform distribution, while the Pareto distribution provides significantly wider results. This is coherent with the narrower range and higher maximum of the true price distribution, reflected in a more dispersed corresponding Pareto distribution.

We now run the multifractal analysis on the housing transactions occurring in London between 1995 and 2016. As can be seen in figure IV.25, the results for each year are very close from one another, especially in the left part of the spectrum (figure IV.25(b)). Due to the presence of many "grey" no-transactions zones for the year 2008 (highlighted in red), the fractal dimension of the support of the measure is one of the smallest one, hence the curve is one of the lowest one. This corresponds to a low fractal dimension and tells more than just the size of the empty zones. In fact, it means that the empty zones are densely spread throughout the city. The fact that the 2008 curve is significantly shifted to the left on both sides compared to the other curves means a higher presence of "spike-type" heterogeneities and a lesser presence of "cup-type" heterogeneities in the spatial distribution of this variable. This is a sign of increase in inequality in the sense that some isolated people are still able to buy expensive houses while the affordability is problematic for their would-be neighbours. Interestingly, the only year that matches the situation of 2008 is the last one available: 2016.

The results when the methodology is applied to New York transactions are quite similar to those for London (figure IV.26). The same loss in height and increase in width for the left portion of the spectrum is observed around

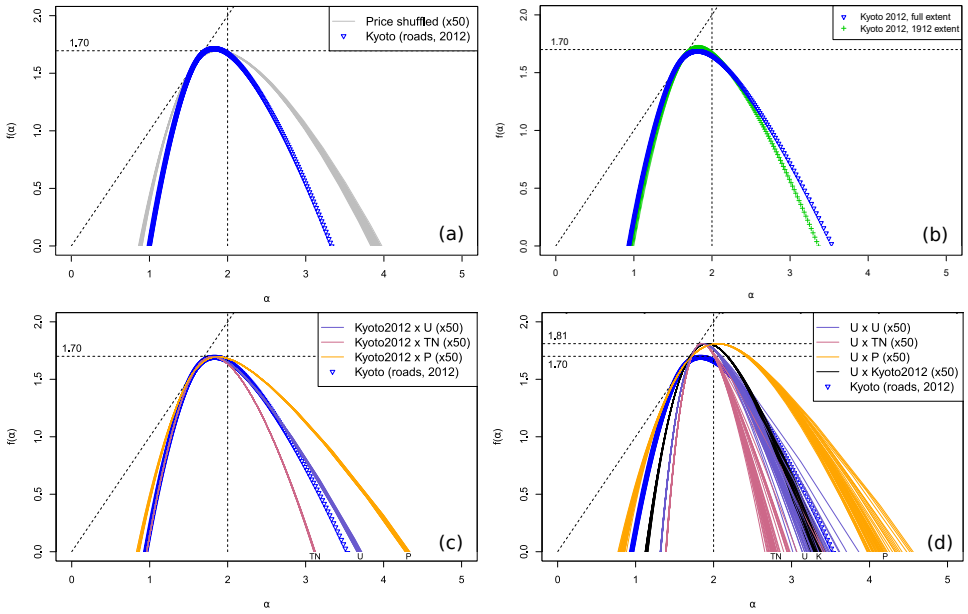

FIGURE IV.23. **Spectra for 2012 Kyoto and models.** (a) True Kyoto distribution (blue triangles) and spatially reshuffled distribution (grey lines). (b) Full Kyoto distribution compared to the extent of 1912 (green crosses). (c) Uniform (U), truncated normal (TN), Pareto (P) and true (red circles) distributions mapped over 2012 Kyoto true spatial distribution. (d) Same distributions and true price distribution (K) uniformly drawn into space.

the 2008 crisis. The spectra are however significantly larger on both sizes, although the very steep left half and asymetrical shape is an indication of low multifractality (compare for example to the results of Murcio et al. (2015)). This confirms (and quantifies) the visual impression that the prices are more evenly spread for New York in the map of figure IV.7. Note that all of New York is considered here to maximize the number of datapoints per analysis.

The spectra for these Kyoto, London and New York datasets are plotted together with the 2014 Paris dataset against the spectra representing the early 20^{th} century in figure IV.27. It could be hypothesized that the increase in spectrum height for the modern city is representative of densification. For example, the eastern half of Kyoto city is much more compact in 2012 than it was in 1912. Unfortunately, it can also be an artefact of the lower resolution, so no definite conclusions can be drawn.

The evolution of the width of the spectrum is more interesting. For example, comparing the 2012 spectrum to the 1912 spectrum for Kyoto, there is an observable loss of extreme α values, corresponding to the steepest spatial increase in price, while the relatively homogeneous zones, i.e. those

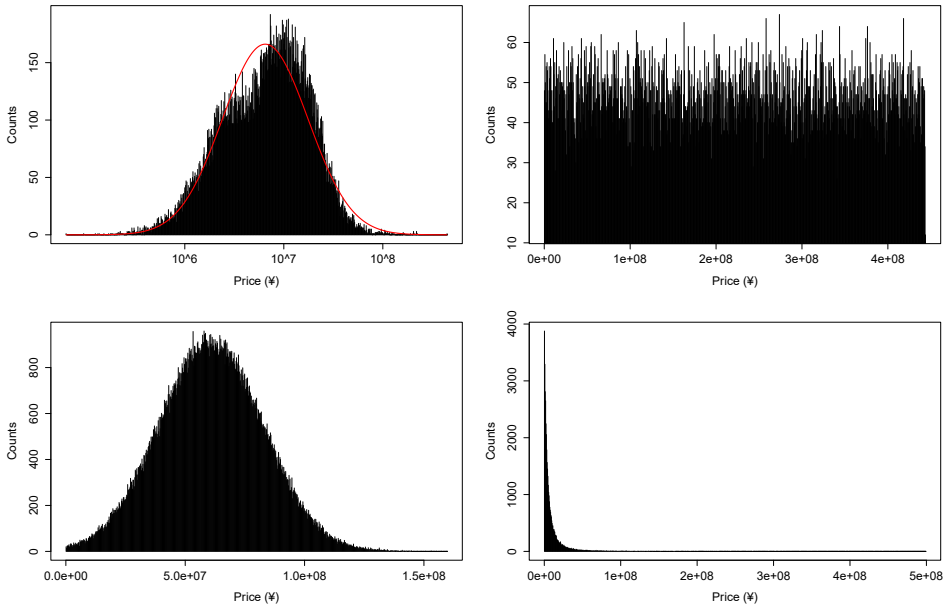

FIGURE IV.24. **2012 price distributions.** Top left: real Kyoto price distribution (note the logarithmic x-axis), top right: uniform distribution, bottom left: truncated normal distribution, bottom right: Pareto distribution.

around $\alpha = 2$, are of higher $f(\alpha)$ dimensions in the 2012 case. This is representative of a noticeable increase in local homogeneity. It can also be noted that the shape is more symmetric in 1912 compared to 2012, with a rounder left half of the spectrum. It means that the diversity in 2012 is created more by (small) local "bumps", and less by (small) local "gaps" compared to 1912.

Interestingly, despite resulting from datasets representing different real estate variables, the spectra for modern London, Kyoto and Paris match on the left (most stable) half of the spectra, while remaining the narrowest ones on the right part of the spectra. Similarly the two datasets representing the early 20^{th} century match on the left part, and stay close on the right part. This trend of multifractal loss in modern cities has already been observed for road networks Ariza-Villaverde et al. (2013); Nie et al. (2015); Murcio et al. (2015). Although, the New York transactions curve is in the middle on the left half, its steepness is also an indication of loss of multifractality.

The D_0, D_1 and D_2 generalized dimensions for Kyoto in 1912, 2012 and 2012 intersected with 1912 boundaries, for the uniform, polycentric and DLA models for 1912 data and shuffled model for 2012 data, as well as for Manhattan assessed tax land value in 2016 and London house price transactions in 2016 can be found in table IV.6. We recall from chapter II that $D(0)$

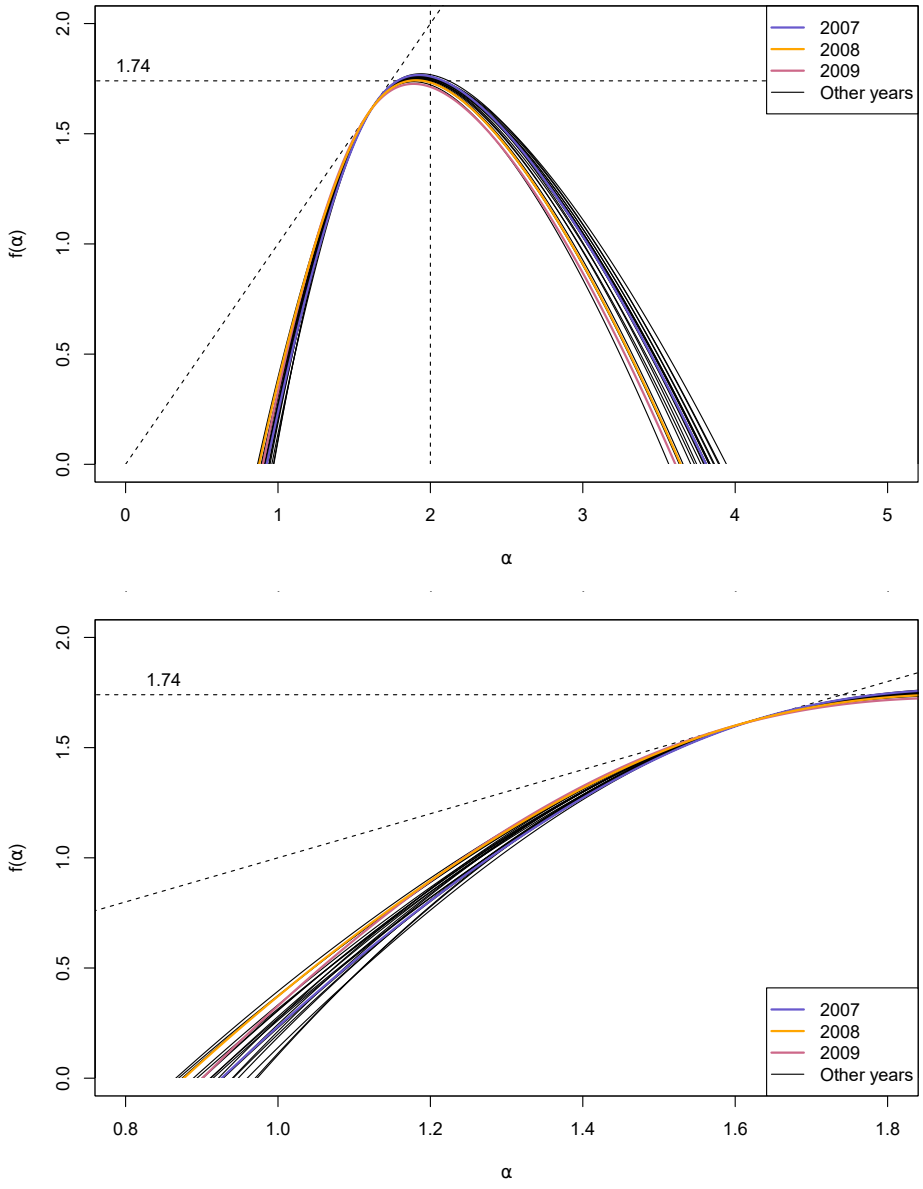

FIGURE IV.25. **London house transactions from 1995 to 2016.** (a) Full spectrum. (b) Zoom on the left part.

is the fractal dimension of the physical space supporting the measure (corresponding to the spectrum maximum height). The dimension $D(1)$ is the information (or entropy) dimension, which provides a measure of the density evenness in the data (corresponding to the point where the spectrum touches the identity line). Finally, $D(2)$ is the correlation dimension, which provides a measure of scattering in the data. Those values show the same decrease in multifractality for modern data as the spectra in the main text. Three problematic values with slightly higher D_1 than D_0 have been obtained for Kyoto in 2012 (1.74 vs 1.70), DLA 1 ranked (1.70 vs 1.67) and DLA 1.5

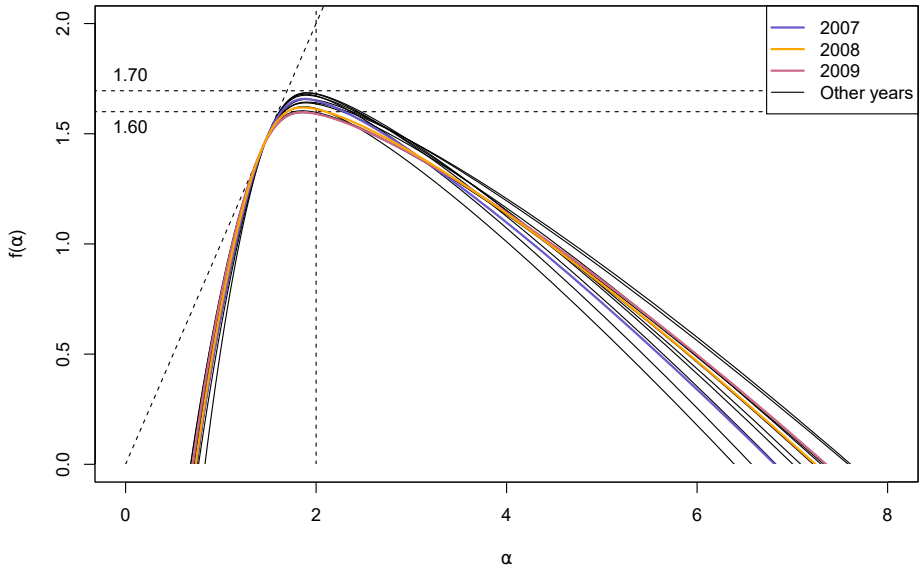

FIGURE IV.26. **New York house transactions from 2003 to 2015.** Note the different x-axis scale compared to the other plots.

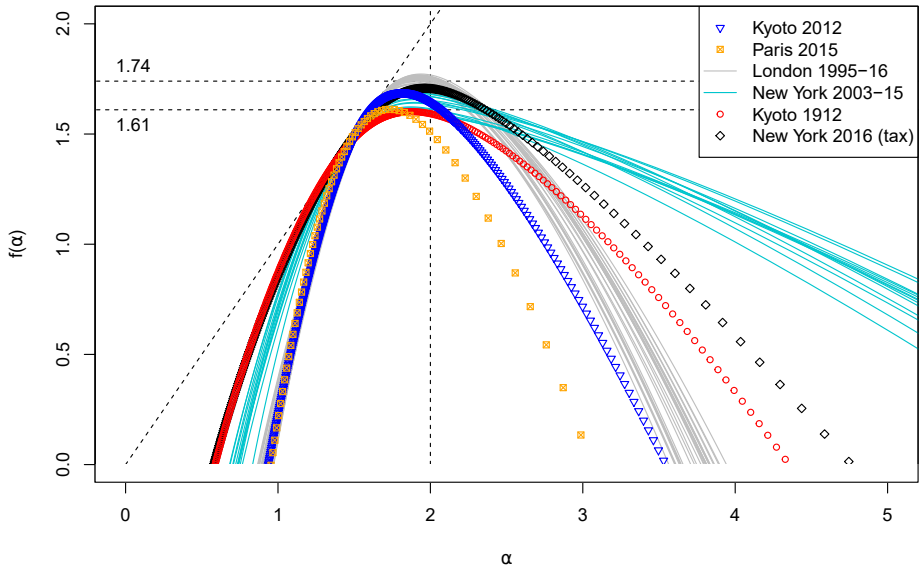

FIGURE IV.27. **Real estate spectra.** Spectra corresponding to Kyoto road valuations in 2012 transformed into land prices (blue triangles), Paris square meter prices in 2014 weighted by population (orange crossed squares), london transactions from 1995 to 2016 (grey lines), New York transactions from 2003 to 2015 (aquamarine lines), Kyoto assessed tax land value in 1912 (red circles), New York assessed land value in 2016 (black diamonds).

ranked (1.78 vs 1.74). This is an indication of small irregularities in the multifractal scaling.

TABLE IV.6. **D_0, D_1 and D_2 generalized dimensions for the previous analyses.**

Model	D_0	D_1	D_2
Kyoto 1912	1.61	1.50	0.23
Kyoto 2012	1.70	1.74	1.70
Kyoto 2012 (part.)	1.72	1.70	1.58
Uniform (1912)	1.91	1.34	0.03
Polycentric (1912)	1.91	1.57	0.14
DLA 1 (ranked)	1.67	1.70	1.23
DLA 1.5 (ranked)	1.74	1.78	1.35
DLA 1 (noise)	1.67	1.62	0.98
DLA 1.5 (noise)	1.74	1.54	0.70
Shuffled (2012)	1.68	1.51	1.37
Manhattan 2016	1.71	1.51	1.37
London 2016	1.80	1.76	1.60

In summary, the sufficiently wide spectrum for the real dataset indicate that multifractality offers a valid methodology to analyse land prices in cities. This is in concordance with Hu et al. (2012) who also found multifractality for land price distributions in Wuhan City in China. In addition, the methodology allowed to differentiate between real and simulated data, between different time periods, and to identify to some extent the 2008 financial crisis. This proves that the methodology can be informative.

2.3. Income in London, New-York and Paris. The results of multifractal analysis applied to income data in Paris (2014), New York (2010) and London (2002 to 2013) is shown in figure IV.28. Recall that the variable considered is the average income (median income for Paris) multiplied by the population count in each IRIS, CT and LSOA (respectively). These geographies being quite large, the monofractal dimensions of all curves are low, especially for Paris. All curves are relatively narrow indicating weaker multifractality than for the house prices. The curves for London around the 2008 crisis in particular are the narrowest. However, the difference with the rest of the full period is not conclusive, as all the curves match on the left half of the spectra. A much finer analysis of the curves in terms of segregation is presented in chapter V where they are compared to the results of classical indicators.

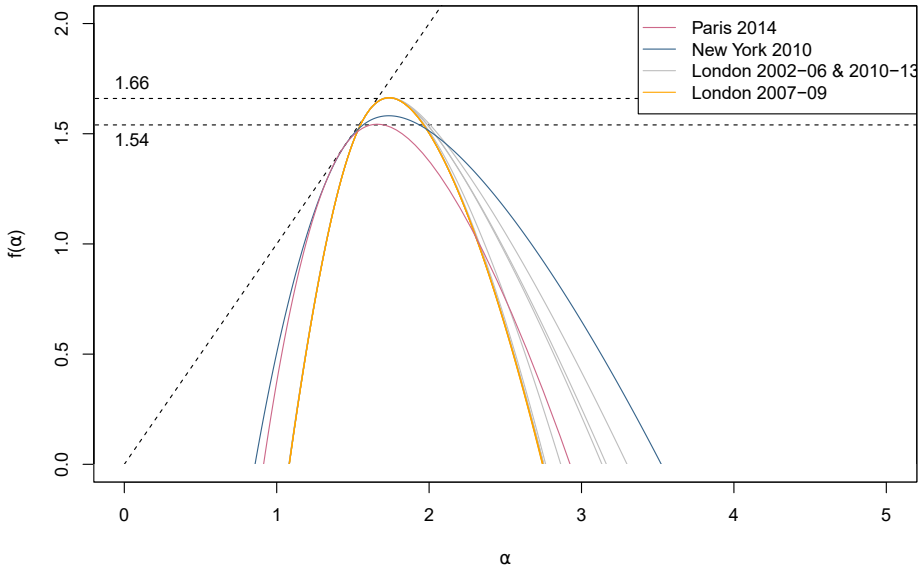

FIGURE IV.28. **Income spectra.** Spectra corresponding to Paris in 2014, New York in 2010 and London from 2002 to 2013 (with years 2007,08 and 09 highlighted in yellow).

3. Comparisons between measures

We present the results of the previous section complemented by energy and land-use diversity analyses grouped respectively for New York, Paris and London. The goal is to make comparisons between measures and to relate the results to the elements of the discussion occurring in the previous chapters. We will in particular evaluate the pertinence of each measure and show that income alone is not sufficient to study inequality. We will also point out how we could use multifractality to guide future city planning.

3.1. Manhattan. Detailed results for energy are shown in figure IV.29. The only significant difference is between the "global" measures (total energy, total electricity and total fuel) and the partial sub-measures, both being gathered in distinct group. As expected, the partial measures offer less diversity than the global measures. Overall, energy is harmoniously distributed between its different sources, and we can consider total energy alone.

The spectra corresponding to the land assessed tax value in 2016, house transactions (2010), income in 2010, energy in 2009 and land-use entropy in 2009 can be seen in figure IV.30. The spectra for land prices and energy consumption are quite similar, in particular on the left part. This was to be expected since they are based on linear transformations of the same land use dataset. The income spectrum appears to be homothetic to the tax value distribution, which comforts the idea that the taxes are intelligently calculated. It is however much narrower than the actual transaction spectrum.

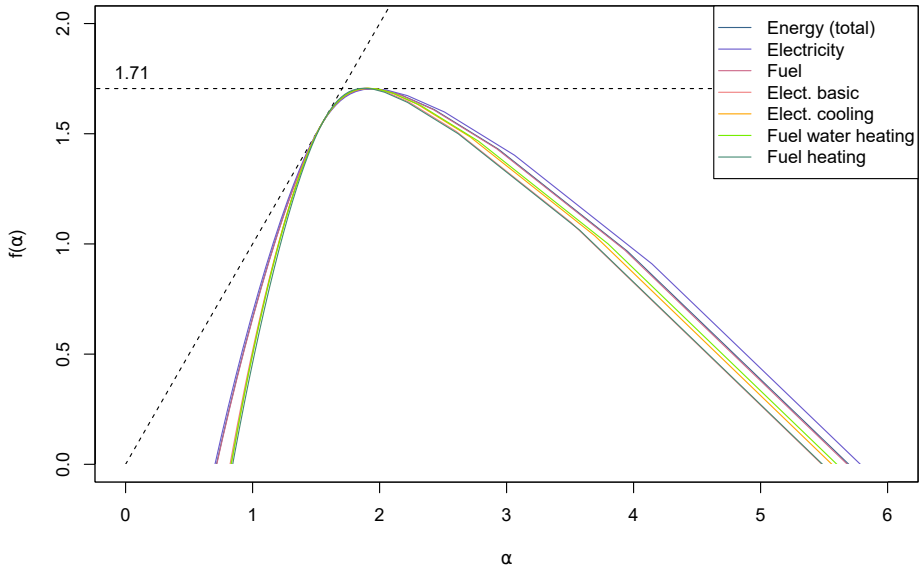

FIGURE IV.29. **Energy in Manhattan in 2009.** Spectra corresponding to the total energy consumption in Manhattan in 2009. Energy is divided into electricity and fuel consumption, further subdivided into basic and cooling use and into water heating and heating (respectively).

This means than some local distributions, in particular the cup type carried by the right part of the spectrum, are not matched. Finally, the entropy spectrum is extremely narrow and includes a steep left part, which indicates almost no multifractality. This can be explained by the "smoothing" to the land use diversity induced by the multi-scale entropy function.

These curves support the idea presented in chapter I that income alone does not contain all the information on inequality. Although a tight correlation can be seen between income and the transaction and energy distributions, they only match on a part of the spectra. The parts of the spectra where they do not match are indicative of the type of neighbourhood whose development should be prioritized if we were to make the house affordability match the current spatial distribution of income. Alternatively, we may decide that the current income spatial distribution is not satisfactory and should be more homogeneous. In that case, we should aim to narrow both curves at the same time.

3.2. Paris. The income and square meter price distributions are very similar in Paris, as can be seen in figure IV.31. There is however an observable asymmetry, with the price spectrum being slightly tilted to the right, while the income spectrum is slightly tilted to the left. The broad resolution of the IRIS and the fact that the true prices are only deduced from the

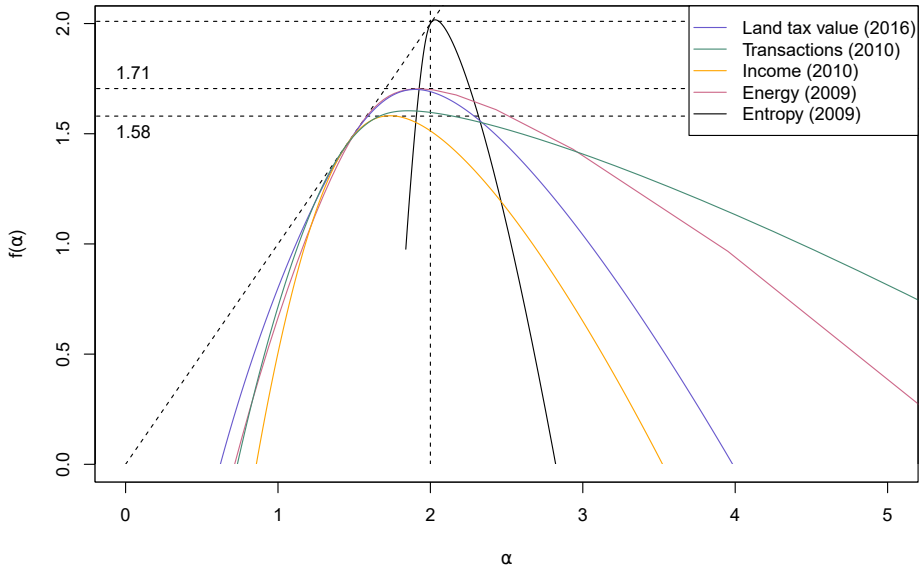

FIGURE IV.30. **Diverse urban measures in Manhattan.** Spectra corresponding to the land assessed tax value (2016), transactions (2010), income (2010), energy (2009) and land-use entropy (2009) distributions.

square meter price does not allow to draw firm conclusions on this asymmetry, although it is a direction that may be worth investigating should more data become available.

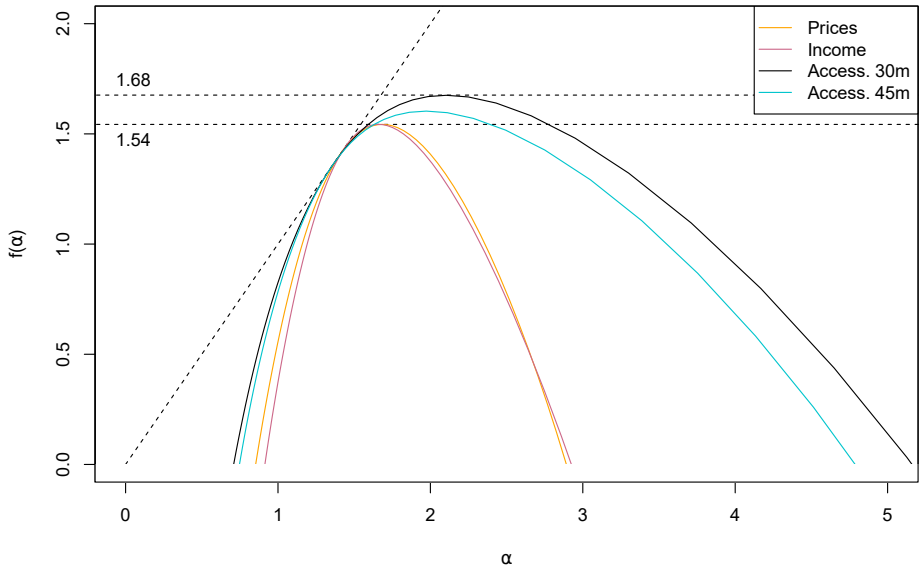

FIGURE IV.31. **Diverse urban measures in Paris in 2014.** Spectra corresponding to the square meter prices, income, and 30 and 45 minutes accessibility distributions.

The spectra corresponding to the 30 and 45 minutes accessibility are however noticeably different from the spectra we have encountered so far. Their shape is very "round", particularly in the left part. This indicates a pronounced multifractality. It also shows that accessibility alone can not fully explain the house prices. As referenced in chapter I, it has been hypothesized that the origin of fractality could be the result of cities growing by bottom up processes resulting from an intense competition for space constrained by the underlying transport network (Batty, 2008*b*). As a matter of fact, these accessibility measures are directly built on the transport network and support the competition assumption not only creating fractality, but also multifractality.

Considering these results, it could be interesting to try the multifractal methodology directly on networks. Although this fall out of scope of this thesis, it is to be noted that some work has been done in this direction for the standard moment method (Palla et al., 2010; Wang et al., 2012; Liu et al., 2015; Song et al., 2015; Rendon de la Torre et al., 2017). These articles use the sand-box algorithm which is a super-sampling box-counting method. It is however possible to extend these methods to suit the multiplier method required for the analysis of urban data, and to adapt a gliding-box algorithm instead of a sand-box algorithm.

3.3. London. All the previous curves for London, together with energy distribution can be seen in figure IV.32. Energy consumption is divided into total consumption with minor differences between the true distribution and the potential distribution if improved, and lightning, heating and water heating costs. Similarly to New York, all the energy curves are grouped together. We referenced in chapter II a case made by Joyeux and Ripple (2007) that energy distribution is not explained by income alone, so that measures of standard of living should take into account both parameters. These results confirm this idea. The difference between the income distribution and the house transaction distribution is particularly striking.

In summary, we have shown that multifractality is better suited to capture the spatial patterning of a variable rather than its value distribution. We have also evidenced that the multifractality of land prices has globally evolved from a "maximum" multifractality situation to an almost "minimal" situation nowadays, representing an homogenisation and loss of diversity. We have enlightened the (limited) potential of multifractality to detect crisis situations. We have also shown that real estate and energy consumption measures could provide additional insights on inequality compared to income alone in our case. We have put forward some evidence that job accessibility

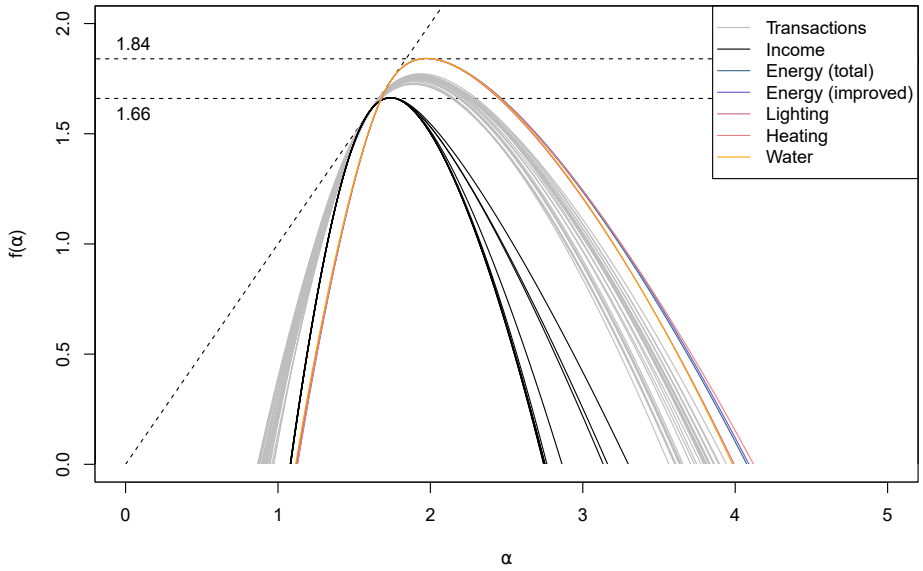

FIGURE IV.32. **Diverse urban measures in London from 1995 to 2016.** Spectra corresponding to the transactions, income, and energy distributions.

is not sufficient to explain the spatial distribution of prices. Finally, we have demonstrated with a land use analysis that multifractality does not always exist in potential urban measures.

CHAPTER V

Evaluation of the multifractal spectrum compared to the traditional inequality and segregation indicators

We evidence throughout this chapter that multifractal analysis is a potent inequality indicator free of the issues usually associated with analysing spatial inequality, such as the modifiable areal unit problem or the lack of useful details provided by global economic segregation indices. Our purpose is not to redo all the analyses previously presented with the classical indicators. We select instead some striking results that should suffice to evidence the advantages and some limitations of our methodology.

The first section recalls the formal definitions of the indices that will be used in the rest of the chapter. The second section presents three independent analyses using the Kyoto land price data, the income distributions for Paris, London and New York, and the property transactions time series for London and New York. The first analysis, also presented in Salat et al. (2018), will underline some incoherences in the results computed by the classical indicators that do not exist with our methodology. The second analysis will serve as a basis to discuss which "dimensions" of segregation are best described by the spectrum. The third analysis will acknowledge the limits of multifractals in detecting crisis, although we show that they are less prone to fall in some traps that the a-spatial inequality measures did not manage to avoid.

1. Formal definitions

According to Sen (1973), a-spatial inequality indices can be sorted into two main categories: descriptive and normative indices. Descriptive indices take the distribution (generally income) directly and apply a function to it to extract information. Normative indices (the Dalton index and the Atkinson Index) apply a utility function first to the distribution to link it to a notion of "economic welfare". Since the definition of such a utility function is both subjective and reliant on complex local policies and living cost practices, we will focus exclusively on the purely objective descriptive indices. Out of these, we retain the well-known Gini coefficient (G), and the less intuitive

Theil coefficient (T) defined in chapter I. We also consider the relative dispersion (RD) to represent the broader family of indices characterizing the difference to the mean (also including variance, variation coefficient, logarithmic standard deviation e.g.). For a distribution $\{x_i\}_{1\leq i\leq n}$ of n observations of average μ, it is defined as

$$\text{RD} = \frac{\sum_i |\mu - x_i|}{n\mu}. \tag{55}$$

The result is a number in the interval $[0, \frac{2(n-1)}{n}]$, or more simply [0,2[, when $n \to +\infty$.

In turn, economic segregation measures can be divided into two main categories depending on whether the studied variable is categorical or ordinal. Our measures are all ordinal, so we only need to take the ordinal indices into considerations. These indices all work on the same principle: comparing the variation inside each neighbourhood to the global variation inside the city.

Assume that the space is divided into n different neighbourhoods, denote $\{n_k\}_{1\leq k\leq n}$ the population count inside each neighbourhood, and denote $\{\mu_k\}_{1\leq k\leq n}$ the average value inside each neighbourhood. Then, the neighbourhood Sorting Index (NSI) is defined as

$$\text{NSI} = \sqrt{\frac{\frac{\sum_k n_k(\mu_k-\mu)^2}{n}}{\frac{\sum_i (x_i-\mu)^2}{n}}}. \tag{56}$$

In simpler terms, the NSI index is the fraction between the variance of the average values per neighbourhood and the total variance in the city. The centile gap index is defined as

$$\text{CGI} = 1 - \frac{1}{4n}\sum_i \left| P_i - P_i^{med} \right|, \tag{57}$$

where P_i is the percentile of household i in the city's distribution, and P_i^{med} is the percentile of the median household of the neighbourhood to which household i belongs in the city's distribution. The main advantage of the CGI index is that is does not require the full distribution of the variable, but only the distribution by percentile (or a broader unit). Since we have the full distribution for our variables, we will not compute the CGI index.

In order to take into account the variance inside each neighbourhood rather than only the average value, Reardon et al. (2006) have added a layer of complexity to the NSI index. Define first a segregation measure S

comparing inter-neighbourhood variation and total variation by

$$S(v) = \sum_{k=1}^{N} \frac{n_k}{nv}(v - v_k), \tag{58}$$

where the variable v is the chosen variation function, and v_k is its value inside neighbourhood k. Depending on the choice of a variation function, the index takes different names. The Ordinal Information Theory Index (OITI) and Ordinal Variation Ratio Index (OVRI) are defined respectively for the following variation functions v_1 and v_2

$$v_1 = \frac{1}{K} \sum_{i=1}^{K} -[c_i \log(c_i) + (1 - c_i) \log(1 - c_i)]; \tag{59}$$

$$v_2 = \frac{1}{K} \sum_{i=1}^{K} 4c_i(1 - c_i), \tag{60}$$

where K is the number of ordinal categories considered and c_i is the cumulative proportion of values inside a sample (here, either a singleton or a neighbourhood) of category i or below. Other possibilities that we will not consider here include the Ordinal Square Foot Index (OSFI)

$$v_3 = \frac{1}{K} \sum_{i=1}^{K} 2\sqrt{c_i(1 - c_i)} \tag{61}$$

and Ordinal Absolute Difference Index

$$v_4 = \frac{1}{K} \sum_{i=1}^{K} 1 - |2c_i - 1| \,. \tag{62}$$

All the indicators presented in this section return a value within $[0, 1]$.

2. Tables and analyses

We present first a comparison between multifractal analysis and classical indices on Kyoto land prices and its model. This comparison will establish that multifractal analysis can provide more coherent results across situations, in particular since its results are not changed by modifying the definition of administrative boundaries. The second section is devoted to the analysis of income distributions. Income is the classical variable associated to inequality. It will show that multifractal analysis is in accordance with the a-spatial inequality indicators. More importantly, it will reveal multifractality as a potent tool to assess the exposure and clustering dimensions of segregation, which is usually a prerogative of categorical segregation analysis. Finally the third section will use the house transactions in London and New York to

critically compare multifractal analysis and a-spatial inequality indicators in a situation of crisis.

2.1. Land prices in Kyoto (and models). For the practical computation of the segregation measures in this section, Kyoto has been divided into 100 artificial square neighbourhoods of same size.

The results for 1912 Kyoto are shown in table V.1 for the full residential land price distribution (Tot.), for a partial price distribution (Part.) that excludes a few outstandingly expensive lots (such as the Imperial palace), as well as for the uniform (Unif.), truncated normal (TN) and Pareto (Pareto) price distributions mapped over the true spatial distribution. The RD, Gini, Theil and NSI coefficients concord with multifractal analysis (figure IV.20) and indicate similar values between the partial and Pareto distributions on the one side, and between the truncated normal and uniform distribution on the other side. Also in accordance with the multifractal analysis, the RD and Gini coefficients indicate more distributional variety for the partial and Pareto distributions than for the uniform and truncated normal ones. This translates into higher levels of spatial segregation for the truncated normal and uniform distributions, which is coherent with the values of the NSI coefficient. It is noteworthy that the NSI coefficient is made irrelevant for the full price distribution. Indeed, its definition offers no counter to the Imperial palace making all other lots negligible compared to it. In contrast, multifractal analysis is more resilient to unique outstanding value, which can only add to the total variety. Finally, by construction, the OITI and OVRI indicate no difference between all price models.

TABLE V.1. **Classical inequality measures for different price distributions based on 1912 Kyoto.**

Indicator	Tot.	Part.	Price:Unif.	Price:TN	Price:Pareto
RD	0.998	0.904	0.498	0.402	0.905
Gini	0.666	0.606	0.332	0.281	0.610
Theil	1.833	0.786	0.192	0.133	0.734
NSI	0.033	0.234	0.500	0.502	0.338
OITI	0.147	0.147	0.147	0.147	0.147
OVRI	0.166	0.165	0.166	0.166	0.166

Another set of results is presented in Table V.2. The partial 1912 distribution has been mapped over the uniform spatial distribution (Unif.), over one centre and five centres polycentric models (C1A4 and C5A1B3), and over one seed and three seeds DLA models (DLA1 and DLA3). None of the indicators show segregation for the uniform distribution, which is expected.

OITI and OVRI failed to distinguish between C1A4, DLA1 and DLA3 models, and NSI between C1A4 and DLA1 models. The C5A1B3 model shows significantly less segregation than the C1A4 model because it is made roughly of 5 copies of the same concentric distribution, even though the repartition would feel identical from an inhabitant perspective. This shows that these measures are not completely free from the modifiable areal unit problem (MAUP), contrary to the multifractal analysis.

TABLE V.2. **Classical inequality measures for different space distributions based on 1912 Kyoto.**

Indicator	Part.	Space:Unif.	C1A4	C5A1B3	DLA1	DLA3
NSI	0.234	0.043	0.530	0.396	0.451	0.241
OITI	0.147	0.004	0.480	0.170	0.488	0.451
OVRI	0.165	0.002	0.442	0.155	0.511	0.476

The results for 2012 Kyoto are shown in Table V.3 for the entire dataset (Tot.), for the part of the dataset that corresponds to the extent of the 1912 city (Part.), for a shuffling of the full dataset (Shuffled), and for the uniform (Price: Unif.), truncated normal (Price: TN), and Pareto (Price: Par.) distributions mapped over the real city. The RD, Gini and Theil coefficients are by construction invariant through price shuffling. Overall, the same decrease of inhomogeneity between 1912 and 2012 is picked up by all coefficients, especially the spatial ones (NSI, OITI, OVRI). Contrary to the multifractal analysis, the shuffled distribution appears more homogeneous than the real distribution, which is true at the broader scale used to compute the NSI, OITI and OVRI coefficients, but not at the micro-scale used for multifractal analysis. Also contrary to the multifractal analysis, the partial distribution is slightly more unequal than the total one. This is due to the property of multifractal analysis that the spectrum of the total measure must be wider than the spectrum of a part of it. In a sense, multifractality "adds" all the variety in the measure whereas the classical indicators are "rescaled" inside each subset. Finally, the ranking between price distributions is similar to the one found in figure IV.23.

2.2. Income distributions. The results when the inequality and segregation measures are applied to our three income distributions are shown in table V.4. To make the variables coherent with the multifractal analysis, we have kept the same definitions: mean income for London and Manhattan, and median income multiplied by population count for Paris. Several scales were chosen for the segregation measures: a common artificial subdivision into 100 neighbourhoods, a common artificial subdivision into 2500

TABLE V.3. **Classical inequality measures for different space distributions based on 2012 Kyoto.**

Indicator	Tot.	Part.	Shuffled	Price:Unif.	Price:TN	Price:Par.
RD	0.701	0.768	0.701	0.498	0.282	0.991
Gini	0.479	0.520	0.479	0.332	0.199	0.661
Theil	0.400	0.479	0.400	0.192	0.067	1.02
NSI	0.267	0.376	0.044	0.251	0.260	0.203
OITI	0.041	0.074	0.002	0.041	0.041	0.041
OVRI	0.043	0.079	0.002	0.043	0.043	0.043

neighbourhoods and specific subdivisions according to greater administrative areal units (the 14 Communal Districts (CD) and 140 Census Blocks (CB) for New York, the 33 Local Authorithy Districts (LAD), more commonly known as Boroughs, for London, and the 248 Communes for Paris for which data was available).

TABLE V.4. **Classical inequality measures for the income distributions in Manhattan (2010), London (2013) and Paris (2014).** The Theil index is given in millions. NY refers to New York, L to London and P to paris. The number or code following the letter indicates which scale the results refer to.

Indicator	NYCD	NY100	NYCB	NY2500	LLAD
RD	0.696	0.696	0.696	0.696	0.211
Gini	0.479	0.479	0.479	0.479	0.149
Theil (M)	113	113	113	113	1617
NSI	0.789	0.659	0.407	0.896	0.585
OITI	0.468	0.212	0.107	0.618	0.200
OVRI	0.481	0.228	0.113	0.607	0.218
Indicator	L100	L2500	P100	PCom.	P2500
RD	0.211	0.211	0.416	0.416	0.416
Gini	0.149	0.149	0.302	0.302	0.302
Theil (M)	1617	1617	66.5	66.5	66.5
NSI	0.631	0.831	0.404	0.582	0.740
OITI	0.167	0.558	0.116	0.235	0.437
OVRI	0.184	0.549	0.127	0.244	0.431

The inequality measures rank the cities in the same order as the spectra of figure IV.28. The segregation measures return very different values depending on the chosen scale. The three cities are ranked in the same order for fixed scales, however the broadest scale implies low segregation everywhere and almost equal segregation levels in London and New York, while

the finest scale implies distinct but close segregation levels in all three cities. These indices only provide a global estimate of segregation and can only be taken into account for a specific scale. Multifractal spectra are unchanged by modifications of the boundary definitions. As a matter of fact, Semecurbe et al. (2016) propose a method to use multifractality to detect and quantify the MAUP for measures based on population densities.

It is difficult to interpret them in relation with the five dimensions of segregation identified by Massey and Denton (1988). Recall that they were

- **Evenness** is defined as the "differential distribution of two social groups among areal units in a city";
- **Exposure** is the "degree of potential contact, or possibility of interaction, between minority and majority group members within geographic areas of the city";
- **Concentration** is the "relative amount of physical space occupied by a minority group in the urban environment";
- **Centralisation** is the the "degree to which a group is spatially located near the centre";
- **Clustering** is the "extent to which areal units/minority adjoin one another".

Also, refer to figure I.1 for an illustration.

Concentration and centralisation are methodologically ignored by multifractal analysis. Indeed, an uniformly rich neighbourhood is indistinguishable form an uniformly poor neighbourhood as both case will correspond to $\alpha = 2$. It is therefore impossible to count directly the amount of space occupied by a specific income category, and it is *a fortiori* impossible to know if this space is located near the centre or not. Evenness, for the same reason, is taken into account locally rather than globally. However, the $D(1)$ value of the generalized dimension is based on the information dimension and is generally interpreted as a measure of the density evenness in the data. This dimension can be identified on the spectrum at the point where it touches the identity line.

Information about exposure and clustering can be extracted from the spectrum. Exposure is best represented by the extremities of the spectrum, since they correspond to isolated elements surrounded by homogeneous elements (for example an exceptionally rich individual near the left extremity, and exceptionally poor near the right extremity). The steeper the part of the curve is, the less exposure exists. Clustering is best represented by the width and roundness of the top spectrum. A very narrow spectrum indicates that almost all neighbourhoods are locally homogeneous, which is exactly clustering. These features are well visible in figure V.1 where the methodology is

applied to the two examples of figure I.1 representing clustering and low exposure[1]. As an example, a right tilted spectrum, for example, indicates that the rich individuals tend to cluster together while the poor individuals are more frequently found in heterogeneous locations. According to figure IV.28, this is the case for Paris and even more clearly for New York.

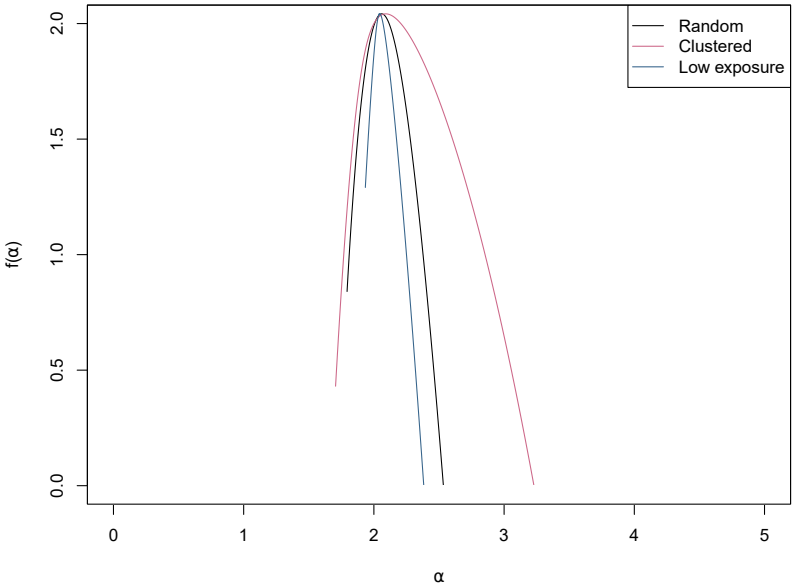

FIGURE V.1. **Multifractal analysis of low exposure and clustering examples from chapter I.** The spectra result from the examples of figure I.1. The increase in roundness of the top of the curve for clustering and in steepness of the extremities for low exposure are well visible.

Note that exposure is not necessarily reciprocal. Indeed, it is defined as the "degree of potential contact, or possibility of interaction". Imagine for example that a neighbourhood contains only white individuals, except for exactly one black individual. Then, the probability that any given white individual would encounter a black individual while walking through the neighbourhood is extremely low. In contrast, every single person encountered by the black individual is white. In this case, the black population is exposed to the white population, but the white population is not exposed to the black population. This observation is by nature true in every case where the size of the minority group is extremely small compared to the size of the majority group. However, if the size of the minority group becomes large compared to the number of neighbourhoods, then, by construction,

[1]The fact that the spectra are very narrow and incomplete is due to the fact that the datasets are not multifractal *per se*, however the figure clearly shows that the spectra evolve in the way we expect when the exposure is decreased or when the clustering is increased.

members of the minority group that are isolated inside their neighbourhoods are no longer representative of their own group. In fact, one cannot say that an hypothetical entire black population is exposed to an hypothetical white population because a few of its individual happen to live isolated in fully white neighbourhoods. In our case, the rich or poor individuals in neighbourhoods for which α remains close to 2 are indeed exposed, however their number are (mathematically) negligible compared to the number of individuals of the same category living in neighbourhoods for which α is further away from 2. For this reason, exposure is better represented at the extremities[2].

In the end, our spectra offer a much more precise characterization of segregation than the global indices. They imply that in New York it is common to have poor individuals living somewhat isolated and being very exposed to rich individuals, while rich individuals cluster together and are rarely exposed to poverty. This is also true, but to a significantly lesser extent in Paris. Meanwhile, in London the situation is more equilibrated. The narrow spectrum indicates that the neighbourhoods are more even (in the sense of homogeneity), however the symmetrical higher portion of the spectrum suggests that the situation is relatively balanced between the poor and the rich. This proves that multifractal analysis can adapt the notions of exposure and clustering, which are normally limited to categorical variables, to a continuous framework using an ordinal variable.

2.3. Housing transactions in New York and London. The results by year for the inequality indicators applied to the transactions occurring in New York between 2003 and 2015 are shown in table V.5. The segregation indices presented no significant differences and are subject to the scale issues identified above. They are therefore not reported here.

The mean and standard deviations of the RD, Gini and Theil coefficients are respectively 1.143, 0.771 and 11488k, and 0.123, 0.051, and 4327k. We highlight the differences to the mean in figure V.2 to visualize if these indicators picked up the financial crisis. As a matter of fact, they did in the same

[2]An analogy can be drawn with the property stating that the set of accumulation points of any series defined on a countably compact space is non-empty. Denote u the series and K the space. By definition, any covering of K by open sets contains a finite covering of K. Since u has an infinite number of elements, at least one of the open sets of K must contain an infinite number of elements of u. This is true at any scale, which concludes the proof of the property. Heuristically, the series u is concentrated around its accumulation points, and any open set not containing an accumulation point can be ignored if one wants to characterize the topological structure of u. Our case is very similar: multifractal analysis infers the measure's behaviour at an infinitesimally small scale and any neighbourhood that does not contain a sizeable "peak" (our equivalent of an accumulation point) can be ignored to characterize the overall repartition of the population.

TABLE V.5. **Classical inequality measures applied to transactions in New York from 2003 to 2015.** The Theil index is given in thousands.

Indicator	2003	2004	2005	2006	2007	2008	2009
RD	0.971	0.962	0.974	1.089	1.219	1.135	1.052
Gini	0.695	0.691	0.697	0.749	0.800	0.777	0.737
Theil (k)	4965	6714	8692	12202	15179	10276	6775
Indicator		2010	2011	2012	2013	2014	2015
RD		1.151	1.223	1.256	1.236	1.291	1.297
Gini		0.786	0.808	0.818	0.808	0.826	0.827
Theil (k)		9154	11570	12756	14022	17655	19373

relatively limited way as the multifractal analysis in figure IV.26 (the plot amplifies the differences). The Theil coefficient performs slightly worse than the other coefficients since it did not identify the small variations around 2004 and 2013.

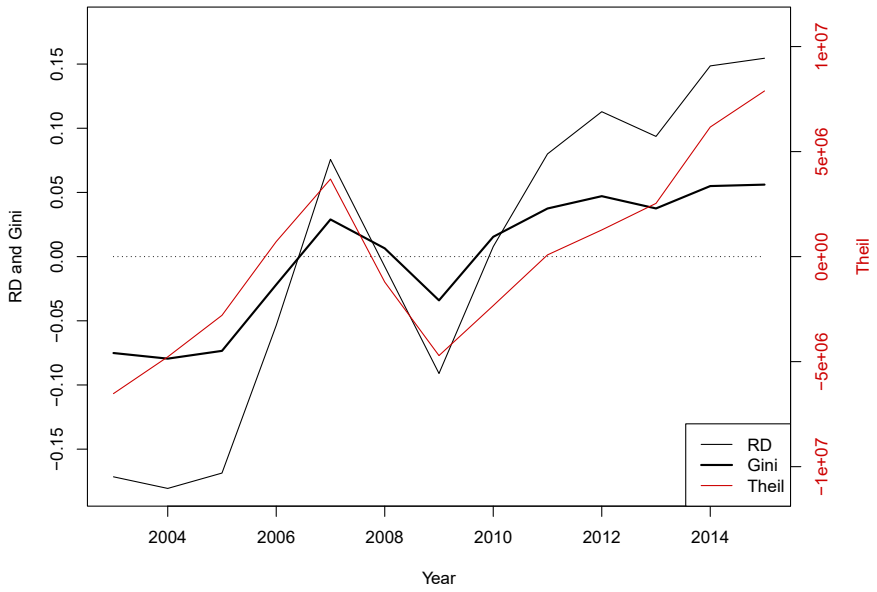

FIGURE V.2. **Difference to the mean of the RD, Gini and Theil coefficients applied to the transactions in New York from 2003 to 2015.** Note that the left axis of the plot is for the RD and Gini coefficients, while the right axis is for the Theil coefficient.

A similar table is created for the transactions in London between 1995 and 2016, see table V.6.

As before, we also plot the difference to the mean in figure V.3. The Theil index indicates a steady increase and does not identify the 2008 crisis,

TABLE V.6. **Classical inequality measures applied to transactions in London from 1995 to 2016.** Note that the Theil index is given in thousands.

Indicator	1995	1996	1997	1998	1999	2000	2001	2002
RD	0.536	0.551	0.564	0.561	0.550	0.555	0.518	0.483
Gini	0.372	0.381	0.390	0.389	0.382	0.386	0.362	0.340
Theil (k)	1149	1249	1437	1638	1943	2352	2562	2939
Indicator	2003	2004	2005	2006	2007	2008	2009	2010
RD	0.439	0.441	0.452	0.474	0.489	0.515	0.539	0.559
Gini	0.310	0.308	0.314	0.328	0.338	0.354	0.370	0.384
Theil (k)	3168	3487	3713	4076	4595	4736	4747	5402
Indicator		2011	2012	2013	2014	2015	2016	
RD		0.577	0.586	0.600	0.592	0.534	0.509	
Gini		0.396	0.402	0.411	0.408	0.372	0.356	
Theil (k)		5597	5845	6368	7112	7368	7942	

while the RD and Gini index are particularly close and suddenly decrease during the crisis. The mean and standard deviations for the RD, Gini and Theil coefficients are respectively 0.528, 0.366 and 4065k, and 0.048, 0.031 and 2075k. These all indicate less inequality in London than in New York, which is coherent with the spectra.

The classical indicators are more efficient than multifractality to characterize the evolution of inequality around the 2008 crisis. In fact, the curves in figures V.2 and V.3 follow a similar horizontal "Z" shape, however the crisis is interestingly located in the decrease part of the shape for New York, while it is located in the second increase for London. This may be due to the crisis producing a particularly pronounced deterring effect in New York for the highest investors (as can be seen in figure IV.6), temporarily narrowing the spread of the transaction prices distribution. In comparison, although the 2008 curves stand out visually in figures IV.26 and IV.25, it is a result of a mix of low minimum α, maximum α and maximum $f(\alpha)$, while no single value characterizes efficiently the crisis period. However, a decrease in inequality after 2013 in London as evidenced by figure V.3 should not exist in view of figure IV.3. This is clearly due to the large increase in maximum price paid making other transactions look equally cheap compared to it. We can relate this issue to the outstandingly expensive imperial palace in Kyoto having the same consequences as evidenced in the previous section. It is a major flaw of these indices.

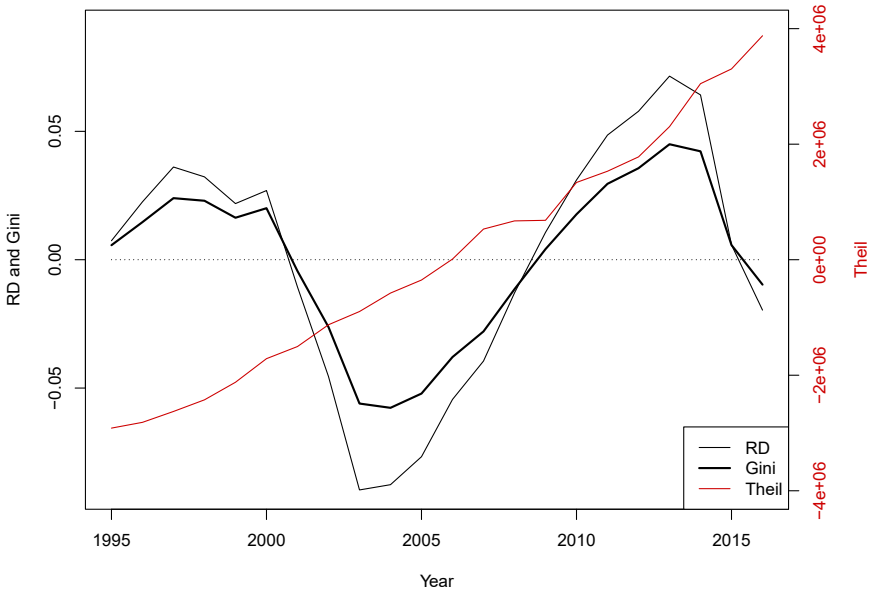

FIGURE V.3. **Difference to the mean of the RD, Gini and Theil coefficients applied to the transactions in London from 1995 to 2016.** Note that the left axis of the plot is for the RD and Gini coefficients, while the right axis is for the Theil coefficient.

Further considerations and conclusions

One of the limits when creating segregation measures for ordinal variables is computational performance. For example, exposure and clustering may be easy to code for a few (ideally two) categories, but become difficult to adapt in the case of a continuous ordinal variable. One strategy could be to discretise the variable into many categories and use a categorical algorithm, however this is likely to prove difficult for the computer. As a matter of fact, the operation of sampling the ordinal variable is added to the operation of sampling the two natural spatial dimensions. Even the global measures such as the NSI, CGI, OITI and OVRI may require intensive computations if custom neighbourhoods are created and the performance declines steeply when the scale is decreased. In contrast, the moment strategy in the multifractal methodology ensures that complex operations inside each neighbourhood are never required. The process remains manageable at all scales.

Chapter V has proved that multifractal analysis is not sensitive to the modifiable areal unit problem contrary to the global segregation measures. Section 2.1 in particular shows that it can yield more coherent and resilient results. Reardon and O'Sullivan (2004); Reardon et al. (2006) additionally suggest that the measure should be insensitive to order preserving change in the distribution. Sections 2.1 and 2.2 of chapter IV demonstrate that the multifractal spectrum is largely dominated by the spatial repartition of the variable (as identified in figure IV.18, IV.20 and IV.23). However, we argue that its ability to pick up differences in the value distribution of the variable when appropriate, such as when the distribution is randomized (figures IV.20 and IV.23), is an advantage.

It was also required that the measure would have "scale interpretability", meaning that it reaches 0 when group proportions are uniform and the maximum value only when there is no proximity between any two members of each group. Instead, our measure reaches its maximum value (the fractal dimension of its support) when the spatial distribution is uniform, and its minimum value (0) when groups are isolated. This situation is equivalent, up to an easy inversion. Other criteria that were devised for multi-categorical segregation, but that can have an interpretation for ordinal segregation are briefly discussed in relation to our method in appendix B. In conclusion,

the multifractal approach fares well against the generally agreed criteria in the field, while offering a computationally efficient improvement over classical measures, particularly since it has an important and unique capacity to quantify the exposure and clustering dimensions of segregation, even for ordinal variables, as identified in chapter V.

This fulfils our first and primary goal, which was to improve the characterisation of the spatial patterns that emerge from inequality over the current existing methods. We also aimed at consolidating the nascent literature that suggests that the multifractal framework is well adapted to study cities (and may be more truthful to reality than monofractal analysis). We have proved in chapter IV that cities often do present the scaling properties that make the multifractal framework relevant. Indeed, we have identified particularly convincing multifractal patterns for real estate measures in several cities spread across the globe: London, Paris, New York and Kyoto. We have also shown that income and energy consumption are good candidates for multifractal analysis. However, all measures are not suitable, as section 3.1 of chapter IV has illustrated for the diversity of land use measure.

We now recall the main practical results of chapters IV and V. Sections 2.1 and 2.2 of chapter IV have enlightened a decrease in multifractality with modernisation that can be understood as an arguably positive reduction of inequality, but also as a negative loss of diversity that can imply situations where all properties become unaffordable. These two sections have also presented convincing similarities in the independent evolution of the spatial repartition of real estate measures across three different continents during the 20th century. Section 3 of chapter IV has revealed discrepancies between the spectra of income and the spectra of the other measures. Finally, Section 2.2 of chapter IV, complemented by section 2.2 of chapter V, led to an observation that in New York the rich tend to live clustered and isolated from the poor, contrary to London which presents a different profile composed of clustered, but balanced in terms of economic class exposure, neighbourhoods. As a matter of fact, there has been an active strategy to orient London's recent development in that direction. More than just observing these situations, multifractal analysis has allowed to obtain a detailed quantification containing a full range of values.

Outside from the academic analysis of current and past situations, the fact that the information contained inside the spectra is delivered over this range of values (rather than through a unique global parameter) makes it particularly useful for practical urban planning. We can not only observe if inequality is evolving through time or space, but we can also observe how it is evolving and observe which end of the distribution is most affected by

the evolution. Ideally, we would want to go further and be able to predict how a development scenario will impact inequality before it is actually implemented. A natural extension to this thesis would therefore be to couple the methodology with urban modelling tools. We make a step in that direction in appendix A where we present an agent-based model that emphasises the role of economic segregation in the process of choosing a domestic property to buy. Contrary to other locational models that are oriented towards relating the population distribution to economic efficiency, we focus on building a model that correctly represents the evolution of economic segregation following a new urban development.

Another natural extension of this work could consist in finding other applications to the identified multifractal urban patterns. One could think for example of testing if industrial energy consumption measures are multifractal, and if the spectrum can be associated with economic efficiency.

In conclusion, we have devised a new computationally efficient methodology to study the spatial patterns emerging from inequality in the urban environment that solves many of the issues usually encountered in this field. It provides richer insights due to its results being presented as a continuous spectrum instead of one global parameter. We have taken particular care to develop an interpretative framework for our results focused on studying inequality and have presented the analysis in a way that aims at emphasizing the advantages of the multifractal methodology for comparing diverse situations and their evolutions through time. This is done to invite planners and policy makers to incorporate the impact on inequality induced by their future projects.

APPENDIX A

An agent-based model to test the impact on inequality of future urban development planning

We define an agent-based representing people relocating inside a city according to the purchasing power granted by their income and their preferences in terms of the economic composition of their neighbourhoods, where neighbourhood is defined by accessibility rather than physical proximity. This model can be used (or can be added to an existing model) to test the impact on inequality of future urban development planning scenarios. Its main originality lies in the strong integration of social considerations in the agents' locational choices. It is aimed at producing a correct economic segregation output, rather than at identifying the dynamics that favour economic productivity. We first present a brief overview of modelling in urban science and justify our approach within this framework. We then detail the construction of our model and define a basic autonomous system that can be used as a null model.

1. Models in Urban Science

A city is more than a physical space as it is also the support of intensive human activity. There are several ways of representing the space-activity pair (Batty, 2013). If the emphasis is on interactions between people or between activity sectors and if the friction of distance is the only required spatial element, then an immaterial network representation and its associated tools are ideal. When a network is inherently spatial, such as a street network, space syntax offers an extensive analysis method (Hillier and Hanson, 1984). However, for our purpose, we are required to link immaterial interactions dynamics with their induced spatial patterning. We therefore turn our attention to another archetype of models: the land use-interaction models. They have evolved from aggregative static systems in the fifties to dynamic systems that take into account micro-scale interactions nowadays. According to Batty (2008*a*, 2016), this transition is explained by the progress in computational power that allows handling bigger and more disaggregated systems, and by the role of policy making that drove the attention towards testing the dynamic impact of public investments on cities.

To successfully implement such a model, one has to define a system and choose a way of iterating it through time. To that end, the methodology has settled around three main basic iteration principles that can be further complexified and combined (Batty, 2007). The cellular automata (CA) approach uses a static grid whose cells' state at time t_k is determined by the states of their neighbouring cells at time t_{k-1} (Engelen et al., 1995; White et al., 1997; Batty, 1997). The agent-based model (ABM) approach relies on agents that can move freely through the space and whose characteristics are modified by their interactions with other agents and with the environment after each movement iteration (Batty, 2005; Heppenstall, 2012). A third, more aggregated, approach is based on the gravity interaction equation (Wilson, 1971). Flows between different zones of a city are assumed to depend proportionally with some characteristics of the origin and of the destination zones and inversely proportionally with the distance separating said zones. Several inter-dependent interaction equations can be looped together allowing the system starts evolving through time. This process is the basis of the well-known land-use transport interaction (LUTI) model (Wegener, 2014).

Although Wegener (2011) warns that excessively small scale should not become harmful to the model's usefulness, we are more interested in completely disaggregated models, since multifractality identifies patterns from the characteristics of the system at an infinitesimal scale. Cellular automata appears to be a reasonable approach to represent the local evolutions of house prices due to gentrification or pauperisation. It has been shown in particular that the fractal nature of cities can be recovered from this type of growth processes (White and Engelen, 1993, 1994; Batty and Longley, 2014). Contrary to the price patterning inside the city which is mostly stable, or at least controlled, the income distribution is best described through agent-based modelling. Income is carried by agents who make decisions as to where they want to live, creating the actual income spatial distribution.

Agents decisions are usually modelled through location theory (McDonald and McMillen, 2011; Wegener, 2013; Delloye, 2018). In that configuration, it is assumed that agents try minimize a utility function taking into account rent price and travel cost. However, since we are only interested in the spatial distribution of inequality, we can consider two agents sharing the same income as interchangeable, independently of their source of income. As a consequence, we do not need to take into account where specific agent would chose to locate in relation with their sector of activity. We need instead to take into account how agents belonging to specific social categories would choose to locate in relation with their neighbours' social categories.

Interestingly, Ibraimovic and Hess (2018) have recently made a strong case that social interactions should not be ignored in location models as it is too often the case.

Some successful modelling platforms have already been implemented, such as the well known UrbanSim (Waddell, 2002; Waddell et al., 2003), which includes real estate location behaviour modelling (Waddell, 2000), and more recently SimMobility (Adnan et al., 2016), which can be applied to add the role of accessibility into microsimulation of real estate dynamics (Zhu et al., 2018). Mustafa (2018) in particular has created a rich integrated cellular automata and agent-based model to simulate future urbanization. However, we want to create a rather simple environment where we can fully control both the real estate market and accessibility, and, more importantly, that emphasizes the role of social interactions in the decision making processes of agents. We therefore choose to test our policy scenarios on our own ad hoc model based on cellular automata and agent-based modelling principles. We follow Wegener (2011) who argues that models should be multi-level, and integrate space, time and policies.

A question remains about defining the time scale for our models. It has been argued that cities are systems that remain far from equilibrium (Pumain, 2017; Batty, 2017). The necessity to translate this observation in urban modelling has been argued by Jin and Wegener (2013); Simmonds et al. (2013). The way we intend to tackle this issue is by creating an autonomous model that represent perpetual movement inside a city. This model is used as a null model representing the non-equilibrium state of the city. Scenarios are run for a few decades for short-range scenarios and for a few centuries for long-range scenarios until the city stabilizes back to its regular perpetual movement state.

2. Model construction: autonomous null model

We now implement an autonomous null model that translates the "normal" movements inside the city. This model is an hybrid between CA and ABM. It is composed of a grid of real estate prices, a transport network and a street network defining the topology (i.e. the notion of neighbourhood), and agents each possessing an income and a preferential accommodation choosing behaviour. Each year, a number of agents leave the system (either by dying or by moving elsewhere), and a number of agents arrive into the system, inducing movements inside the city from the new entrants and occasionally from agents no longer satisfied by their changing environment.

Since the aim is to study the spatial distribution of income, two agents with the same salary are interchangeable in this model. In practice, we create

a bigger "reservoir" of agents and we draw from it the agents that get involved with buying houses (hence excluding the renting market). In particular, migration is translated by a change to the general profile of the population reservoir, rather than by an exchange of uniquely identified agents. Similarly, the global distribution is stable enough that we do not have to model sharp changes in income resulting for example from climbing the social ladder or from divorce at an individual scale. The rules governing the evolution of the autonomous model are flexible and its core functioning is simple enough to easily support the addition of extra layers of parameters. We finally use data from London to test the model.

2.1. The city. It is modelled by a grid whose unit represents a distance of about 100 meters. Each cell has a distribution of prices and availability attached to it. In addition, there exists a street network and a transport network linking cells to other cells.

2.2. Topology. For each cell in the grid, two types of neighbourhoods are defined. The *true neighbourhood* consists of all the cells within a 7 minutes walking distance (or 6 cells) from the original cell through the street network. The *extended neighbourhood* gathers all the cells within a distance from the original cell corresponding to 25 minutes through the transport network, as well as the cells within a 5 minutes walking distance from these cells. Note that the true neighbourhood is not included in the extended one, so that the two definitions are separated.

2.3. Agents. An agent x is characterized by a set of parameters $A_x = \{a_0, I_0, t, g, r, T_s, T_r, T_d, B\}$, where a_0 is their age at time t when they first interact with the system, I_0 is the yearly income they will earn when they reach age T_s and start working, g is the rate at which their salary increases until they reach retirement at age T_r, at which point they will earn $r \times I_0$ until they eventually die at age T_d, and B is their location choosing behaviour (see below). In practice, we set g, r and T_r globally, while T_s and T_d depend only on I_0. The subset $\{a_0, I_0, t_0, B\}$ is therefore enough to fully characterize an agent.

Since the data available to us is more precise for individuals than for households, we add a step consisting in merging up to three agents into "household" agents according to household composition data. This is done by summing the I_0 of several agents sharing the same a_0[1], while taking the average of T_s and T_d, and choosing a B at random.

[1]Preferentially to defining complex age compatibility rules and then compute the average age of the household

2.4. Income function. It is defined for an agent of age a with parameters $A_x = \{a_0, I_0, t, g, r, T_s, T_r, T_d, B\}$ by

$$I(a) = \begin{cases} 0 \text{ if } a < T_s \\ I_0 * g^{(a-T_s)} \text{ if } T_s \leq a \leq T_r \\ I_0 * r \text{ if } T_r < a \leq T_d \end{cases} . \tag{63}$$

In simpler terms, if $t = t_k$, then the agent's income at time t_n will be $I(a_0 + n - k)$.

2.5. Behaviour. An agent has one of the following preferences regarding the composition of their true neighbourhood when they choose a location to move in.

- (SQ) *Status-quo*: the agent wants to live in a cell whose true neighbourhood are similar (income wise) to their current one;
- (MS) *Maximum similarity*: the agent wants to live in a cell whose true neighbourhood is in majority of the same income level as their own;
- (KH) *King of the hill*: the agent wants to live in a place whose true neighbourhood is poorer on average than they are;
- (PB) *Prince of Bel-Air*: the agent wants to live in a place whose true neighbourhood is richer on average than they are;
- (RR) *Rooted*: the agent will not move no matter what happens in the neighbourhood.

An agent has one of the following preferences regarding the composition of their extended neighbourhood when they choose a location to move in.

- (sq) *Status-quo*: the agent wants to live in a cell whose extended neighbourhood are similar (income wise) to their current one;
- (mo) *Maximum opportunity*: the agent wants to live in a cell whose extended neighbourhood maximizes income;
- (np) *No preference.*

Every agent is assigned a random combination of one true neighbourhood and one extended neighbourhood behaviour. If an exogenous agent draws SQ or sq, then the income of their current (initial) neighbourhood is chosen randomly.

In practice, denoting the sorted income distributions

- i_x for agent x (singleton);
- I_t^x inside the initial true neighbourhood of agent x;
- I_e^x inside the initial extended neighbourhood of agent x;
- I_t^k inside the true neighbourhood of cell k;
- I_e^k inside the extended neighbourhood of cell k,

then, the agent tries to optimize the following functionals:

$$SQ = \arg\min_k \left\{ \left| \text{mean}(I_t^x) - \text{mean}(I_t^k) \right| \right\} \tag{64}$$

$$MS = \arg\min_k \left\{ \left| i_x - \text{mean}(I_t^k) \right| \right\} \tag{65}$$

$$KH = \mathbb{1}\left(i_x > \text{mean}(I_t^k) \right) \tag{66}$$

$$PB = \mathbb{1}\left(i_x < \text{mean}(I_t^k) \right) \tag{67}$$

$$sq = \arg\min_k \left\{ \left| \text{mean}(I_e^x) - \text{mean}(I_e^k) \right| \right\} \tag{68}$$

$$mo = \arg\max_k \left\{ \text{mean}(I_e^k) \right\} \tag{69}$$

where $\mathbb{1}(\cdot)$ is equal to 1 if the condition is verified, 0 otherwise (the cell is chosen randomly among all the results equal to 1). Rich agents have priority for choosing their cells.

The behaviours can alternatively be defined in the following more precise, but more computationally intensive, way.:

$$SQ = \arg\min_k \left\{ \sum_p \left| I_t^x[p] - I_t^k[p] \right| \right\} \tag{70}$$

$$MS = \arg\min_k \left\{ \sum_p \left| i_x - I_t^k[p] \right| \right\} \tag{71}$$

$$MS = \arg\max_k \left\{ \sum_p \mathbb{1}\left(I_t^k[p] - \varepsilon < i_x < I_t^k[p] + \varepsilon \right) \right\} \tag{72}$$

$$KH = \arg\max_k \left\{ \sum_p \mathbb{1}\left(i_x > I_t^k[p] \right) \right\} \tag{73}$$

$$PB = \arg\max_k \left\{ \sum_p \mathbb{1}\left(i_x < I_t^k[p] \right) \right\} \tag{74}$$

$$sq = \arg\min_k \left\{ \sum_p \left| I_e^x[p] - I_e^k[p] \right| \right\} \tag{75}$$

Alternatively, heuristic rules such as MS requires that more than half of the cells of the neighbourhood lie within $i_x \pm \varepsilon$, or KH requires that more than half the cells are lower than i_x can be considered.

2.6. Affordability. Each year, a number of properties become available, as determined in the next section. A number of agents exceeding that number make the choice of buying a property and start competing to get the most suitable one. Each unoccupied property is given a rating based on the agent's B (For example by normalizing the true and extended behaviours

out of 100 and adding the two scores). This rating is then modified by an affordability index given by

$$aff(x) = \begin{cases} \exp(-\exp((0.7(N+p)-x)/5)) & \text{if } x \leq N+p \\ \dfrac{1}{1+\exp((x-1.5(N+p))/6)} & \text{if } x > N+p \end{cases}, \tag{76}$$

where x is the price of the considered property, N is the usual ratio between price paid to income for the city (for example, $N = 6 \cdot I$ in London), and p is 0 if the agent comes from the reservoir, or p is the price of the vacated property if the agent just sold his current house. In mathematical terms, the affordability function is a Gompertz function on the first part, and a classical logistic function on the second part. Its shape can be seen in figure A.1.

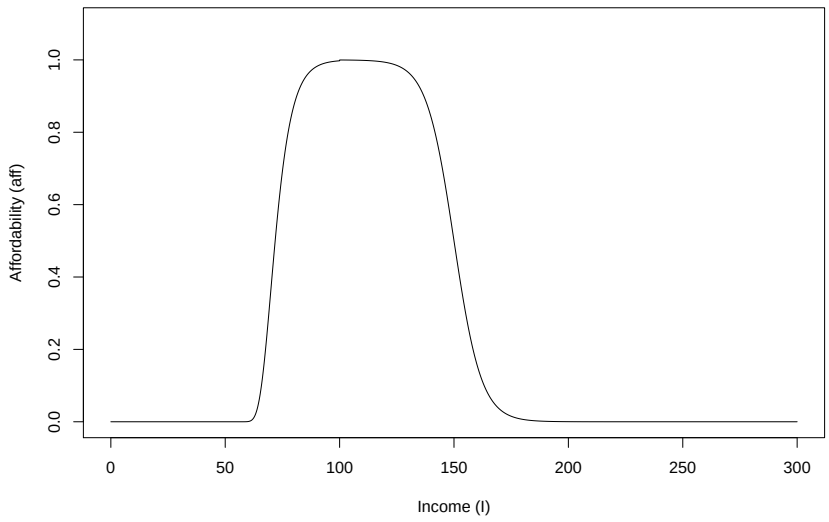

FIGURE A.1. **Affordability function.** The x-axis is normalized so that $N + p = 100$.

A freeze period l_{freeze} during which a property cannot be vacated (unless death occurs) is then added to the property corresponding to the estimated length of the mortgage:

$$l_{freeze} = \text{floor}(3 \cdot ltv \cdot (P-p)/I), \tag{77}$$

where ltv is the loan to value coefficient, P is the price of the property and p is the same as above.

2.7. Autonomous model. An initial reservoir of agents is created by drawing the parameters A_x according to the data and by merging some agents into households accordingly. An initial grid of property availability

and prices is created and filled with initial compatible agents (by construction, SQ is always a compatible behaviour).

At each time step t_k:

1. A number of agents with age 0 and other parameters drawn from the global distribution are added to the reservoir;
2. All agents whose age is greater than T_d die whether they are in the reservoir or occupying a grid cell;
3. Empty grid cells are filled with random agents whose age is within $[T_d - 35, T_d - 18]$;
4. Agents who are too dissatisfied with the evolution of their neighbourhood vacate the cells they occupy and are added to a waiting list;
5. A number of additional agents (set by the data) choose to vacate the cells they occupy for reasons best known to them;
6. Empty grid cells are filled first with agents on the waiting list, then with agents from the reservoir competing according to their B and purchase power;
7. Grid cell prices are raised/lowered depending on the average income in the cell true neighbourhood.

The steps are ordered in a way designed to take into account the dynamic of agents whose B is not compatible with the property they have inherited or who wish to sell their newly inherited property to get a more expensive one. In the fourth step, agents become dissatisfied if at any time the average income in the neighbourhood falls out of the interval $[I^x_{t/e}(1-q), I^x_{t/e}(1+q)]$ for a chosen q (unless their behaviour is RR). Finally, in step 7, if I^k_t increases or decreases by more than $(1 \pm l)$, then the prices carried by cell k are increased or decreased by $(1 \pm m)$.

2.8. Initial data. The model was set up according to London data. The following sources were used either directly or indirectly to evaluate the different parameters:

- Age distribution in London (Data, ONS:2017*a*);
- Income distribution for individuals in London (Data, HMRC:2014*b*);
- Income characteristics and housing tenure (Data, DWP:2012*b*);
- Life expectancy in England and Wales (Data, ONS:2007-11);
- Household composition (Data, ONS:2011);
- Price paid data in London (Data, HMLR:1995-16);
- Mortgage characteristics and loan to value (Data, GLA:2018,F);

This data provides the initial distribution of age (a_0) and income (I_0) in the city. The initial grid of prices and availability is established according

to the Land Registry dataset already used in chapter IV to compute the spectra of real estate measures in London. All years between 1995 and 2016 are considered to establish the availability. Redundancy is not an issue here since if a same property has been sold twice during that period, then it means that the probability of it being available was twice the average. All the prices are adjusted to the standard of 2016 according to the global inflation in the city. Other parameters are derived as reported in table A.1.

TABLE A.1. **Global parameters of the model.**

Model parameter	Value
Yearly income rise (g)	0.8%
Pension rate (r)	68.21%
Starting age (T_s)	18 + {1 every decile}
Retirement age (T_r)	65
Life expectancy (T_d)	79 + {1 very hexadecile}
Price paid to income (P)	$6 \cdot I$
Loan to value (ltv)	65%
Dissatisfaction (q)	0.5
Income measured change (l)	0.75%
Price readjustment (m)	0.05%

In addition, we found that 32% of households are composed of one individual, 53% of one family (simplified in 2 incomes counted) and 15% of more than one family (simplified in 3 incomes counted). The total number of tenured households is 1.635 Millions out of a total population of 8.825 Millions. Each year, 118000 properties are vacated in total (i.e. counting properties vacated both at step 4 and at step 5). Finally, the distribution of behaviours B is set according to table A.2. The birth rate in London was found to be around 130000 birth per year.

TABLE A.2. **Behaviour distribution.**

Behaviour (B)	Value
SQ	40%
MS	10%
KH	5%
PB	5%
RR	40%
sq	25%
mo	70%
np	5%

Additional data relating to tenure by household composition, the spatial distribution inside London of ages and income, and mortgage length can be used as controls to ensure that the agents autonomous movements stay in line with the real distributions.

The model was coded in Java by Dr Sarah Wise, UCL. After the initial steps, the income distribution created by the agents behaviours when competing to fill the property grid cells produced the encouraging spectrum of figure A.2.

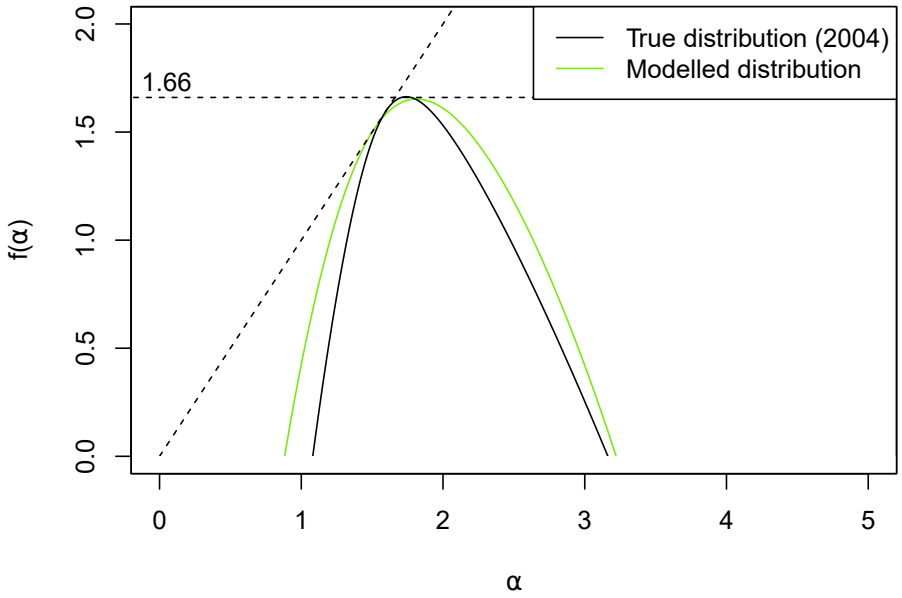

FIGURE A.2. **Spectrum of the income distribution predicted by our model.** The real distribution and the predicted distribution are close.

APPENDIX B

Additional criteria for segregation measures

(Reardon and O'Sullivan, 2004) (partially based on James and Taeuber (1985)) suggest that a good segregation measure should have:

(1) **Location equivalence.** This means that if the local environment of two points have the same population composition, then treating them as one single environment should not change segregation. In the case of multifractal analysis, such two local environment will correspond to the same α value, so the α distribution will not change. However, the corresponding $f(\alpha)$ may change if enough points are removed. This criterion can be related to *organizational equivalence* from James and Taeuber (1985), which states that when units are subdivided with preserved proportions or combined, then segregation does not change. In our case, we only have the property that combining several units with the same spectra will result in a unit with still the same spectrum. In addition, figure IV.21 shows that dividing an area (New York) into several similar areas (its boroughs) results in similar spectra.

(2) **Population density invariance/Size invariance.** This criteria is equivalent to invariance through linear transformation of the variable distribution, which is a well known property of multifractals.

(3) **Composition invariance.** It means that increasing uniformly the proportion of one category, but not of the others should leave segregation invariant. This criterion is presented as controversial, and we stand with the opposite point of view.

(4) **Transfers and exchanges.** It means that it is expected that individuals moving to or exchanging their place with other individual of an area where their category is less represented will reduce segregation. In our case, the multifractal spectrum conversely shrinks when people move towards area where their category is over-represented.

(5) **Additive spatial decomposability.** It is presented as "If X spatial sub-areas are aggregated into Y larger spatial areas, then a segregation measure should be decomposable into a sum of within- and between-area components." This is a done through the σ-additivity property when the measure is defined pre-multifractal analysis.

(6) **Additive grouping decomposability.** It is presented as "If M groups are clustered in N supergroups, then a segregation measure should be decomposable into a sum of independent within- and between-supergroup components." This does not make sense in our context, since it contradicts the continuous nature of our ordinal variables.

Bibliography

Abeysinghe, T. and Hao, W. Y. (2014), 'Income inequality in Singapore: Do housing prices play a role?'. SCAPE Working Paper Series. Paper No. 2014/01. URL.

Adnan, M., Pereira, F., Lima Azevedo, C., Basak, K., Lovric, M., Raveau, S., Zhu, Y., Ferreira, J., Zegras, C. and Ben-Akiva, M. (2016), SimMobility: A Multi-Scale Integrated Agent-based Simulation Platform, *in* '95th Annual Meeting, Transportation Research Board', Washington D.C.

Andersen, H. S. (2002), 'Excluded Places: The Interaction Between Segregation, Urban Decay and Deprived Neighbourhoods', *Housing, Theory and Society* **19**(3-4), 153–169.
DOI: 10.1080/140360902321122860

Apparicio, P., Martori, J. C., Pearson, A. L., Fournier, r. and Apparicio, D. (2014), 'An Open-Source Software for Calculating Indices of Urban Residential Segregation', *Social Science Computer Review* **32**(1), 117–128.
DOI: 10.1177/0894439313504539

Arbesman, S., Kleinberg, J. M. and Strogatz, S. H. (2009), 'Superlinear scaling for innovation in cities', *Physical Review. E, Statistical, Nonlinear, and Soft Matter Physics* **79**(1), 016115.
DOI: 10.1103/PhysRevE.79.016115

Arcaute, E., Hatna, E., Ferguson, P., Youn, H., Johansson, A. and Batty, M. (2015), 'Constructing cities, deconstructing scaling laws', *Journal of The Royal Society Interface* **12**(102), 20140745.
DOI: 10.1098/rsif.2014.0745

Arcaute, E., Molinero, C., Hatna, E., Murcio, R., Vargas-Ruiz, C., Masucci, A. P. and Batty, M. (2016), 'Cities and regions in Britain through hierarchical percolation', *Royal Society Open Science* **3**(4), 150691.
DOI: 10.1098/rsos.150691

Ariza-Villaverde, A. B., Jiménez-Hornero, F. J. and De Ravé, E. G. (2013), 'Multifractal analysis of axial maps applied to the study of urban morphology', *Computers, Environment and Urban Systems* **38**, 1–10.
DOI: 10.1016/j.compenvurbsys.2012.11.001

Arneodo, A., Audit, B., Decoster, N., Muzy, J.-F. and Vaillant, C. (2002), Wavelet Based Multifractal Formalism: Applications to DNA Sequences,

Satellite Images of the Cloud Structure, and Stock Market Data, *in* A. Bunde, J. Kropp and H. J. Schellnhuber, eds, 'The Science of Disasters', Springer Berlin Heidelberg, Germany, pp. 26–102.
DOI: 10.1007/978-3-642-56257-0_2
ISBN: 978-3-642-62531-2 / 978-3-642-56257-0 (reprint, 2012)

Arneodo, A., Grasseau, G. and Kostelich, E. J. (1987), 'Fractal dimensions and $f(\alpha)$ spectrum of the Hénon attractor', *Physics Letters A* **124**(8), 426–432.
DOI: 10.1016/0375-9601(87)90546-9

Atkinson, A. B. (1970), 'On the measurement of inequality', *Journal of Economic Theory* **2**(3), 244–263.
DOI: 10.1016/0022-0531(70)90039-6

Atkinson, A. B. (1983), *The economics of inequality*, 2nd edn, Clarendon Press; Oxford University Press, Ney York, NY; Oxford, UK.
ISBN: 978-0-19-877209-5 / 978-0-19-877208-8

Atkinson, A. B. (2015), *Inequality: what can be done?*, Harvard University Press, Cambridge, MA.
ISBN: 978-0-674-50476-9

Atkinson, R. and Bridge, G., eds (2005), *Gentrification in a global context: the new urban colonialism*, Housing and society series, Routledge, London, UK; New-York, NY.
ISBN: 978-0-415-32950-7 / 978-0-415-32951-4

Atmanspacher, H., Scheingraber, H. and Wiedenmann, G. (1989), 'Determination of $f(\alpha)$ for a limited random point set', *Physical Review A, General Physics* **40**(7), 3954–3963.
DOI: 10.1103/PhysRevA.40.3954

Bacry, E., Delour, J. and Muzy, J.-F. (2001), 'Modelling financial time series using multifractal random walks', *Physica A: Statistical Mechanics and its Applications* **299**(1-2), 84–92.
DOI: 10.1016/S0378-4371(01)00284-9

Bacry, E., Muzy, J.-F. and Arneodo, A. (1993), 'Singularity spectrum of fractal signals from wavelet analysis: Exact results', *Journal of Statistical Physics* **70**(3-4), 635–674.
DOI: 10.1007/BF01053588

Banavar, J. R., Maritan, A. and Rinaldo, A. (1999), 'Size and form in efficient transportation networks', *Nature* **399**, 130–132.
DOI: 10.1038/20144

Barner, M., Cottineau, C., Molinero, C., Salat, H., Stanilov, K. and Arcaute, E. (2018), Multiscale entropy in the spatial context of cities. ArXiv: 1711.09817.

Barnsley, M. F. (1988), Chapter 2 Metric Spaces; Equivalent Spaces; Classification of Subsets; and the Space of Fractals, *in* 'Fractals everywhere', Academic Press, Boston, MA, pp. 69–86.
ISBN: 978-0-12-079062-3

Barunik, J., Aste, T., Di Matteo, T. and Liu, R. (2012), 'Understanding the source of multifractality in financial markets', *Physica A: Statistical Mechanics and its Applications* **391**(17), 4234–4251.
DOI: 10.1016/j.physa.2012.03.037

Batty, M. (1997), 'Cellular Automata and Urban Form: A Primer', *Journal of the American Planning Association* **63**(2), 266–274.
DOI: 10.1080/01944369708975918

Batty, M. (2005), *Cities and complexity: understanding cities with cellular automata, agent-based models, and fractals*, MIT Press, Cambridge, MA.
ISBN: 978-0-262-02583-6

Batty, M. (2007), 'Model cities', *Town Planning Review* **78**(2), 125–151.
DOI: 10.3828/tpr.78.2.3

Batty, M. (2008*a*), Fifty Years of Urban Modeling: Macro-Statics to Micro-Dynamics, *in* S. Albeverio, D. Andrey, P. Giordano and A. Vancheri, eds, 'The Dynamics of Complex Urban Systems', Physica-Verlag HD, Heidelberg, Germany, pp. 1–20.
DOI: 10.1007/978-3-7908-1937-3_1
ISBN: 978-3-7908-1936-6

Batty, M. (2008*b*), 'The Size, Scale, and Shape of Cities', *Science* **319**(5864), 769–771.
DOI: 10.1126/science.1151419

Batty, M. (2013), *The new science of cities*, MIT Press, Cambridge, MA.
ISBN: 978-0-262-01952-1

Batty, M. (2016), 'Classifying urban models', *Environment and Planning B: Planning and Design* **43**(2), 251–256.
DOI: 10.1177/0265813516630803

Batty, M. (2017), Cities in Disequilibrium, *in* J. Johnson, A. Nowak, P. Ormerod, B. Rosewell and Y.-C. Zhang, eds, 'Non-Equilibrium Social Science and Policy', Springer International Publishing, Cham, Switzerland, pp. 81–96.
DOI: 10.1007/978-3-319-42424-8_6
ISBN: 978-3-319-42422-4 / 978-3-319-42424-8

Batty, M. (2018), Science in Planning: Theory Methods and Models, *in* 'Planning Knowledge and Research', Routledge, New York, NY.
ISBN: 978-1-138-23375-1 / 978-1-138-23376-8

Batty, M. and Longley, P. (1986), 'The fractal simulation of urban structure 1986', *Environment and Planning A* **18**(5), 1143–1179.

Batty, M. and Longley, P. (1994), *Fractal cities: a geometry of form and function*, Academic Press, London, UK.
ISBN: 978-0-12-455570-9

Batty, M. and Longley, P. (2014), Modelling Spatial Morphologies: Fractal Patterns from Cellular Automata, *in* R. Abrahart and L. See, eds, 'Geo-Computation, Second Edition', CRC Press, pp. 23–48.
DOI: 10.1201/b17091-3
ISBN: 978-1-4665-0328-1

Bell, W. (1954), 'A probability model for the measurement of ecological segregation', *Social Forces* **32**(4), 357–364.
JSTOR: 2574118

Benzi, R., Paladin, G., Parisi, G. and Vulpiani, A. (1984), 'On the multi-fractal nature of fully developed turbulence and chaotic systems', *Journal of Physics A: Mathematical and General* **17**(18), 3521–3531.
DOI: 10.1088/0305-4470/17/18/021

Berry, K. J. and Mielke, P. W. (1992), 'Indices of Ordinal Variation', *Perceptual and Motor Skills* **74**(2), 576–578.
DOI: 10.2466/pms.1992.74.2.576

Bettencourt, L. M. A. (2013), 'The Origins of Scaling in Cities', *Science* **340**(6139), 1438–1441.
DOI: 10.1126/science.1235823

Bettencourt, L. M. A. and Lobo, J. (2016), 'Urban scaling in Europe', *Journal of The Royal Society Interface* **13**(116), 20160005.
DOI: 10.1098/rsif.2016.0005

Bettencourt, L. M. A., Lobo, J., Helbing, D., Kühnert, C. and West, G. B. (2007), 'Growth, innovation, scaling, and the pace of life in cities', *Proceedings of the National Academy of Sciences* **104**(17), 7301–7306.
DOI: 10.1073/pnas.0610172104

Brown, G., Michon, G. and Peyrière, J. (1992), 'On the multifractal analysis of measures', *Journal of Statistical Physics* **66**(3-4), 775–790.
DOI: 10.1007/BF01055700

Brueckner, J. K., Thisse, J.-F. and Zenou, Y. (1999), 'Why is central Paris rich and downtown Detroit poor?', *European Economic Review* **43**(1), 91–107.
DOI: 10.1016/S0014-2921(98)00019-1

Buonocore, R., Aste, T. and Di Matteo, T. (2016), 'Measuring multiscaling in financial time-series', *Chaos, Solitons & Fractals* **88**, 38–47.
DOI: 10.1016/j.chaos.2015.11.022

Buonocore, R. J., Aste, T. and Di Matteo, T. (2017), 'Asymptotic scaling properties and estimation of the generalized Hurst exponents in financial data', *Physical Review E* **95**(4).
DOI: 10.1103/PhysRevE.95.042311

Burgess, E. W. (1928), 'Residential Segregation in American Cities', *The Annals of the American Academy of Political and Social Science* **140**(1), 105–115.
DOI: 10.1177/000271622814000115

Ceriani, L. and Verme, P. (2012), 'The origins of the Gini index: extracts from Variabilità e Mutabilità (1912) by Corrado Gini', *The Journal of Economic Inequality* **10**(3), 421–443.
DOI: 10.1007/s10888-011-9188-x

Chakravorty, S. (1996), 'A Measurement of Spatial Disparity: The Case of Income Inequality', *Urban Studies* **33**(9), 1671–1686.
DOI: 10.1080/0042098966556

Chen, Y. (2008), 'A Wave-Spectrum Analysis of Urban Population Density: Entropy, Fractal, and Spatial Localization', *Discrete Dynamics in Nature and Society* **2008**, 1–22.
DOI: 10.1155/2008/728420

Chen, Y. (2014), 'Multifractals of central place systems: Models, dimension spectrums, and empirical analysis', *Physica A: Statistical Mechanics and its Applications* **402**, 266–282.
DOI: 10.1016/j.physa.2014.01.061

Chen, Y. (2016), 'Defining Urban and Rural Regions by Multifractal Spectrums of Urbanization', *Fractals* **24**(01), 1650004.
DOI: 10.1142/S0218348X16500043

Chen, Y. and Wang, J. (2013), 'Multifractal characterization of urban form and growth: the case of Beijing', *Environment and Planning B: Planning and Design* **40**(5), 884–904.
DOI: 10.1068/b36155

Chen, Y. and Zhou, Y. (2004), 'Multi-fractal measures of city-size distributions based on the three-parameter Zipf model', *Chaos, Solitons & Fractals* **22**(4), 793–805.
DOI: 10.1016/j.chaos.2004.02.059

Cheng, Q. (1999*a*), 'The gliding box method for multifractal modeling', *Computers & Geosciences* **25**(9), 1073–1079.
DOI: 10.1016/S0098-3004(99)00068-0

Cheng, Q. (1999*b*), 'Multifractality and spatial statistics', *Computers & Geosciences* **25**(9), 949–961.
DOI: 10.1016/S0098-3004(99)00060-6

Cheng, Q. and Agterberg, F. P. (1996), 'Comparison between two types of multifractal modeling', *Mathematical Geology* **28**(8), 1001–1015.
DOI: 10.1007/BF02068586

Chhabra, A. B., Meneveau, C., Jensen, R. V. and Sreenivasan, K. R. (1989), 'Direct determination of the $f(\alpha)$ singularity spectrum and its application to fully developed turbulence', *Physical Review A* **40**(9), 5284–5294.
DOI: 10.1103/PhysRevA.40.5284

Chhabra, A. B. and Sreenivasan, K. R. (1991), 'Negative dimensions: Theory, computation, and experiment', *Physical Review A, Atomic, Molecular, and Optical Physics* **43**(2), 1114–1117.
DOI: 10.1103/PhysRevA.43.1114

Chodrow, P. S. (2017), 'Structure and information in spatial segregation', *Proceedings of the National Academy of Sciences* **114**(44), 11591–11596.
DOI: 10.1073/pnas.1708201114

Codes (2018), weblink. R codes used for the main analyses.

Cortese, C. F., Falk, R. F. and Cohen, J. K. (1976), 'Further Considerations on the Methodological Analysis of Segregation Indices', *American Sociological Review* **41**(4), 630–637.
DOI: 10.2307/2094840

Cottineau, C., Hatna, E., Arcaute, E. and Batty, M. (2017), 'Diverse cities or the systematic paradox of Urban Scaling Laws', *Computers, Environment and Urban Systems* **63**, 80–94.
DOI: 10.1016/j.compenvurbsys.2016.04.006

Dalton, H. (1920), 'The Measurement of the Inequality of Incomes', *The Economic Journal* **30**(119), 348–361.
DOI: 10.2307/2223525

Data (DWP:2012*b*), weblink 1, weblink 2. Department for Work & Pensions (DWP), Family Resources Survey and Household Below Average Income series, year 2012-13.

Data (FCA:2017*b*), weblink 1, weblink 2. Financial Conduct Authority (FCA), Product sales data and Mortgage lending statistics, 2017.

Data (GLA:2018), weblink. Greater London Authority (GLA), Housing in London report 2018.

Data (HMLR:1995-16), weblink. HM Land Registry (HMLR), Price Paid Data for the years 1995 to 2016.

Data (HMRC:2014*b*), weblink. HM Revenue & Customs (HMRC), request under the Freedom of Information act, year 2014-15.

Data (KC:2012*a*), weblink. Kyoto City Open Data website.

Data (LonEnergy:2008-16), weblink. Ministry of Housing, Communities & Local Government (MHCLG), Energy Performance of Buildings Data:

England and Wales, 2008-2016.

Data (LonIncome:2002-13), weblink. Greater London Authority (GLA), GLA Household Income Estimates from 2002 to 2013.

Data (NY:2002-18), weblink. NYC Planning, PLUTO database since 2002.

Data (NYIncome:2010), weblink. Census Tract FactFinder website.

Data (NY:Sales), weblink. New York City Open Data, Annualized Rolling Sales.

Data (ONS:2007-11), weblink. Office for National Statistics (ONS), Trend in life expectancy at birth and at age 65 by socio-economic position based on the National Statistics Socio-economic Classification, England and Wales: 1982-1986 to 2007-2011.

Data (ONS:2011), weblink. London Datastore, 2011 Census Snapshot: Households and Families, based on the 2011 Census by the Office for National Statistics (ONS).

Data (ONS:2017*a*), weblink. Office for National Statistics (ONS), Estimates of the population for the UK, England and Wales, Scotland and Northern Ireland, year 2017.

Data (ParIncome:2014*a*), weblink. Institut National de la Statistique et des Etudes Economiques (INSEE), Revenus, pauvreté et niveau de vie en 2014, 2014.

Dawkins, C. J. (2007), 'Space and the Measurement of Income Segregation', *Journal of Regional Science* **47**(2), 255–272.
DOI: 10.1111/j.1467-9787.2007.00508.x

Delloye, J. (2018), Urban morphodynamics : reconciling location theory and complex systems, PhD thesis, Université Catholique de Louvain, Belgique.
https://dial.uclouvain.be/pr/boreal/object/boreal:200833.

Derrible, S. and Kennedy, C. (2010*a*), 'Characterizing metro networks: state, form, and structure', *Transportation* **37**(2), 275–297.
DOI: 10.1007/s11116-009-9227-7

Derrible, S. and Kennedy, C. (2010*b*), 'The complexity and robustness of metro networks', *Physica A: Statistical Mechanics and its Applications* **389**(17), 3678–3691.
DOI: 10.1016/j.physa.2010.04.008

Di Matteo, T. (2007), 'Multi-scaling in finance', *Quantitative Finance* **7**(1), 21–36.
DOI: 10.1080/14697680600969727

Di Matteo, T., Aste, T. and Dacorogna, M. (2003), 'Scaling behaviors in differently developed markets', *Physica A: Statistical Mechanics and its Applications* **324**(1-2), 183–188.
DOI: 10.1016/S0378-4371(02)01996-9

Duncan, O. D. and Duncan, B. (1955), 'A Methodological Analysis of Segregation Indexes', *American Sociological Review* **20**(2), 210–217.
DOI: 10.2307/2088328

Dzioubinski, O. and Chipman, R. (1999), Trends in consumption and production: household energy consumption, *in* 'DESA discussion paper series, no. 6', United Nations, Dept. of Economic and Social Affairs, New York, NY. URL.

Engelen, G., White, R., Uljee, I. and Drazan, P. (1995), 'Using cellular automata for integrated modelling of socio-environmental systems', *Environmental Monitoring and Assessment* **34**(2), 203–214.
DOI: 10.1007/BF00546036

Evertsz, C. J. G. and Mandelbrot, B. B. (1992), Multifractal Measures, *in* H.-O. Peitgen, H. Jürgens and D. Saupe, eds, 'Chaos and fractals: new frontiers of science', Springer-Verlag, New York, NY.
ISBN: 978-0-38-797903-8

Falconer, K. J. (2003), *Fractal geometry: mathematical foundations and applications*, 2nd edn, Wiley, Chichester, UK.
ISBN: 978-0-470-84861-6 / 978-0-470-84862-3

Farzanegan, M. R., Gholipour, H. and Nguyen, J. (2017), Housing costs and inequality in post-revolutionary Iran, *in* 'European Public Choice Society Annual Meeting 2017, School of Public Policy', Central European University, Budapest, Hungary. URL.

Fielding, A. J. (2004), 'Class and space: social segregation in Japanese cities', *Transactions of the Institute of British Geographers* **29**(1), 64–84.
DOI: 10.1111/j.0020-2754.2004.00114.x

Fotheringham, A. S., Batty, M. and Longley, P. A. (1989), 'Diffusion-limited aggregation and the fractal nature of urban growth', *Papers of the Regional Science Association* **67**(1), 55–69.
DOI: 10.1007/BF01934667

Frankhauser, P. (1994), *La fractalité des structures urbaines*, Collection Villes, Anthropos : Diffusion, Economica, Paris, France.
ISBN: 978-2-7178-2668-5 (1999 edition)

Frankhauser, P. (2004), Comparing the morphology of urban patterns in Europe. a fractal approach, *in* P. Borsdorf and P. Zembri, eds, 'European Cities: Insights on Outskirts, Structures', ESF COST Office, Brussels, Belgium, pp. 79–105.
ISBN: 9782110856630

Frankhauser, P., Tannier, C., Vuidel, G. and Houot, H. (2018), 'An integrated multifractal modelling to urban and regional planning', *Computers, Environment and Urban Systems* **67**, 132–146.

DOI: 10.1016/j.compenvurbsys.2017.09.011

Frisch, U. and Parisi, G. (1983), Turbulence and predictability of geophysical flows and climate dynamics, *in* 'Varenna Summer School LXXXVIII'.

Fujita, K. and Hill, R. C. (1997), Together and equal: place stratification in Osaka, *in* P. P. Karan and K. Stapleton, eds, 'The Japanese City', The University Press of Kentucky, Lexington, KY, pp. 106–133.
JSTOR: j.ctt130j6ms.10
ISBN: 978-0-81-312035-5

Garrett, T. J. (2011), 'Are there basic physical constraints on future anthropogenic emissions of carbon dioxide?', *Climatic Change* **104**(3-4), 437–455.
DOI: 10.1007/s10584-009-9717-9

Gini, C. (1912), *Variabilità e mutabilità : contributo allo studio delle distribuzioni e delle relazioni statistiche*, Tipografia di Paolo Cuppin, Bologna, Italia. URL.

Glaeser, E. L., Kahn, M. E. and Rappaport, J. (2008), 'Why do the poor live in cities? The role of public transportation', *Journal of Urban Economics* **63**(1), 1–24.
DOI: 10.1016/j.jue.2006.12.004

Gomez-Lievano, A., Patterson-Lomba, O. and Hausmann, R. (2016), 'Explaining the prevalence, scaling and variance of urban phenomena', *Nature Human Behaviour* **1**(1), 0012.
DOI: 10.1038/s41562-016-0012

Grassberger, P. and Procaccia, I. (2004), Measuring the Strangeness of Strange Attractors, *in* B. R. Hunt, T.-Y. Li, J. A. Kennedy and H. E. Nusse, eds, 'The Theory of Chaotic Attractors', Springer, New York, NY, pp. 170–189. DOI: 10.1007/978-0-387-21830-4_12.
ISBN: 978-1-4419-2330-1 / 978-0-387-21830-4

Gu, G.-F. and Zhou, W.-X. (2006), 'Detrended fluctuation analysis for fractals and multifractals in higher dimensions', *Physical Review E* **74**(6), 061104.
DOI: 10.1103/PhysRevE.74.061104

Haag, G. (1994), 'The rank-size distribution of settlements as a dynamic multifractal phenomenon', *Chaos, Solitons & Fractals* **4**(4), 519–534.
DOI: 10.1016/0960-0779(94)90063-9

Halsey, T. C., Jensen, M. H., Kadanoff, L. P., Procaccia, I. and Shraiman, B. I. (1987), 'Fractal measures and their singularities: The characterization of strange sets', *Nuclear Physics B - Proceedings Supplements* **2**(Supplement C), 501–511.
DOI: 10.1016/0920-5632(87)90036-3

Heppenstall, A. J., ed. (2012), *Agent-based models of geographical systems*, Springer, Dordrecht, Netherlands.
ISBN: 978-90-481-8926-7

Hillier, B. and Hanson, J. (1984), *The social logic of space*, Cambridge University Press, Cambridge, MA.
ISBN: 978-0-511-59723-7

Holschneider, M. (1988), 'On the wavelet transformation of fractal objects', *Journal of Statistical Physics* **50**(5-6), 963–993.
DOI: 10.1007/BF01019149

Howard, B., Parshall, L., Thompson, J., Hammer, S., Dickinson, J. and Modi, V. (2012), 'Spatial distribution of urban building energy consumption by end use', *Energy and Buildings* **45**, 141–151.
DOI: 10.1016/j.enbuild.2011.10.061

Hu, S., Cheng, Q., Wang, L. and Xie, S. (2012), 'Multifractal characterization of urban residential land price in space and time', *Applied Geography* **34**, 161–170.
DOI: 10.1016/j.apgeog.2011.10.016

Hu, S., Cheng, Q., Wang, L. and Xu, D. (2013), 'Modeling land price distribution using multifractal IDW interpolation and fractal filtering method', *Landscape and Urban Planning* **110**, 25–35.
DOI: 10.1016/j.landurbplan.2012.09.008

Huang, Y. X., Schmitt, F. G., Hermand, J.-P., Gagne, Y., Lu, Z. M. and Liu, Y. L. (2011), 'Arbitrary-order Hilbert spectral analysis for time series possessing scaling statistics: Comparison study with detrended fluctuation analysis and wavelet leaders', *Physical Review E* **84**(1).
DOI: 10.1103/PhysRevE.84.016208

Huang, Y. X., Schmitt, F. G., Lu, Z. M., Fougairolles, P., Gagne, Y. and Liu, Y. L. (2010), 'Second-order structure function in fully developed turbulence', *Physical Review E* **82**(2).
DOI: 10.1103/PhysRevE.82.026319

Ibraimovic, T. and Hess, S. (2018), 'A latent class model of residential choice behaviour and ethnic segregation preferences', *Housing Studies* **33**(4), 544–564.
DOI: 10.1080/02673037.2017.1373749

Ihlen, E. A. and Vereijken, B. (2013), 'Multifractal formalisms of human behavior', *Human Movement Science* **32**(4), 633–651.
DOI: 10.1016/j.humov.2013.01.008

Jacobs, J. (1961), *The death and life of great American cities*, New York: Random House, New York, NY.
ISBN: 978-0-394-42159-9

Jaffard, S., Lashermes, B. and Abry, P. (2007), Wavelet Leaders in Multifractal Analysis, *in* T. Qian, M. I. Vai and Y. Xu, eds, 'Wavelet Analysis and Applications', Birkhauser, Basel, pp. 201–246.
DOI: 10.1007/978-3-7643-7778-6_17
ISBN: 978-3-7643-7777-9

Jakubs, J. F. (1981), 'A distance-based segregation index', *Socio-Economic Planning Sciences* **15**(3), 129–136.
DOI: 10.1016/0038-0121(81)90028-8

James, D. R. and Taeuber, K. E. (1985), 'Measures of Segregation', *Sociological Methodology* **15**, 1–32.
DOI: 10.2307/270845

Jargowsky, P. A. (1996), 'Take the Money and Run: Economic Segregation in U.S. Metropolitan Areas', *American Sociological Review* **61**(6), 984–998.
DOI: 10.2307/2096304

Jargowsky, P. A. (2002), Sprawl, concentration of poverty, and urban inequality, *in* G. D. Squires, ed., 'Urban sprawl: Causes, consequences, & policy responses', Urban Institute Press, Washington, D.C, pp. 39–72.
ISBN: 978-0-87766-709-4

Jargowsky, P. A. and Kim, J. (2005), 'A measure of spatial segregation: The generalized neighborhood sorting index'. National Poverty Center Working Paper Series. Paper No. 05-3. URL.

Jiang, Z.-Q., Xie, W.-J., Zhou, W.-X. and Sornette, D. (2018), Multifractal analysis of financial markets. ArXiv: 1805.04750.

Jin, Y. and Wegener, M. (2013), 'Guest Editorial', *Environment and Planning B: Planning and Design* **40**(6), 951–954.
DOI: 10.1068/b4006ge

Joyeux, R. and Ripple, R. D. (2007), 'Household energy consumption versus income and relative standard of living: A panel approach', *Energy Policy* **35**(1), 50–60.
DOI: 10.1016/j.enpol.2005.10.012

Kaizoji, T. (2003), 'Scaling behavior in land markets', *Physica A: Statistical Mechanics and its Applications* **326**(1-2), 256–264.
DOI: 10.1016/S0378-4371(03)00145-6

Kantelhardt, J. W. (2012), Fractal and Multifractal Time Series, *in* R. A. Meyers, ed., 'Mathematics of Complexity and Dynamical Systems', Springer, New York, NY, pp. 463–487.
DOI: 10.1007/978-1-4614-1806-1_30
ISBN: 978-1-4614-1805-4 / 978-1-4614-1806-1

Kantelhardt, J. W., Zschiegner, S. A., Koscielny-Bunde, E., Havlin, S., Bunde, A. and Stanley, H. E. (2002), 'Multifractal detrended fluctuation

analysis of nonstationary time series', *Physica A: Statistical Mechanics and its Applications* **316**(1-4), 87–114.
DOI: 10.1016/S0378-4371(02)01383-3

Kasperowicz, R. (2014), 'Economic growth and energy consumption in 12 European countries: a panel data approach', *Journal of International Studies* **7**(3), 112–122.
DOI: 10.14254/2071-8330.2014/7-3/10

Kestener, P. and Arneodo, A. (2003), 'Three-Dimensional Wavelet-Based Multifractal Method: The Need for Revisiting the Multifractal Description of Turbulence Dissipation Data', *Physical Review Letters* **91**(19).
DOI: 10.1103/PhysRevLett.91.194501

Kvalseth, T. O. (1995*a*), 'Coefficients of Variation for Nominal and Ordinal Categorical Data', *Perceptual and Motor Skills* **80**(3), 843–847.
DOI: 10.2466/pms.1995.80.3.843

Kvalseth, T. O. (1995*b*), 'Comment on the Coefficient of Ordinal Variation', *Perceptual and Motor Skills* **81**(2), 621–622.
DOI: 10.1177/003151259508100251

Lashermes, B., Jaffard, S. and Abry, P. (2005), Wavelet Leader based Multifractal Analysis, *in* 'IEEE International Conference on Acoustics, Speech, and Signal Processing. Proceedings', Vol. 4, IEEE, Philadelphia, PA, pp. 161–164.
DOI: 10.1109/ICASSP.2005.1415970
ISBN: 978-0-7803-8874-1

Leitão, J. C., Miotto, J. M., Gerlach, M. and Altmann, E. G. (2016), 'Is this scaling nonlinear?', *Royal Society Open Science* **3**(7), 150649.
DOI: 10.1098/rsos.150649

Lieberson, S. (1981), *A Piece of the Pie: Blacks and White Immigrants Since 1880*, University of California Press, Berkeley, CA.
ISBN: 978-0-52-004362-6

Liu, J.-L., Yu, Z.-G. and Anh, V. (2015), 'Determination of multifractal dimensions of complex networks by means of the sandbox algorithm', *Chaos: An Interdisciplinary Journal of Nonlinear Science* **25**(2), 023103.
DOI: 10.1063/1.4907557

Lloyd, C. D. (2016), 'Are spatial inequalities growing? The scale of population concentrations in England and Wales', *Environment and Planning A* **48**(7), 1318–1336.
DOI: 10.1177/0308518X15621306

Lobmayer, P. and G., W. R. (2002), 'Inequality, residential segregation by income, and mortality in US cities', *Journal of Epidemiology & Community Health* **56**(3), 183–187.

DOI: 10.1136/jech.56.3.183

Longley, P. and Batty, M. (1989), 'On the Fractal Measurement of Geographical Boundaries.', *Geographical Analysis* **21**(1), 47–67.

Lorenz, M. O. (1905), 'Methods of Measuring the Concentration of Wealth', *Publications of the American Statistical Association* **9**(70), 209–219.
DOI: 10.2307/2276207

Louf, R. and Barthelemy, M. (2013), 'Modeling the Polycentric Transition of Cities', *Physical Review Letters* **111**(19).
DOI: 10.1103/PhysRevLett.111.198702

Louf, R. and Barthelemy, M. (2014), 'Scaling: Lost in the Smog', *Environment and Planning B: Planning and Design* **41**(5), 767–769.
DOI: 10.1068/b4105c

Louf, R. and Barthelemy, M. (2015), 'How congestion shapes cities: from mobility patterns to scaling', *Scientific Reports* **4**(1).
DOI: 10.1038/srep05561

Louf, R. and Barthelemy, M. (2016), 'Patterns of Residential Segregation', *PLoS ONE* **11**(6), e0157476.
DOI: 10.1371/journal.pone.0157476

Louf, R., Roth, C. and Barthelemy, M. (2014), 'Scaling in Transportation Networks', *PLoS ONE* **9**(7), e102007.
DOI: 10.1371/journal.pone.0102007

Mainster, M. A. (1990), 'The fractal properties of retinal vessels: embryological and clinical implications', *Eye* **4 (Pt. 1)**, 235–241.
DOI: 10.1038/eye.1990.33

Mandelbrot, B. B. (1982), *The fractal geometry of nature*, W.H. Freeman, San Francisco, CA.
ISBN: 978-0-7167-1186-5

Mandelbrot, B. B. (1997), *Fractals and Scaling in Finance Discontinuity, Concentration, Risk. Selecta Volume E*, Springer, New York, NY.
ISBN: 978-1-4757-2763-0

Mandelbrot, B. B. (1999), 'A Multifractal Walk down Wall Street', *Scientific American* **280**(2), 70–73.
DOI: 10.1038/scientificamerican0299-70

Mandelbrot, B. B., Evertsz, C. J. G. and Hayakawa, Y. (1990), 'Exactly self-similar left-sided multifractal measures', *Physical Review A, Atomic, Molecular, and Optical Physics* **42**(8), 4528–4536.
DOI: 10.1103/PhysRevA.42.4528

Martin, R., Moore, J. and Schindler, S., eds (2015), *The art of inequality: architecture, housing, and real estate: a provisional report*, 1st edn, Temple Hoyne Buell Center for the Study of American Architecture, Columbia

University, New York, NY.
ISBN: 978-1-941332-22-1

Massey, D. S. and Denton, N. A. (1988), 'The Dimensions of Residential Segregation', *Social Forces* **67**(2), 281–315.
DOI: 10.2307/2579183

Massey, D. S. and Denton, N. A. (1993), *American apartheid: segregation and the making of the underclass*, Harvard University Press, Cambridge, MA.
ISBN: 978-0-67-401821-1

Masucci, A. P., Arcaute, E., Hatna, E., Stanilov, K. and Batty, M. (2015), 'On the problem of boundaries and scaling for urban street networks', *Journal of The Royal Society Interface* **12**(111), 20150763.
DOI: 10.1098/rsif.2015.0763

McDonald, J. F. and McMillen, D. P. (2011), *Urban economics and real estate: theory and policy*, 2nd edn, Wiley, Hoboken, NJ.
ISBN: 978-0-470-59148-2

McMillen, D. P. and Smith, S. C. (2003), 'The number of subcenters in large urban areas', *Journal of Urban Economics* **53**(3), 321–338.
DOI: 10.1016/S0094-1190(03)00026-3

Meneveau, C. and Sreenivasan, K. (1989), 'Measurement of $f(\alpha)$ from scaling of histograms, and applications to dynamical systems and fully developed turbulence', *Physics Letters A* **137**(3), 103–112.
DOI: 10.1016/0375-9601(89)90093-5

Morales, R., Di Matteo, T. and Aste, T. (2013), 'Non-stationary multifractality in stock returns', *Physica A: Statistical Mechanics and its Applications* **392**(24), 6470–6483.
DOI: 10.1016/j.physa.2013.08.037

Morales, R., Di Matteo, T., Gramatica, R. and Aste, T. (2012), 'Dynamical generalized Hurst exponent as a tool to monitor unstable periods in financial time series', *Physica A: Statistical Mechanics and its Applications* **391**(11), 3180–3189.
DOI: 10.1016/j.physa.2012.01.004

Morgan, B. S. (1983), 'A Distance-Decay Based Interaction Index to Measure Residential Segregation', *Area* **15**(3), 211–217.
JSTOR: 20001935

Murcio, R., Masucci, A. P., Arcaute, E. and Batty, M. (2015), 'Multifractal to monofractal evolution of the London street network', *Physical Review E* **92**(6).
DOI: 10.1103/PhysRevE.92.062130

Murcio, R. and Rodríguez-Romo, S. (2009), 'Colored diffusion-limited aggregation for urban migration', *Physica A: Statistical Mechanics and its Applications* **388**(13), 2689–2698.
DOI: 10.1016/j.physa.2009.03.021

Mustafa, A. M. E. S. (2018), Spatiotemporal modeling of interactions between urbanization and flood risk: a multi-level approach, PhD thesis, Université de Liège, Belgique. https://orbi.uliege.be/handle/2268/221082.
DOI: 10.13140/RG.2.2.21270.86082

Muzy, J.-F., Bacry, E. and Arneodo, A. (1991), 'Wavelets and multifractal formalism for singular signals: Application to turbulence data', *Physical Review Letters* **67**(25), 3515–3518.
DOI: 10.1103/PhysRevLett.67.3515

Muzy, J.-F., Delour, J. and Bacry, E. (2000), 'Modelling fluctuations of financial time series: from cascade process to stochastic volatility model', *The European Physical Journal B* **17**(3), 537–548.
DOI: 10.1007/s100510070131

Nie, Q., Xu, J. and Liu, Z. (2015), 'Fractal and multifractal characteristic of spatial pattern of urban impervious surfaces', *Earth Science Informatics* **8**(2), 381–392.
DOI: 10.1007/s12145-014-0159-1

Nielsen, F. (2017), 'Inequality and inequity', *Social Science Research* **62**, 29–35.
DOI: 10.1016/j.ssresearch.2016.12.009

Odland, J. (1978), 'The Conditions for Multi-Center Cities', *Economic Geography* **54**(3), 234.
DOI: 10.2307/142837

Ohnishi, T., Mizuno, T., Shimizu, C. and Watanabe, T. (2012), 'Power Laws in Real Estate Prices during Bubble Periods', *International Journal of Modern Physics: Conference Series* **16**, 61–81.
DOI: 10.1142/S2010194512007787

Olsen, L. (1995), 'A Multifractal Formalism', *Advances in Mathematics* **116**(1), 82–196.
DOI: 10.1006/aima.1995.1066

Ossadnik, S. M., Buldyrev, S. V., Goldberger, A. L., Havlin, S., Mantegna, R. N., Peng, C.-K., Simons, M. and Stanley, H. E. (1994), 'Correlation approach to identify coding regions in DNA sequences', *Biophysical Journal* **67**(1), 64–70.
DOI: 10.1016/S0006-3495(94)80455-2

Palla, G., Lovász, L. and Vicsek, T. (2010), 'Multifractal network generator', *Proceedings of the National Academy of Sciences* **107**(17), 7640–7645.

DOI: 10.1073/pnas.0912983107

Pan, W., Ghoshal, G., Krumme, C., Cebrian, M. and Pentland, A. (2013), 'Urban characteristics attributable to density-driven tie formation', *Nature Communications* **4**, 1961.
DOI: 10.1038/ncomms2961

Park, R. E. (1924), 'The Concept of Social Distance As Applied to the Study of Racial Attitudes and Racial Relations', *Journal of Applied Sociology* **8**, 339–344. URL.

Park, R. E. (1926), 'The Concept of Position in Sociology', *Papers and Proceedings of the American Sociological Society* **20**, 1–14. URL.

Peng, C.-K., Buldyrev, S. V., Havlin, S., Simons, M., Stanley, H. E. and Goldberger, A. L. (1994), 'Mosaic organization of DNA nucleotides', *Physical Review. E, Statistical Physics, Plasmas, Fluids, and Related Interdisciplinary Topics* **49**(2), 1685–1689.
DOI: 10.1103/PhysRevE.49.1685

Persons, W. M. (1909), 'The Variability in the Distribution of Wealth and Income', *The Quarterly Journal of Economics* **23**(3), 416–449.
DOI: 10.2307/1884773

Pesin, Y. B. (1997), *Dimension theory in dynamical systems: contemporary views and applications*, Chicago lectures in mathematics series, University of Chicago Press, Chicago, IL.
ISBN: 978-0-226-66221-3 / 978-0-226-66222-0

Pigou, A. C. (1912), *Wealth and welfare*, Macmillan and co., limited, London, UK.
ISBN: 978-1-49-435808-2 (reprint, 2013)

Piketty, T. (2014), *Capital in the twenty-first century*, The Belknap Press of Harvard University Press, Cambridge, MA.
ISBN: 978-0-674-43000-6

Portugali, J. (2011), *Complexity, cognition and the city*, Understanding complex systems, Springer Berlin, Germany.
ISBN: 978-3-642-19451-1 / 978-3-642-27087-1

Portugali, J., Meyer, H., Stolk, E. and Tan, E., eds (2012), *Complexity Theories of Cities Have Come of Age*, Springer Berlin Heidelberg, Germany.
ISBN: 978-3-642-24543-5 / 978-3-642-24544-2

Pumain, D. (2004), 'Scaling Laws and Urban Systems'. Santa Fe Institute Working Papers. Paper No. 2004-02-002. URL.

Pumain, D. (2012), Urban Systems Dynamics, Urban Growth and Scaling Laws: The Question of Ergodicity, *in* J. Portugali, H. Meyer, E. Stolk and E. Tan, eds, 'Complexity Theories of Cities Have Come of Age', Springer Berlin Heidelberg, Germany, pp. 91–103.

DOI: 10.1007/978-3-642-24544-2_6
ISBN: 978-3-642-24543-5 / 978-3-642-24544-2

Pumain, D. (2017), Geography Far from Equilibrium, *in* J. Johnson, A. Nowak, P. Ormerod, B. Rosewell and Y.-C. Zhang, eds, 'Non-Equilibrium Social Science and Policy', Springer International Publishing, Cham, Switzerland, pp. 71–80.
DOI: 10.1007/978-3-319-42424-8_5
ISBN: 978-3-319-42422-4 / 978-3-319-42424-8

Reardon, S. F., Farrell, C. R., Matthews, S. A., O'Sullivan, D., Bischoff, K. and Firebaugh, G. (2009), 'Race and space in the 1990s: changes in the geographic scale of racial residential segregation, 1990-2000', *Social Science Research* **38**(1), 55–70.
DOI: 10.1016/j.ssresearch.2008.10.002

Reardon, S. F., Firebaugh, G., O'Sullivan, D. and Matthews, S. (2006), A New Approach to Measuring Socio-Spatial Economic Segregation, *in* '29th General Conference of The International Association for Research in Income and Wealth', Joensuu, Finland. URL.

Reardon, S. F. and O'Sullivan, D. (2004), 'Measures of Spatial Segregation', *Sociological Methodology* **34**(1), 121–162.
DOI: 10.1111/j.0081-1750.2004.00150.x

Rendon de la Torre, S., Kalda, J., Kitt, R. and Engelbrecht, J. (2017), 'Fractal and multifractal analysis of complex networks: Estonian network of payments', *The European Physical Journal B* **90**(12).
DOI: 10.1140/epjb/e2017-80214-5

Ricci, U. (1916), 'L'Indice di variabilità e la curva dei redditi', *Giornale degli Economisti e Rivista di Statistica* **53 (Anno 27)**(3), 177–228.
JSTOR: 23225478

Riedi, R. (1995), 'An Improved Multifractal Formalism and Self-Similar Measures', *Journal of Mathematical Analysis and Applications* **189**(2), 462–490.
DOI: 10.1006/jmaa.1995.1030

Rodríguez-Romo, S. and Murcio, R. (2014), 'An assessment of similarity measures for aggregates grown from multiple seeds', *Chaos, Solitons & Fractals* **66**, 31–40.
DOI: 10.1016/j.chaos.2014.05.006

Salat, H., Murcio, R. and Arcaute, E. (2017), 'Multifractal methodology', *Physica A: Statistical Mechanics and its Applications* **473**, 467–487.
DOI: 10.1016/j.physa.2017.01.041

Salat, H., Murcio, R., Yano, K. and Arcaute, E. (2018), 'Uncovering inequality through multifractality of land prices: 1912 and contemporary Kyoto',

PLoS One .
DOI: 10.1371/journal.pone.0196737

Salingaros, N. and West, B. (1999), 'A universal rule for the distribution of sizes', *Environment and Planning B* **26**(6), 909–923.
DOI: 10.1068/b260909

Schweitzer, F. and Steinbrink, J. (2002), Analysis and Computer Simulation of Urban Cluster Distributions, *in* K. Humpert, K. Brenner and S. Becker, eds, 'Fundamental Principles of Urban Growth', Müller + Busmann, Wuppertal, Germany, pp. 142–157.
DOI: 10.1.1.143.594

Semecurbe, F., Tannier, C. and Roux, S. (2016), 'Spatial distribution of human population in france: exploring the Modifiable Areal Unit Problem using multifractal analysis', *Geographical Analysis* **48**(3), 292–313.
DOI: 10.1068/b260909

Sen, A. K. (1973), *On Economic Inequality*, Oxford University Press, Oxford, UK.
ISBN: 978-0-19-828193-1 (reprint, 1997)

Sen, A. K. (1997), 'From Income Inequality to Economic Inequality', *Southern Economic Journal* **64**(2), 383.
DOI: 10.2307/1060857

Simmonds, D., Waddell, P. and Wegener, M. (2013), 'Equilibrium versus Dynamics in Urban Modelling', *Environment and Planning B: Planning and Design* **40**(6), 1051–1070.
DOI: 10.1068/b38208

Song, Y.-Q., Liu, J.-L., Yu, Z.-G. and Li, B.-G. (2015), 'Multifractal analysis of weighted networks by a modified sandbox algorithm', *Scientific Reports* **5**(1).
DOI: 10.1038/srep17628

Squires, G. D., ed. (2002), *Urban sprawl: causes, consequences, & policy responses*, Urban Institute Press, Washington, D.C.
ISBN: 978-0-87766-709-4

Stanley, H. E. and Meakin, P. (1988), 'Multifractal phenomena in physics and chemistry', *Nature* **335**, 405–409.
DOI: 10.1038/335405a0

Stearns, L. B. and Logan, J. R. (1986), 'Measuring Trends in Segregation: Three Dimensions, Three Measures', *Urban Affairs Quarterly* **22**(1), 124–150.
DOI: 10.1177/004208168602200107

Stosic, T. and Stosic, B. (2006), 'Multifractal analysis of human retinal vessels', *IEEE Transactions on Medical Imaging* **25**(8), 1101–1107.

DOI: 10.1109/TMI.2006.879316

Taeuber, K. E. and Taeuber, A. F. (1965), *Negroes in cities; residential segregation and neighborhood change*, Chicago Aldine Publication Co, Chicago, IL.
ISBN: 978-0-20-236279-3 (reprint, 2009)

Talu, S. (2013), 'Multifractal Geometry in Analysis and Processing of Digital Retinal Photographs for Early Diagnosis of Human Diabetic Macular Edema', *Current Eye Research* **38**(7), 781–792.
DOI: 10.3109/02713683.2013.779722

Tannier, C., Morer, M. and Ansel, D. (2016), Spatial Decision-Making: Between Individual Choices and Collective References, *in* P. Frankhauser and D. Ansel, eds, 'Deciding Where to Live', Springer VS, Wiesbaden, Germany, pp. 127–149.
DOI: 10.1007/978-3-658-15542-1_6
ISBN: 978-3-658-15542-1

Tannier, C. and Thomas, I. (2013), 'Defining and characterizing urban boundaries: A fractal analysis of theoretical cities and Belgian cities', *Computers, Environment and Urban Systems* **41**, 234–248.
DOI: 10.1016/j.compenvurbsys.2013.07.003

Tannier, C., Thomas, I., Vuidel, G. and Frankhauser, P. (2011), 'A Fractal Approach to Identifying Urban Boundaries', *Geographical Analysis* **43**(2), 211–227.

Tannier, C., Vuidel, G., Houot, H. and Frankhauser, P. (2012), 'Spatial accessibility to amenities in fractal and nonfractal urban patterns', *Environment and Planning B: Planning and Design* **39**(5), 801–819.

Theil, H. (1967), *Economics and information theory*, Volume 7 of Studies in mathematical and managerial economics, North-Holland Pub. Co.; Rand McNally, Amsterdam, Netherlands; Chicago, IL.

Thomas, I., Frankhauser, P. and Badariotti, D. (2012), 'Comparing the fractality of european urbanneighbourhoods: do national contexts matter?', *Journal of Geographical Systems* **37**, 189–208.
DOI: 10.1007/s10109-010-0142-4

Tribus, M. and McIrvine, E. C. (1971), 'Energy and Information', *Scientific American* **225**(3), 179–188.
DOI: 10.1038/scientificamerican0971-179

Tricot, C. (1982), 'Two definitions of fractional dimension', *Mathematical Proceedings of the Cambridge Philosophical Society* **91**(01), 57.
DOI: 10.1017/S0305004100059119

Vicsek, T., Family, F. and Meakin, P. (1990), 'Multifractal Geometry of Diffusion-Limited Aggregates', *Europhysics Letters (EPL)* **12**(3), 217–222.

DOI: 10.1209/0295-5075/12/3/005

Waddell, P. (2000), 'A Behavioral Simulation Model for Metropolitan Policy Analysis and Planning: Residential Location and Housing Market Components of Urbansim', *Environment and Planning B: Planning and Design* **27**(2), 247–263.
DOI: 10.1068/b2627

Waddell, P. (2002), 'UrbanSim: Modeling Urban Development for Land Use, Transportation, and Environmental Planning', *Journal of the American Planning Association* **68**(3), 297–314.
DOI: 10.1080/01944360208976274

Waddell, P., Borning, A., Noth, M., Freier, N., Becke, M. and Ulfarsson, G. (2003), 'Microsimulation of Urban Development and Location Choices: Design and Implementation of UrbanSim', *Networks and Spatial Economics* **3**(1), 43–67.
DOI: 10.1023/A:1022049000877

Wang, D., Fu, B., Lu, K., Xiao, L., Zhang, Y. and Feng, X. (2010), 'Multifractal analysis of land use pattern in space and time: A case study in the Loess Plateau of China', *Ecological Complexity* **7**(4), 487–493.
DOI: 10.1016/j.ecocom.2009.12.004

Wang, D.-L., Yu, Z.-G. and Anh, V. (2012), 'Multifractal analysis of complex networks', *Chinese Physics B* **21**(8), 080504.
DOI: 10.1088/1674-1056/21/8/080504

Watson, T. (2006), 'Metropolitan Growth, Inequality, and Neighborhood Segregation by Income', *Brookings-Wharton Papers on Urban Affairs* **2006**, 1–52.
DOI: 10.1353/urb.2006.0029

Watson, T. (2009), "Inequality and the Measurement of Residential Segregation by Income In American Neighborhoods". National Bureau of Economic Research Working Paper. Paper No. 14908.
DOI: 10.3386/w14908

Wegener, M. (2011), 'From Macro to Micro-How Much Micro is too Much?', *Transport Reviews* **31**(2), 161–177.
DOI: 10.1080/01441647.2010.532883

Wegener, M. (2013), Employment and Labour in Urban Markets in the IRPUD Model, *in* F. Pagliara, M. de Bok, D. Simmonds and A. Wilson, eds, 'Employment Location in Cities and Regions', Springer Berlin Heidelberg, Berlin, Germany, pp. 11–31.
DOI: 10.1007/978-3-642-31779-8_2
ISBN: 978-3-642-31778-1

Wegener, M. (2014), Land-Use Transport Interaction Models, *in* M. M. Fischer and P. Nijkamp, eds, 'Handbook of Regional Science', Springer Berlin Heidelberg, Berlin, Germany, pp. 741–758.
DOI: 10.1007/978-3-642-23430-9_41
ISBN: 978-3-642-23429-3

Wendt, H., Roux, S. G., Jaffard, S. and Abry, P. (2009), 'Wavelet leaders and bootstrap for multifractal analysis of images', *Signal Processing* **89**(6), 1100–1114.
DOI: 10.1016/j.sigpro.2008.12.015

West, G. B. (1997), 'A General Model for the Origin of Allometric Scaling Laws in Biology', *Science* **276**(5309), 122–126.
DOI: 10.1126/science.276.5309.122

West, G. B. (2006), Size, Scale and the Boat Race; Conceptions, Connections and Misconceptions, *in* D. Pumain, ed., 'Hierarchy in Natural and Social Sciences', Vol. 3, Springer-Verlag, Berlin, Heidelberg, pp. 71–80.
DOI: 10.1007/1-4020-4127-6_4
ISBN: 978-1-4020-4126-6

West, G. B. (2017), *Scale: the universal laws of growth, innovation, sustainability, and the pace of life in organisms, cities, economies, and companies*, Penguin Press, New York, NY.
ISBN: 978-1-59420-558-3

White, R. and Engelen, G. (1993), 'Cellular Automata and Fractal Urban Form: A Cellular Modelling Approach to the Evolution of Urban Land-Use Patterns', *Environment and Planning A* **25**(8), 1175–1199.
DOI: 10.1068/a251175

White, R. and Engelen, G. (1994), 'Urban systems dynamics and cellular automata: Fractal structures between order and chaos', *Chaos, Solitons & Fractals* **4**(4), 563–583.
DOI: 10.1016/0960-0779(94)90066-3

White, R., Engelen, G. and Uljee, I. (1997), 'The use of constrained cellular automata for high-resolution modelling of urban land-use dynamics', *Environment and Planning B: Planning and Design* **24**(3), 323–343.
DOI: 10.1068/b240323

Wilson, A. G. (1971), 'A Family of Spatial Interaction Models, and Associated Developments', *Environment and Planning A: Economy and Space* **3**(1), 1–32.
DOI: 10.1068/a030001

Witten, T. A. and Sander, L. M. (1981), 'Diffusion-Limited Aggregation, a Kinetic Critical Phenomenon', *Physical Review Letters* **47**(19), 1400–1403.
DOI: 10.1103/PhysRevLett.47.1400

Wong, D. W. S. (1993), 'Spatial Indices of Segregation', *Urban Studies* **30**(3), 559–572.
DOI: 10.1080/00420989320080551

Yakubo, K., Saijo, Y. and Korosak, D. (2014), 'Superlinear and sublinear urban scaling in geographical networks modeling cities', *Physical Review. E, Statistical, Nonlinear, and Soft Matter Physics* **90**(2), 022803.
DOI: 10.1103/PhysRevE.90.022803

Yamu, C. and Frankhauser, P. (2015), 'Spatial accessibility to amenities, natural areas and urban green spaces: using a multiscale, multifractal simulation model for managing urban sprawl', *Environment and Planning B: Planning and Design* **42**(6), 1054–1078.
DOI: 10.1068/b130171p

Yamu, C. and van Nes, A. (2017), 'An Integrated Modeling Approach Combining Multifractal Urban Planning with a Space Syntax Perspective', *Urban Science* **1**(4), 37.
DOI: 10.3390/urbansci1040037

Yano, K., Nakaya, T., Isoda, Y., Brown, P. and Savas, M., eds (2007), *Virtual Kyoto: Exploring the past, present and future of Kyoto*, Nakanishiya Shuppan, Kyoto, Japan, chapter 3, Meiji-Taisho Era in Virtual Kyoto (1868-1926), pp. 48–69.
ISBN: 978-4-7795-0100-5

Yano, K., Nakaya, T., Isoda, Y. and Kawasumi, T. (2009), Chapter 6 Virtual Kyoto as 4D-GIS, *in* H. Lin and M. Batty, eds, 'Virtual Geographic Environments', Esri Press, Redlands, CA, pp. 69–86.
ISBN: 978-1-58948-318-7

Yano, K., Nakaya, T., Isoda, Y., Takase, Y., Kawasumi, T., Matsuoka, K., Seto, T., Kawahara, D., Tsukamoto, A., Inoue, M. and Kirimura, T. (2008), 'Virtual Kyoto: 4DGIS Comprising Spatial and Temporal Dimensions', *Chigaku Zasshi (Jounal of Geography)* **117**(2), 464–478.
DOI: 10.5026/jgeography.117.464

Yano, K., Nakaya, T., Kawasumi, T. and Tanaka, S., eds (2011), *Historical GIS of Kyoto*, Nakanishiya Shuppan, Kyoto, Japan.
ISBN: 978-4-7795-0542-3

Yntema, D. B. (1933), 'Measures of the Inequality in the Personal Distribution of Wealth or Income', *Journal of the American Statistical Association* **28**(184), 423–433.
DOI: 10.1080/01621459.1933.10503242

Youn, H., Bettencourt, L. M. A., Lobo, J., Strumsky, D., Samaniego, H. and West, G. B. (2016), 'Scaling and universality in urban economic diversification', *Journal of The Royal Society Interface* **13**(114), 20150937.

DOI: 10.1098/rsif.2015.0937

Zhu, Y., Diao, M., Ferreira Jr., J. and Zegras, P. C. (2018), Integrating accessibility measures into the microsimulation of daily real estate market dynamics, *in* 'Applied Urban Modelling 2018 conference'.